

# Gene Profiles during Root Canal Treatment in Experimental Rat Periapical Lesions

Zulema Rosalia Arias Martinez, DDS,\* Koji Naruishi, DDS, PhD,\*  
 Keisuke Yamashiro, DDS, PhD,\* Fumio Myokai, DDS, PhD,\* Teruo Yamada, PhD,<sup>†</sup>  
 Kaori Matsuura, DDS, PhD,\* Naoko Namba, DDS,\* Hideo Arai, DDS, PhD,\*  
 Junzo Sasaki, MD, PhD,<sup>‡</sup> Yoshimitsu Abiko, DDS, PhD,<sup>§</sup> and Shogo Takashiba, DDS, PhD\*

## Abstract

The purpose of this study was to profile gene expression in periapical lesions during root canal treatment (RCT). Periapical lesions were induced experimentally by exposing the pulp in Sprague-Dawley rats. After 3 wk, the animals received root canal filling (RCF) and were sacrificed 1 or 4 wk later. From the periapical tissues, total RNA was extracted and processed for cDNA-microarray analysis. The lesions were histologically and radiographically confirmed to expand 4 wk after pulp exposure (inflammation phase) and to stabilize 4 wk after RCF (healing phase). In approximately 30,000 genes on the microarray, 203 genes were up-regulated to more than 5-fold (e.g., IL-1 $\beta$ ), and 864 genes were down-regulated to less than 20% of baseline level (e.g., caspase 8) in inflammation phase. Compared with inflammation phase, we found that 133 genes were up-regulated (e.g., IL-1 $\alpha$ ) and 50 genes were down-regulated (e.g., defensin  $\alpha$ 5) in healing phase. Corresponding to the gene expression profiles, accumulation of IL-1 $\alpha$  and IL-1 $\beta$  was observed in the periapical lesions by immunohistochemistry. These gene profiles might be useful in diagnosing the healing process of periapical lesions. (*J Endod* 2007;33:936–943)

## Key Words

Gene profiles, IL-1 $\alpha$ , IL-1 $\beta$ , periapical lesion, root canal treatment

From the \*Department of Pathophysiology–Periodontal Science, Okayama University Graduate School of Medicine, Dentistry and Pharmaceutical Sciences, Okayama, Japan; <sup>†</sup>Department of Cytology and Histology, Okayama University Graduate School of Medicine, Dentistry and Pharmaceutical Sciences, Okayama, Japan; <sup>‡</sup>Department of Biochemistry and Molecular Biology, Nihon University School of Dentistry at Matsudo, Chiba, Japan.

Address requests for reprints to Dr. Shogo Takashiba, DDS, PhD, Department of Pathophysiology–Periodontal Science, Okayama University Graduate School of Medicine, Dentistry and Pharmaceutical Sciences, 2-5-1 Shikata-cho, Okayama 700-8525, Okayama, Japan. E-mail address: stakashi@cc.okayama-u.ac.jp.

0099-2399/\$0 - see front matter

Copyright © 2007 by the American Association of Endodontists.

doi:10.1016/j.joen.2007.04.016

Periapical periodontitis is mainly caused by bacterial infection within the root canal (1), and periapical tissue destruction is caused by endogenous inflammatory mediators released during interaction between bacteria and host cells, mainly polymorphonuclear neutrophils (PMNs), lymphocytes, plasma cells, and macrophages (2). However, the pathological mechanisms that are responsible for apical tissue destruction such as bone degradation are not fully understood.

After developing periapical lesions, endodontic treatment (root canal treatment, RCT) has been performed traditionally to remove the infectious agents in root canal (3). By means of RCT, inflammatory reactions against infectious antigen in periapical lesions decrease gradually, and lead to the healing process (2, 3).

Clinically, judgment of the success of RCT is abundant but inconclusive. In many clinical cases, the success has been evaluated by radiographic healing of periapical lesions (4). Also, it may be evaluated by a decrease in clinical symptoms such as spontaneous pain, percussive pain, and pus discharge from canal. Considering the inflammatory responses in periapical lesions, success should be evaluated by decrease in inflammatory reactions. However, molecular mechanisms regulating inflammatory processes, especially the healing process after RCT in periapical lesions, are still poorly understood.

Comprehensive gene expression analysis with cDNA microarray is a powerful tool to investigate the etiology and pathophysiology of diseases including periapical lesions (5, 6). The altered gene expression pattern detected by cDNA microarray analysis suggests that changes of complex inflammatory reactions during RCT are likely to be involved in the development and consequences of the disease. In the present study, we established an in vivo model of the periapical lesions with RCT to clarify the molecular pathophysiology of the disease. Using cDNA microarray analysis, we report for the first time a global gene expression analysis in periapical lesions with RCT. We analyzed the gene expression profiles in periapical lesions to clarify the molecular mechanisms of the disease, and we also investigated changes in gene expression relating to the therapeutic effects. The possible targets for diagnosis of healing process in periapical lesions using immunohistochemical analysis were determined from these data. Our approach should contribute to the development of novel diagnostic systems in periapical lesions during RCT.

## Materials and Methods

### Animals

Male Sprague-Dawley (SD) rats 10 weeks of age were purchased from CLEA Japan (Tokyo, Japan). Rats were fed standard rodent chow and water ad libitum, and housed under a 12-hour light–dark cycle. Rats were acclimated to the animal facility for 5 days before any experimental handling. The protocol was approved by the Animal Care Committee of the Okayama University Graduate School of Medicine, Dentistry and Pharmaceutical Sciences.

### Experimental Animal Models of Periapical Lesions During RCT

The animals were anesthetized with sodium pentobarbital (50 mg/kg; nembutal sodium; Dainippon-Sumitomo Pharma, Osaka, Japan). Periapical lesions were induced

experimentally by exposing the pulp in the lower first molars of the rats. After 3 wk, root canals were mechanically disinfected with reamers and files, and irrigated with standard saline solution, then root canals were obturated using gutta-percha point (Showa Yakuhin Kako, Tokyo, Japan) and sealer (Canals N, Showa Yakuhin Kako) with lateral condensation technique. Finally the occlusal cavity was sealed with glass-ionomer cement (Fuji Ionomer Type II: GC, Tokyo, Japan). According to experimental protocol (Fig. 1A), 4 rats were assigned to 3 groups: a nontreatment group (healthy,  $n = 4$ ; 3 for RNA sample, 1 for tissue section); an inflammation group (inflammation,  $n = 4$ ; 3 for RNA sample, 1 for tissue section); and an RCT group (healing,  $n = 4$ ; 3 for RNA sample, 1 for tissue section). Inflammation group has not received RCT throughout experiments. Periapical inflammatory reactions were evaluated by radiographic examination in a time dependent manner using a portable X-ray machine (MAX-DC 70: Morita, Osaka, Japan). At the same time, periapical tissues were evaluated histologically in each group of rats.

### RNA Preparation

In the three specimens from each group, tissues surrounding periapical area were dissected out with the use of a low-speed handpiece and excavator. The samples were immediately inserted in RNAlater (Ambion, Austin, TX) to perform microarray analysis. Then the samples of each group were pooled into 1 tube and homogenized using a Mixer

Mill MM 301 (Retsch, Haan, Germany) and total RNA was isolated using RNeasy Fibrous Tissue Mini Kit (QIAGEN, Hilden, Germany). The RNA integrity was determined using Agilent 2100 bioanalyzer, and RNA6000 Pico LabChip Kit (Agilent, Palo Alto, CA) and the ratio of the amount of 28S to 18S ribosomal RNAs approached about 2:1.

### Microarray Analysis

Rat genome 230 2.0 arrays, which contained approximately 30,000 probes corresponding to known rat genes, were purchased from Affymetrix (Santa Clara, CA). For cDNA microarray analysis, a series of reverse-transcription, second-strand cDNA synthesis, and probe generation were accomplished and processed according to manufacturer's instruction (Affymetrix). Briefly, first-strand cDNA was synthesized with SuperScript II and a T7-(dT)<sub>24</sub> primer from total RNA and then double-strand cDNA was synthesized with *Escherichia coli* RNase H, *E. coli* DNA polymerase I, and *E. coli* DNA ligase (all from Affymetrix). After the double-stranded cDNA were purified with GeneChip Sample Cleanup Module (Affymetrix), cRNA was prepared using a MEGAscript T7 kit (Ambion). After a second cycle of amplification and biotin labeling with a GeneChip IVT labeling kit (Affymetrix), 20  $\mu\text{g}$  of labeled cRNA was fragmented by mild alkaline treatment, at 94°C for 35 min with GeneChip Sample Cleanup Module (Affymetrix). The Rat genome 230 2.0 arrays were hybridized as described in the GeneChip Expression Analysis Technical Manual (Affymetrix). After hybridization, the microarray was rinsed with  $0.2 \times \text{SSC}$  (3 mmol/L NaCl, 0.3 mmol/L Na-citrate) and then scanned with an array scanner (Scanner 3000, Affymetrix). Scanned images were analyzed using GeneChip Operating Software (Version 1.1: Affymetrix) and GeneSpring software (version 7.2: Tomy Digital Biology, Tokyo, Japan). In brief, the hybridization efficiencies were equalized by median value of control probe set to each array, and the genes with higher signal intensities than *bioB* derived from *E. coli* as an internal control for hybridization were subjected for further analysis. The genes (probe sets) showing greater than a fold-change greater than 5.0 or less than 0.2 were selected as changed genes. Next, pathway analysis was performed using Ingenuity pathways analysis (IPA) software ([www.ingenuity.com](http://www.ingenuity.com), Ingenuity® Systems, Inc, CA), a web-delivered application that enables biologists to discover, visualize, and explore potentially relevant pathobiologic networks. Data sets containing the genes accession numbers and their corresponding expression fold-change values were imported into IPA software (Ingenuity Systems, Inc.). Focus genes identified by the IPA program were categorized based on location, cellular components, and reported biochemical, biologic, and molecular functions using the software. The program queried the Ingenuity Systems' Pathway Knowledge Base for interactions between the focus genes and all other gene objects stored in the knowledge base, and generated a set of networks ranked by score. The score is the negative log of a p value and indicates the likelihood of the focus genes being found in the networks caused by random chance. A score of 3 indicates that there is a 1/1,000 chance that the focus genes are in the network due solely to chance. Therefore, scores of 3 or greater represent a 99.9% confidence level. Biologic functions were then calculated and assigned to each network.

### Quantitative RT-PCR

The quantitative reverse transcription polymerase chain reaction (qRT-PCR) was performed using Chromo 4 Real-time PCR Detector (Bio-Rad, Hercules, CA) according to the manufacturer's instructions. Briefly, 5  $\mu\text{g}$  of total RNA extracted from the periapical samples were reverse-transcribed with oligo (dT)<sub>12-18</sub> primer, dNTPs and SuperScript II (all from Invitrogen, Carlsbad, CA) in a total volume of 20  $\mu\text{L}$ , and 0.1  $\mu\text{L}$  of this reaction mixture was mixed with both SYBR Green PCR Master Mix (Applied Biosystems, Foster City, CA) and the gene-

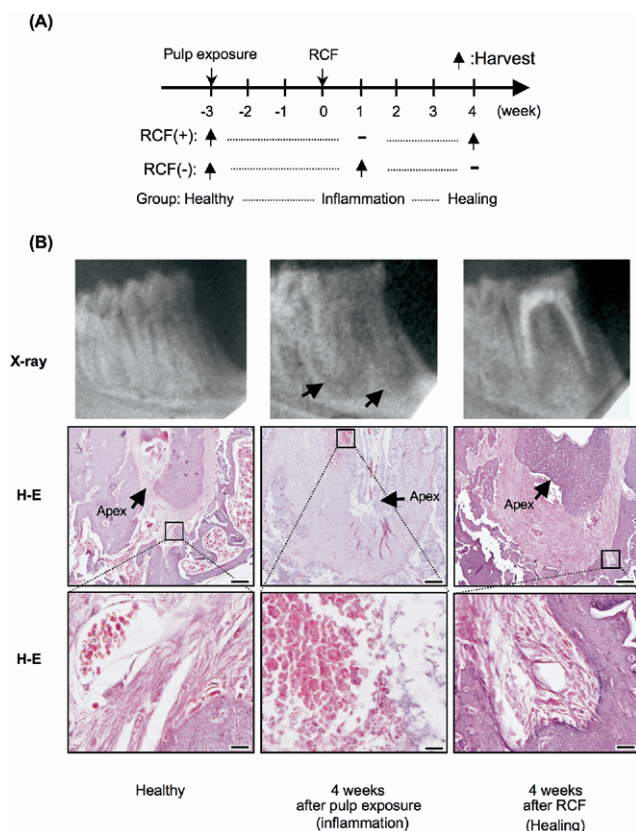


**Figure 1.** Establishment of in vivo experimental model of periapical lesions with RCT. (A) Experimental protocol. (B) Representative radiographical (X-ray, top panel) and histological (hematoxylin and eosin staining, middle and bottom panel) evaluation in each group. In radiographic data in top panel, arrow heads show the radiolucent area. We stained 3 sections on a glass slide for each group, and selected the most representative view. In the inflammation phase, infiltrated leukocytes were observed. Scale bars: middle panel, 500  $\mu\text{m}$ ; bottom panel, 100  $\mu\text{m}$ .

specific primers. The PCR primers were designed by Primer 3 ([http://frodo.wi.mit.edu/cgi-bin/primer3/primer3\\_www.cgi](http://frodo.wi.mit.edu/cgi-bin/primer3/primer3_www.cgi)) and have been shown in a supplementary Table. The real-time PCR was performed using Chromo 4 Real-time PCR Detector (Bio-Rad) according to the manufacturer's instructions. The all amplification of selected genes conditions consisted of an initial 10 min denaturation step at 95°C followed by 40 cycles of denaturation at 95°C for 15 sec, annealing and elongation at 55°C for 1 min. Three independent assays were performed for each gene, and we deleted outlier from the further analysis.  $\beta$ -Actin was used as an internal control for the relative quantification of the target messages, because there were no significant difference in  $\beta$ -actin mRNA level among the samples by preliminary experiments using the microarray and real-time PCR.

### Immunohistochemistry

To confirm the Microarray data, one rat in each group was sacrificed, and periapical area with tooth of each rat was harvested carefully for histological examination. Tissues were fixed in 4% paraformaldehyde and decalcified by K-CX decalcifying solution (FALMA, Tokyo, Japan). The decalcified tissues were embedded in paraffin wax, and three sagittal sections 5- $\mu$ m thick were cut and placed together on one glass slide for histological (hematoxylin and eosin staining) and immunohistochemical examination.

The tissue sections were deparaffinized in xylene and rehydrated. Sections were rinsed in phosphate-buffered saline solution (PBS) (–) and incubated with 3% H<sub>2</sub>O<sub>2</sub> in methanol for 20 min to quench endogenous peroxidase activity and the sections were rinsed with PBS (–). Primary antibodies were incubated 30 min at room temperature in a humid chamber. Primary antibodies used in this study were rat anti-IL-1 $\alpha$  antibody (Cat. No. sc-9983, Santa Cruz Biotechnology, Santa Cruz, CA) and rat anti-IL-1 $\beta$  antibody (Cat. No. sc-7884, Santa Cruz). After sections were rinsed with PBS containing 0.2% Tween 20 (PBST), peroxidase-conjugated goat anti-rat immunoglobulin (Nichirei, Tokyo, Japan) was incubated for 30 min at room temperature and rinsed with PBST. Finally, the sections were developed with 3, 3'-diaminobenzidine tetrahydrochloride (DAB; Vector Laboratories, Burlingame, CA) and mounted with coverslips.

### Statistical Analysis

Statistical analysis in quantitative RT-PCR (qRT-PCR) were carried out using StatView 5.0 software (Abacus Concepts, Berkeley, CA). Comparisons between two groups were performed with unpaired Student's *t* test, and *p* values of less than 0.05 were considered statistically significant.

## Results

### Establishment of Experimental Animal Models of Periapical Lesions

Experimental protocol has shown in Fig. 1A. To confirm the establishment of inflammatory reaction in periapical area, we examined the degree of the inflammation by both radiographic and histologic examination (Fig. 1B). We observed that there was a dramatic inflammatory reaction, infiltration of leukocytes, and thickness of periodontal ligament 4 wk after pulp exposure in periapical area. Further, the inflammatory reaction decreased slightly 4 wk after RCF as expected. From these results, we categorized the inflammatory stages around periapical region to three groups (Healthy, Inflammation, and Healing). No clinical signs of infection or mortality were observed throughout experiments. There were no significant differences in body weight of rats among each group.

### Microarray Analysis

Global gene expression patterns were generated from Affymetrix Genechip microarrays using total RNA isolated from periapical tissues of each group. We compared the gene expression patterns among each group (Healthy vs. Inflammation, Healthy vs. Healing, and Inflammation vs. Healing) and used a 5-fold change in expression as the experimental cut-off value that would imply significance. In the 30,000 genes on the array 203 genes were up-regulated to more than 5-fold (IL-1 $\beta$ , MMP-12, PDGF- $\alpha$ , etc.) and 864 genes were down-regulated to less than 20% of baseline level (*Cathepsin E*, *Caspase 8*, *Calmodulin 3*, etc.) in the inflammation compared with the healthy control (Table 1). In addition, 410 genes were up-regulated to over 5-fold (IL-1 $\beta$ , *Cathepsin L*, *Integrin  $\beta$ 6*, etc.) and 826 genes were down-regulated to less than 20% of baseline level (*MMP-8*, *Defensin Rat NP-3 precursor*, *Cyclin E*, etc.) in the healing phase compared with the healthy control (Table 2). Furthermore, 133 genes were up-regulated to over 5-fold (*IL-1 $\alpha$* , *MMP-3*, *Integrin  $\beta$ 6*, etc.) and 50 genes were down-regulated to less than 20% of baseline level (*Mast cell protease 9*, *Defensin Rat NP-3 precursor*, *Defensin- $\alpha$ 5*, etc.) in the healing phase compared with the inflammation (Table 3). To validate the alternation of gene expression levels that were detected on the microarrays, qRT-PCR analysis was performed using RNA obtained from the same tissue samples used in the microarray experiment (Fig. 2). Because the amount of tissue was limited, RNA of the rats belonging to the same experimental group was pooled. As shown in Fig. 2, we analyzed several genes, IL-1 $\beta$ , caspase 8, cathepsin L, IL-1 $\alpha$ , and defensin- $\alpha$ 5 using qRT-PCR. Besides caspase 8 gene, we demonstrated that gene expression patterns correlated, but generally higher fold-changes were observed in qRT-PCR experiments compared with those obtained in the microarray experiments.

The ingenuity analysis shows possible interactions among the gene products which were up- or down-regulated in the microarray experiments. As seen in supplementary Fig. 1–3, the pathway analysis revealed that interactions of genes during RCT are complex as expected. Especially, we found that increase of IL-1 $\alpha$  gene is an important factor in healing phase after the inflammation phase (Supplementary Fig. 3). Also, we found that the tumor necrosis factor (TNF) gene and transforming growth factor (TGF)  $\beta$ 1 gene might play a central role in healing phase, although the expression of their genes does not show obvious change during RCT.

### Expression of IL-1 $\alpha$ and IL-1 $\beta$

The pathways presented in the supplemental figures are possible interactions but do not directly implicate IL-1 $\alpha$  and IL-1 $\beta$  in the process of healing. Since both IL-1 $\alpha$  and IL-1 $\beta$  are known to be involved in the process of inflammation (7), we investigated further their expression at protein levels. The expression of IL-1 $\alpha$  or IL-1 $\beta$  protein in rat periapical lesions was assessed by immunohistochemistry (IHC). As shown in Fig. 3, the strong staining of IL-1 $\alpha$  was observed in periapical lesions at healing phase compared with inflammation phase. Furthermore, we observed that there was no significant difference between inflammation phase and healthy controls in IL-1 $\alpha$  staining. On the other hand, the strong staining of IL-1 $\beta$  was observed in periapical areas at inflammation phase compared with healthy controls. Moreover, we observed that there was no significant difference between inflammation phase and healing phase in IL-1 $\beta$  staining.

## Discussion

Inflammatory processes are thought to play an important role in the pathogenesis of periapical periodontitis (7). An accumulation of various cell types, neutrophils, macrophages, and lymphocytes in the periapical lesions has been observed to be associated with the develop-

**TABLE 1.** Gene Profiles in Inflamed Tissue Compared with Healthy Control

Function	Gene Name	Accession #	Fold Change	
Up-regulated (total 203 genes)	Cytokine-related	Chemokine (CXC motif) ligand 1	NM_030845	170.00
		*IL-1 $\beta$	NM_031512	6.48
	Enzymes	Colony stimulating factor 1	AW535553	5.22
		MMP-12	NM_053963	54.2
		Plasminogen activator	NM_013151	15.7
		Prostaglandin-endoperoxide synthase 2	U03389	8.99
		MMP14	A1176440	8.31
		Carboxypeptidase X1	A1577849	7.72
	Growth factor-related	Lysyl oxidase	NM_017061	6.43
		Insulin-like growth factor binding protein-5	BF399783	27.6
		PDGF- $\alpha$	AA866419	10.5
		Insulin-like growth factor-2	BI299621	6.56
		Epidermal growth factor	NM_022294	6.18
	Kinases	Fibroblast growth factor-3	BF410980	5.06
		MAPK4	BE117850	9.65
	Cellular matrix	CaM-kinase II inhibitor $\alpha$	A1236027	6.94
		Collagen type XVIII $\alpha$ 1	A101782	9.79
		Laminin $\alpha$ 1	BI281952	9.28
		Collagen type XIV $\alpha$ 1	A1599143	7.20
		Procollagen, type XV	AA800298	6.86
Transcription regulator	Cadherin 13	NM_138889	5.40	
	Runt related transcription factor 2	BF403180	10.50	
Others	Jun-B oncogene	NM_021836	5.41	
	Heat shock 70kD protein 1A	NM_031971	27.90	
	Fibulin 2	AA944398	7.27	
Down-regulated (total 864 genes)	Cytokine-related	Myosin heavy chain 11	X16262	6.06
		Dynamin 1	NM_080689	5.11
	Enzymes	Erythropoietin receptor	NM_017002	0.112
		Tumor Necrosis factor (ligand) superfamily	BF286267	0.161
		Interferon regulatory factor 7	BF411036	0.179
		Mast cell protease 8	NM_021598	0.011
		Cathepsin E	NM_012938	0.070
		MMP-8	NM_022221	0.093
	Growth factor-related	*Caspase 8	NM_022277	0.104
		Cytochrome c oxidase	X15030	0.156
		Dipeptidylpeptidase 4	J02997	0.156
		Hepatocyte growth factor inhibitor 1	BI280343	0.151
		Calmodulin 3	NM_012518	0.100
	Kinases	Phosphatidylinositol-4-phosphate 5-kinase	BF406008	0.126
		Cyclin-dependent kinase inhibitor 3	BE113362	0.136
		G protein-coupled receptor kinase 6	NM_031657	0.138
		Protein kinase C, $\delta$	A1171093	0.148
		Mitogen activated protein kinase 1	BI282894	0.184
		Proteoglycan 2, bone marrow	NM_031619	0.052
		Lectin	NM_012976	0.118
Cellular matrix	Cadherin 1	NM_031334	0.122	
	Integrin $\beta$ 7	AF003598	0.157	
	Tubulin $\beta$ 2	AA892044	0.174	
Transcription regulator	GATA binding protein 1	NM_012764	0.080	
	Calmodulin binding protein 1	AW528001	0.186	
Others	Fc receptor, IgE	M17153	0.029	
	Leptin receptor	AF304191	0.056	
	Cyclin B1	L11995	0.061	
	Cyclin E	AW913890	0.086	
	CD47 antigen	NM_019195	0.104	

\*Confirmed by qRT-PCR.

ment of periapical periodontitis (8). Increased numbers of inflammatory cells or high levels of inflammatory mediators such as cytokines and proteases have been reported in periapical lesions (9). Thus, several *in vitro* studies may contribute to clarify the pathophysiology of periapical lesions that lead to periapical healing (9–11), but conclusive evaluations rely on clinical examination in patients with periapical lesions. In fact, the radiographic evaluation is frequently used for the assessment of RCT or even epidemiologic clinical studies (12, 13). However, radiographic examination is not sufficient for the evaluation of healing during

RCT because bone remodeling is much slower than biological responses; therefore several molecular markers must be selected for diagnosis of periapical healing to evaluate more scientifically and reasonably. In this case we may use exudate as samples for checking several molecular markers.

At first, to identify candidate genes regulated by performing RCT comprehensively, we established the *in vivo* models for periapical lesions with RCT and confirmed the inflammation and healing phase during RCT radiographically and histologically (Fig. 1B). Histological

**TABLE 2.** Gene Profiles in Healing Phase after Root Canal Filling Compared with Healthy Control

Function	Gene Name	Accession #	Fold Change	
Up-regulated (total 410 genes)	Cytokine-related			
	IL-1 $\beta$	NM_031512	21.9	
	Interferon regulatory factor 6	BF410603	19.6	
	IL-1 $\alpha$	NM_017019	19.3	
	Chemokine (C-C motif) ligand 2	NM_031530	15.5	
	Chemokine (C-C motif) ligand 3	U22414	12.9	
	Enzymes	MMP-3	NM_133523	17.4
		Prostaglandin E synthase	AB048730	14.8
		MMP-10	NM_133514	11.9
		Lysil Oxidase	NM_017061	11.5
		Plasminogen activator, urokinase	X83537	11.3
		*Cathepsin L	AI176595	9.95
		MMP-14	X83537	9.85
		TIMP-1	NM_053819	7.73
		Cathepsin C	AW920064	5.85
		PDGF- $\alpha$	AA866419	18.2
	Growth factor-related	Epidermal growth factor receptor	M37394	13.7
		Fibroblast growth factor-3	BF410980	5.27
		Integrin $\beta$ 6	AI070686	59.1
	Cellular matrix	Collagen type V $\alpha$ 3	NM_021760	27.4
Procollagen, type XII, $\alpha$ 1		BE108345	11.2	
Hypoxia inducible factor 1, $\alpha$ subunit		AI029318	14.4	
Transcription regulator	CCAAT/enhancer binding protein, $\beta$	NM_024125	8.26	
	JUN-B oncogene	NM_021836	7.65	
	Claudin 1	AI137640	21.6	
Others	Heat shock 70kD protein 1A	NM_031971	20.0	
	Heat shock 27kD protein 1	NM_031970	20.0	
	Down-regulated (total 826 genes)			
Enzymes				
Kinases	Mast cell protease 9	NM_019323	0.01	
	MMP-8	NM_022221	0.01	
	Cathepsin E	NM_012938	0.08	
	Chymase 1, mast cell	NM_013092	0.09	
	Dipeptidylpeptidase 4	J02997	0.13	
Cellular matrix	Protein kinase C, $\theta$	AI171083	0.15	
	MMP-14	NM_031020	0.18	
Transcription regulator	Proteoglycan 2, bone marrow	NM_031619	0.01	
	Tubulin $\beta$ 5	AB011679	0.15	
	Integrin $\beta$ 7	AF003598	0.20	
Others	GATA binding protein 1	NM_012764	0.01	
	CCAAT/enhancer binding protein, $\epsilon$	NM_017095	0.06	
	GATA binding protein 2	NM_033442	0.13	
	Defensin NP-4 precursor 1	U16684	0.01	
	*Defensin, $\alpha$ 5, Paneth cell-specific	U16686	0.01	
	Defensin Rat NP-3 precursor	U16683	0.01	
	Cathelicidin	AA998531	0.02	
	Cyclin-dependent kinase inhibitor 3	BE113362	0.07	
	Cyclin A2	AA998516	0.07	
	Cyclin B1	L11995	0.07	
Cyclin E	AW913890	0.08		
Fc receptor, IgE, high affinity I	M17153	0.10		
Leptin receptor	AF304191	0.10		
Cyclin D3	NM_012766	0.17		

\*Confirmed by qRT-PCR.

examinations of the periapical lesions show the increased infiltration of inflammatory cells such as leukocytes at 4 wk after pulp exposure although they were present in a small number (inflammation phase). Further, we observed regenerative bone slightly at 4 wk after RCF (healing phase). Importantly, radiolucent areas have been still observed at periapical lesions at 4 wk after RCF, although the areas reduced by radiographic examination. These findings indicate that periapical lesions at 4 wk after RCF were in the initial phase toward healing. Using this in vivo model, we performed cDNA microarray analysis to clarify the regulation of gene expression comprehensively at periapical lesions with RCT.

Microarray data demonstrates that the expression of several inflammatory cytokine-related genes is altered by inflammatory process. After 4 wk exposure of pulp, we observed that expression of chemokine

(CXC motif) ligand 1, IL-1 $\beta$ , and colony stimulating factor 1 genes increased as expected. Interestingly, gene expression of TNF family decreased. Since different expression patterns were observed, even in genes categorized in similar function, we recognized that gene expression profiles are complex. To determine the biologically relevant networks and pathways of the differentially expressed genes, pathway analysis was done on the up- and down-regulated genes, and integrated total datasets using the IPA software (supplementary Figs. 1–3). The networks describe functional relationships between gene transcripts based on known interactions reported in the literature. Several significant pathways were recognized in up- and down-regulated genes. Since the network was complex as expected, we cannot find an important pathway especially in periapical lesions during RCT. The whole extent of gene expression and interaction cannot entirely be discussed herein; how-

**TABLE 3.** Gene Profiles in Healing Phase after Root Canal Filling Compared with Inflammatory Phase

Function	Gene Name	Accession #	Fold Change
<b>Up-regulated (total 133 genes)</b>			
Cytokine-related	*IL-1 $\alpha$	NM_017019	7.15
	Interferon regulatory factor 6	BF410603	5.67
Enzymes	Carbonic anhydrase 4	NM_019174	17.4
	MMP-12	NM_053963	16.9
	Lipase, endothelial	AA964219	10.5
	Adenosine deaminase	NM_130399	8.42
	MMP-3	NM_133523	7.90
	Interferon gamma induced GTPase	AW525366	5.73
	Integrin $\beta$ 6	A1070686	40.5
Cellular matrix	Claudin 4	BE328951	85.4
	Immunoglobulin heavy chain 1a	A1411947	14.1
Others	PERP, TP53 apoptosis effector	BI286396	12.5
	GO/G1 switch gene 2	A1406939	9.48
	Annexin A8	BM389254	8.95
	Fc receptor, IgG, low affinity lib	X73371	6.13
<b>Down-regulated (total 50 genes)</b>			
Enzymes	Carbonic anhydrase 1	BM383006	0.015
	Pre-eosinophil-associated ribonuclease-2	A1177934	0.066
	Mast cell protease 9	NM_019323	0.114
Cellular matrix	Proteoglycan 2, bone marrow	NM_031619	0.013
	Spectrin $\alpha$ 1	A1639523	0.021
	Myosin VC	BF420807	0.126
	Claudin 5	BI281680	0.180
	Lectin, galactose binding	NM_012976	0.191
	Nucleotide binding protein 2	BF397271	0.050
Transcription regulator	Defensin NP-4 precursor	U16684	0.010
	Defensin NP-3 precursor	U16683	0.010
	*Defensin, $\alpha$ 5, Paneth cell-specific	U16686	0.010
	Cathelicidin	AA998531	0.079
	Transferrin	AA945178	0.136

\*Confirmed by qRT-PCR.

ever, additional investigations can be based on the data recruited by this analysis. We hope that they will help future investigation of molecular mechanisms in healing process after RCT.

By comparing the gene profiles between inflammation and healing phase we focused on the IL-1 gene expression mainly in the events associated with RCT. IL-1 is a pro-inflammatory cytokine that regulates multiple aspects of immune and inflammatory responses (14). The IL-1 family of cytokines includes IL-1 $\alpha$  and IL-1 $\beta$  (15). Since IL-1 $\alpha$  and

IL-1 $\beta$  bind to the same receptors (16), it seems that differential expression of these molecules may explain the differential roles of these molecules among inflammatory reactions during RCT. Interestingly, Matsuo et al. reported previously that the exudates from the canals with small radiolucent areas contained significantly higher IL-1 $\alpha$  levels than those from the canals with large radiolucent areas (17). They mentioned that the tendency to be an increase in the levels of IL-1 $\alpha$  and a decrease in the levels of IL-1 $\beta$  was observed after RCT. Their findings suggest that IL-1 $\alpha$  and IL-1 $\beta$  may play different roles in the healing process of periapical lesions during RCT. Corresponding to their findings, our results showed that IL-1 $\alpha$  expression in healing phase is stronger than that of inflammation phase from our cDNA microarray analysis (Table 3) and IHC data (Fig. 3). In addition, Egusa et al. reported that human gingival epithelial cells clearly increased production of IL-1 $\alpha$  in response to bacterial infection. This report might indicate that IL-1 $\alpha$  level increases by growth of epithelial cells around periapical lesion as seen in healing phase (18). It might be explained, at least in part, the pathophysiology of periapical healing by the different expression of IL-1 $\alpha$  and IL-1 $\beta$ , although the exact mechanisms for the functional discrimination between IL-1 $\alpha$  and IL-1 $\beta$  remains to be elucidated.

Neutrophils are key components of innate immune system (19). They are the first cells to infiltrate at sites of local inflamed lesions where they kill invading pathogens and promote acute inflammation via release of proteases and reactive oxygen species (19, 20). In our experimental in vivo model, we observed that leukocytes infiltrate at periapical lesions in inflammation phase. These data suggest that neutrophils are important for the initiation of periapical lesion formation. Furthermore, it has been generally accepted that neutrophils produced antimicrobial peptides defensins (21), suggesting that neutrophils can protect against severe inflammation and its potential pathological conse-

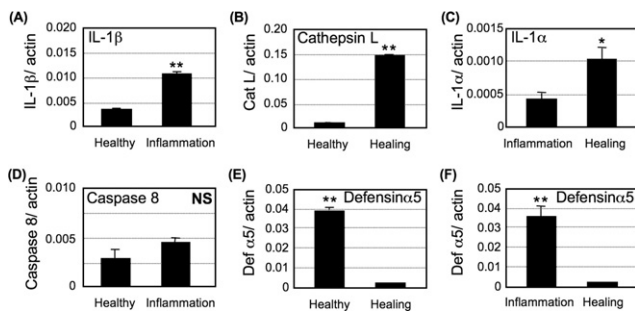


**Figure 2.** Validation of microarray gene expression data by qRT-PCR analysis. Based on the microarray data shown in Table 1–3, several genes were selected and confirmed the expression pattern by triplicate qRT-PCR analysis for each pooled RNA sample. The expression patterns of all the genes indicated with asterisks except caspase 8 (D), correlated to microarray data. (A): IL-1 $\beta$  (Healthy vs Inflammation), (B): *Cathepsin L* (Healthy vs Healing), (C): IL-1 $\alpha$  (Inflammation vs Healing), (D): *Caspase 8* (Healthy vs Inflammation), (E): *Defensin $\alpha$ 5* (Healthy vs Healing), and (F): *Defensin $\alpha$ 5* (Inflammation vs Healing). All values were normalized to  $\beta$ -actin housekeeping genes. Values are mean  $\pm$  SD, ( $n = 3$ ) \*  $p < 0.05$ ; \*\*  $p < 0.01$ ; NS, not significant (Student's  $t$  test).

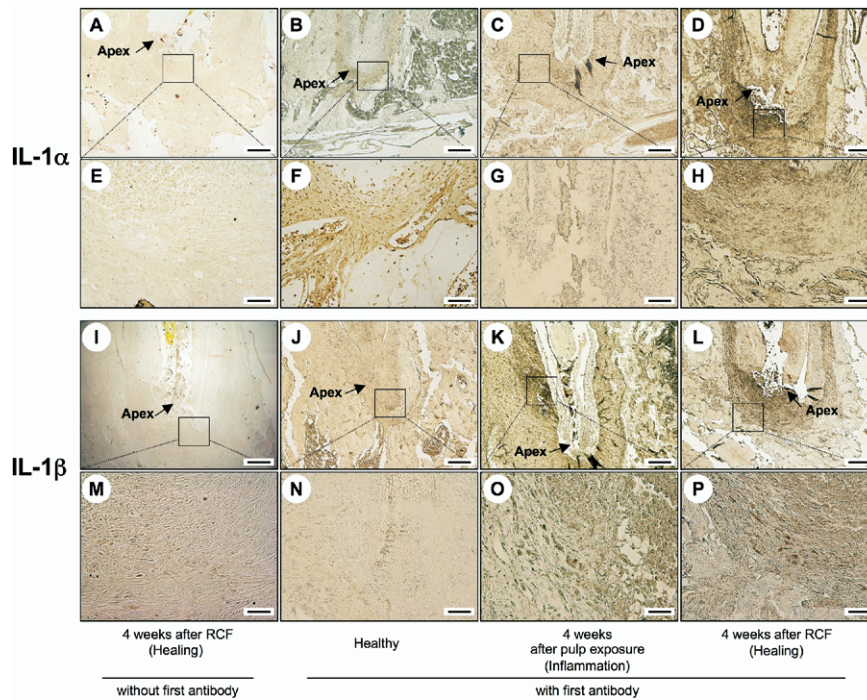


**Figure 3.** Immunohistochemical validation of gene expressions obtained from microarray data in periapical tissues. IL-1 $\alpha$  (A–H) and IL-1 $\beta$  (I–P). Immunohistochemistry was performed by an indirect peroxidase technique described in “Materials and Methods” section. From each group 3 sections were stained on a slide for either IL-1 $\alpha$  and IL-1 $\beta$ , and the most representative staining was selected. Positivity is indicated by a brown color. Negative controls (without the first antibody), A, E, I, M. Scale bars = 500  $\mu$ m for A–D, I–L; 100  $\mu$ m for E–H, M–P.

quences. Mainly, defensins have been isolated from the cytoplasmic granules of neutrophils in human beings (22), rats (23), and rabbits (24). From the present microarray data, we found that the expression of several defensin-related genes, defensin NP-4 precursor, defensin Rat NP-3 precursor and defensin  $\alpha$ 5, were down-regulated at healing phase compared with inflammation phase (Table 3). These findings suggest that infiltration of neutrophils at periapical lesions decreased after RCF. To examine the expression of defensin-related genes in periapical lesions might be useful to create the novel examination systems for diagnosis of periapical healing after RCT in the future.

In summary, cDNA microarray analysis of global gene expression patterns provided new molecular candidates for the diagnosis of periapical healing after RCT using in vivo models. Our findings suggest biological significance of differential gene expression and confirm some results in the literature with regard to molecules known to be involved in the periapical healing. cDNA microarray analysis of a well-controlled model system involving a highly relevant periapical healing is a useful screening tool for identifying novel differentially expressed genes. These genes provide a basis for further studies of periapical healing after RCT, and might be useful as attractive targets for diagnosis.

### Acknowledgments

We thank Dr. K. Yamabe and Dr. O. Rodis for technical support. This study was supported by Grants-in-Aid for Scientific Research (A) (No. 16209056, No. 18209057, and No. 16209063) from the Japan Society for the Promotion of Science.

### Supplementary Material

Supplementary data associated with this article can be found in the online version at doi:10.1016/j.joen.2007.04.016.

### References

1. Torabinejad M, Eby WC, Naidorf JJ. Inflammatory and immunological aspects of the pathogenesis of human periapical lesions. *J Endod* 1985;11:479–8.
2. Marton IJ, Kiss C. Protective and destructive immune reactions in apical periodontitis. *Oral Microbiol Immunol* 2000;15:139–50.
3. Oztan MD. Endodontic treatment of teeth associated with a large periapical lesion. *Int Endod J* 2002;35:73–8.
4. Mikrogeorgis G, Lyrroudia K, Molyvdas I, Nikolaidis N, Pitas I. Digital radiograph registration and subtraction: a useful tool for the evaluation of the progress of chronic apical periodontitis. *J Endod* 2004;30:513–7.
5. Rosa GJ, de Leon N, Rosa AJ. Review of microarray experimental design strategies for genetical genomics studies. *Physiol Genomics* 2006;28:15–23.
6. Dalma-Weiszhausz DD, Warrington J, Tanimoto EY, Miyada CG. The affymetrix GeneChip platform: an overview. *Methods Enzymol* 2006;410:3–28.
7. Fouad AF. IL-1 alpha and TNF-alpha expression in early periapical lesions of normal and immunodeficient mice. *J Dent Res* 1997;76:1548–54.
8. Kronman JH, Goldman M, Lin PS, Goldman LB, Kliment C. Evaluation of intracytoplasmic particles in histiocytes after endodontic therapy with a hydrophilic plastic. *J Dent Res* 1977;56:795–801.
9. Danin J, Linder LE, Lundqvist G, Andersson L. Tumor necrosis factor-alpha and transforming growth factor-beta1 in chronic periapical lesions. *Oral Surg Oral Med Oral Pathol Oral Radiol Endod* 2000;90:514–7.
10. Lee SH, Kim KK, Choi BK. Upregulation of intercellular adhesion molecule 1 and proinflammatory cytokines by the major surface proteins of *Treponema maltophilum* and *Treponema lecithinolyticum*, the phylogenetic group IV oral spirochetes associated with periodontitis and endodontic infections. *Infect Immun* 2005;73:268–76.
11. Danin J, Linder L, Lundqvist G, Wretling B. Cytokines in periradicular lesions: the effect of linezolid treatment. *Oral Surg Oral Med Oral Pathol Oral Radiol Endod* 2003;96:492–8.
12. Kirkevang LL, Wenzel A. Risk indicators for apical periodontitis. *Community Dent Oral Epidemiol* 2003;31:59–67.
13. Kabak Y, Abbott PV. Prevalence of apical periodontitis and the quality of endodontic treatment in an adult Belarusian population. *Int Endod J* 2005;38:238–45.
14. Seymour GJ. Possible mechanisms involved in the immunoregulation of chronic inflammatory periodontal disease. *J Dent Res* 1987;66:2–9.

15. Rosenwasser IJ. Biologic activities of IL-1 and its role in human disease. *J Allergy Clin Immunol* 1998;102:344–50.
16. Boch JA, Wara-aswapati N, Auron PE. Interleukin 1 signal transduction—current concepts and relevance to periodontitis. *J Dent Res* 2001;80:400–7.
17. Matsuo T, Ebisu S, Nakanishi T, Yonemura K, Harada Y, Okada H. IL-1alpha and IL-1beta periapical exudates of infected root canals: correlations with the clinical findings of the involved teeth. *J Endod* 1994;20:432–5.
18. Egusa H, Nikawa H, Makihira S, Yatani H, Hamada T. In vitro mechanisms of interleukin-8-mediated responses of human gingival epithelial cells to *Candida albicans* infection. *Int J Med Microbiol* 2006;296:301–11.
19. Mortensen RF, Zhong W. Regulation of phagocytic leukocyte activities by C-reactive protein. *J Leukoc Biol* 2000;67:495–500.
20. Kadl A, Bochkov VN, Huber J, Leitinger N. Apoptotic cells as sources for biologically active oxidized phospholipids. *Antioxid Redox Signal* 2004;6:311–20.
21. McGirt LY, Beck LA. Innate immune defects in atopic dermatitis. *J Allergy Clin Immunol* 2006;118:202–8.
22. Wilde CG, Griffith JE, Marra MN, Snable JL, Scott RW. Purification and characterization of human neutrophil peptide 4, a novel member of the defensin family. *J Biol Chem* 1989;264:11200–3.
23. Eisenhauer PB, Harwig SS, Szklarek D, Ganz T, Selsted ME, Lehrer RI. Purification and antimicrobial properties of three defensins from rat neutrophils. *Infect Immun* 1989;57:2021–7.
24. Selsted ME, Harwig SS, Ganz T, Schilling JW, Lehrer RI. Primary structures of three human neutrophil defensins. *J Clin Invest* 1985;76:1436–9.

## Oligonucleotide array analysis of cyclic tension-responsive genes in human periodontal ligament fibroblasts

Keisuke Yamashiro<sup>a</sup>, Fumio Myokai<sup>a</sup>, Koichi Hiratsuka<sup>b</sup>, Tadashi Yamamoto<sup>a</sup>,  
Kyoko Senoo<sup>a</sup>, Hideo Arai<sup>a</sup>, Fusanori Nishimura<sup>a,1</sup>,  
Yoshimitsu Abiko<sup>b</sup>, Shogo Takashiba<sup>a,\*</sup>

<sup>a</sup> Department of Pathophysiology–Periodontal Science, Okayama University Graduate School of Medicine, Dentistry and Pharmaceutical Sciences, 2-5-1 Shikata-cho, Okayama 700-8525, Japan

<sup>b</sup> Department of Biochemistry and Molecular Biology, Nihon University School of Dentistry at Matsudo, 2-870-1 Sakae-cho-Nishi Matsudo, Chiba 271-8587, Japan

Received 19 September 2006; received in revised form 7 December 2006; accepted 2 January 2007

Available online 23 January 2007

### Abstract

Mechanical stress results in differential gene expression that is critical to convert the stimulus into biochemical signals. Under physiological stress such as occlusal force, human periodontal ligament fibroblasts (HPLF) are associated with homeostasis of periodontal tissues however the changes in response to mechanotransduction remain uncharacterized. We hypothesized that cyclic tension-responsive (CT) genes may be used to identify a set of fundamental pathways of mechanotransduction. Our goal was to catalogue CT genes in cultured HPLF. HPLF were subjected to cyclic tension up to 16 h, and total RNA was isolated from both tension-loaded and static HPLF. The oligonucleotide arrays analysis revealed significant changes of mRNA accumulation for 122 CT genes, and their kinetics were assigned by the *K*-means clustering methods. Ingenuity Pathway Analysis was completed for HPLF mechanotransduction using 50 CT genes. This analysis revealed that cyclic tension immediately down-regulated all nuclear transcription factors except *v-fos FBJ murine osteosarcoma viral oncogene homolog* (FOS) reacting as an early responsive gene. In turn, transcription factors such as *tumor protein p53 binding protein 2* (TP53BP2), and extra-nuclear molecules such as *adrenergic receptor β2* (ADRB2) were up-regulated after 1–2 h, which may result in fundamental HPLF functions to adapt to cyclic tension. Subsequent inhibition assays using Y27632, a pharmacologic inhibitor of Rho-associated kinase (ROCK), suggested that HPLF has both ROCK-dependent and ROCK-independent CT genes. Mechanical stress was found to effect the expression of numerous genes, in particular, expression of an early responsive gene; FOS initiates alteration of HPLF behaviors to control homeostasis of the periodontal ligament.

© 2007 Elsevier Ltd. All rights reserved.

**Keywords:** Cyclic tension-responsive genes; Oligonucleotide array; Human periodontal ligament fibroblasts; Pathway analysis; Rho-associated kinase

\* Corresponding author. Tel.: +81 86 235 6677;  
fax: +81 86 235 6679.

E-mail address: [stakashi@cc.okayama-u.ac.jp](mailto:stakashi@cc.okayama-u.ac.jp) (S. Takashiba).

<sup>1</sup> Present address: Department of Dental Science for Health Promotion, Division of Cervico-Gnathostomatology, Hiroshima University Graduate School of Biomedical Sciences, 1-2-3 Kasumi Minamiku, Hiroshima 743-0037, Japan

### 1. Introduction

Mechanical stress is thought to play important roles in regulating the function, metabolism or maintenance of connective tissues such as periodontal ligaments. Abnormal mechanical stress may cause destruction of

tissues, and affects many pathological situations. A better understanding about cellular adaptation to changes in mechanical stress may help us design a new strategy in the treatment and prevention of mechanical stress-related disorders such as trauma, tooth/bone resorption, and atrophy or destruction of the connective tissues.

Mechanotransduction is the process by which cells transduce physiological force-induced signals into biochemical responses, and involves differential gene expression that is necessary for mediating adaptations to mechanical stress (Ingber, 2003). Evidence has accumulated that mechanical stress-induced alterations in cell shape and structure are critical for the control of cell contraction, migration, growth, differentiation, and apoptosis (Chicurel, Chen, & Ingber, 1998; Khan & Sheetz, 1997). Mechanical stresses are either transmitted to cells from the extracellular matrix, or generated within the contractile cytoskeleton of individual cells (Wang, Butler, & Ingber, 1993). Force-induced assembly of the focal adhesions and the cytoskeleton are crucial for inducing mechanotransduction in the cytoplasm (Geiger & Bershadsky, 2001; Ingber, 1997), and mediated in large by activation of the Ras-homolog of small GTPase (Rho) (Amano et al., 1997; Ridley & Hall, 1992). Rho acts as a molecular switch that cycles between an inactive GDP-bound and an active GTP-bound conformation interacting with downstream targets (effectors) to elicit cellular responses, and regulate the actin cytoskeleton (Etienne-Manneville & Hall, 2002). Rho-associated kinases (ROCK), the first and the best-characterized Rho effectors, are serine/threonine kinases that are involved in diverse cellular functions including motility, adhesion, smooth-muscle contraction, neuritic outgrowth, centrosome positioning, apoptosis, actin cytoskeleton organization and cell-size regulation. Thus, ROCK have the potential to contribute to various physiological and pathological states (Maekawa et al., 1999; Riento & Ridley, 2003). The Rho/ROCK pathway has been shown to be crucial for mediating mechanotransduction (Chiquet, Renedo, Huber, & Fluck, 2003; Numaguchi, Eguchi, Yamakawa, Motley, & Inagami, 1999) however the precise mechanisms that link mechanical stress to subsequent changes in cellular activities remains unknown.

Periodontal ligament is a connective tissue lying between alveolar bone and tooth root, and not only is a source of osteogenic cells, but also may contain multipotent stem cells that could regenerate cementum and periodontal ligament (Seo et al., 2004). Periodontal ligament fibroblasts (HPLF), in particular, can differentiate in response to a variety of extracellular stimuli to either maintain homeostasis or participate in remodeling of the

periodontal ligament, and repair or regeneration of the surrounding hard tissues (McCulloch, Lekic, & McKee, 2000). These cells are subject to continuous mechanical stress under physiological condition the result of both occlusal and masticatory forces. Several studies have been published that link mechanical stress to intracellular signaling molecules in HPLF (Kletsas, Basdra, & Papavassiliou, 2002; Myokai et al., 2003) however the molecular mechanisms of HPLF mechanotransduction remain elusive. Since it is likely that the expression of many genes is altered in response to mechanical stress it will become necessary to further catalogue these genes with respect to both temporal and subcellular distribution. We hypothesized that comprehensive analysis of cyclic tension-responsive (CT) genes may provide data useful to understand the fundamental mechanisms of mechanotransduction in HPLF.

The GeneChip probe array technology allows a systematic analysis of gene expression changes, and provides significant information for a wide variety of basic biological processes, including development (Abeyta et al., 2004), tumorigenesis (Kasamatsu et al., 2005), and the immune system (Calvano et al., 2005). The array technology allows simultaneous monitoring of the activities of numerous genes because of the technique's sensitivity, specificity, and reproducibility. In the present study, HPLF were loaded with cyclic tension, and the CT genes were identified using the GeneChip probe array. The CT genes identified were further analyzed on a cellular pathway map based on Ingenuity Systems' Pathway Knowledge Base. This was done to identify genetic networks involved in mechanotransduction in HPLF. Moreover, to elucidate the effect of the Rho/ROCK pathway on CT gene expression, we analyzed the CT gene expression in the presence or absence of a pharmacologic inhibitor of ROCK activity.

## 2. Materials and methods

### 2.1. Cell culture and mechanical stress

Periodontal ligament was obtained from periodontally healthy and non-carious teeth extracted for orthodontic reasons from four donors, three Japanese female (21, 24, and 17 years old) and a Japanese male (22 years old), with informed consent. Prior to the experiment, the protocol (no. 43) was approved by the Research Ethics Committee for Human Genome/Gene Analysis Research in Okayama University Graduate School of Medicine, Dentistry, and Pharmaceutical Sciences. HPLF were maintained and expanded in Dulbecco's Modified Eagle's Medium supplemented with 10% fetal

calf serum (both reagents from Invitrogen, Carlsbad, CA) as described previously (Yamamoto et al., 2003). HPLF between the 5th and 9th passages were seeded on 6-well flexible-bottomed culture plates (FLEX II; Flexcell, McKeesport, PA) at a concentration of  $2 \times 10^5$  cells per well, and grown for 2 days to allow them to attach on the culture dish while the control cells were seeded on 6-well fix-bottomed culture plates (FLEX I; Flexcell).

The HPLF grown on the flexible-bottomed plates were subjected to 18% tension (36 kPa) at 6 cycles per minute with the Flexercell Strain Unit for 0.5, 1, 2 or 16 h as described (Myokai et al., 2003). It has been demonstrated that the degree of tension can be calculated after measuring the increase in distance between any two sets of concentric rings of the culture well (Banes, Link, Gilbert, Tay, & Monbureau, 1990).

The Flexercell Strain Unit is designed to apply reproducible cyclic tension or compression to the cells in vitro. Force Analysis showed that deformation of the flexible membrane is not uniform but rather generates a tension gradient with the greatest deformation occurring at the periphery of the well (Banes et al., 1990). Thus, the results represented an average of cells exposed to different degrees of tension. The calculation showed that 18% tension resulted in 6% mean elongation to cells over the entire culture plate surface. Control cells were cultured under identical conditions but remained static.

## 2.2. Oligonucleotide microarray analysis

The oligonucleotide microarray analysis was performed on HPLF at 5 different time points (0, 0.5, 1.0, 2.0, and 16 h) of cyclic tension. HPLF from three donors were used for these analyses. Total RNA was recovered from the tension-loaded and control HPLF using RNeasy Mini Kit (Qiagen, Hilden, Germany). The protocol for microarray analysis was described previously (Hiratsuka et al., 2002). Briefly, single-stranded (ss) cDNA was synthesized from 8  $\mu$ g of total RNA using a T7-(dT)<sub>24</sub> primer (Amersham Biosciences, Piscataway, NJ) with SuperScript II Reverse Transcriptase (Invitrogen). Double-stranded (ds) cDNA was synthesized from the sscDNA, and purified with the GeneChip Sample Cleanup Module (Affymetrix, Santa Clara, CA). Using the dsDNA as a template, cRNA was transcribed with Bio-11-CTP and Bio-16-UTP (Enzo Diagnostics, Farmingdale, NY), purified, fragmented, and hybridized to the array (Human Genome Focus GeneChip probe arrays #900377; Affymetrix) spotted about 8500 known human genes. The arrays were washed, and stained with streptavidin-phycoerythrin (Molecular Probes, Eugene, OR) using an Affymetrix Fluidics Station. Fluorescence

intensities were scanned with an Affymetrix GeneArray Scanner.

Poly-A RNA controls were used to monitor the entire target labeling process. The GeneChip Poly-A RNA Control Kit (Affymetrix; P/N 900433) contained a pre-synthesized mixture of *lys*, *phe*, *thr*, and *dap* from *Bacillus subtilis*. The final concentrations of the controls, relative to the total RNA population, were  $1:1 \times 10^6$ ,  $1:5 \times 10^4$ ,  $1:2.5 \times 10^4$ ,  $1:7.5 \times 10^3$ , respectively. Biotin-labeled cRNAs were used to evaluate sample hybridization efficiency on the microarrays. The GeneChip Eukaryotic Hybridization Control Kit (Affymetrix; P/N 900299 and 900362) contained 20 $\times$  eukaryotic hybridization controls that were composed of a mixture of biotin-labeled cRNA transcripts of *bioB*, *bioC*, *bioD*, and *cre*, prepared in staggered concentrations (1.5, 5, 25, and 100 pM final concentrations for *bioB*, *bioC*, *bioD*, and *cre*, respectively). The 20 $\times$  controls were spiked into the hybridization cocktail independent of RNA sample.

## 2.3. Data analysis

Data analysis was performed as described (Rajagopalan, 2003) using the Affymetrix Microarray Suite software (version 5.0, Affymetrix) and GeneSpring software (version 7.1; Tomy Digital Biology, Tokyo, Japan). In brief, the hybridization efficiencies were equalized by median value of the control probe set to each array, and the genes with higher signal intensities than *bioB* were selected for further analysis.

The microarrays are divided into several hundred thousand probe cells grouped in pairs, perfect match (PM) and mis-match (MM) cells. Therefore, detection cells were made on the basis of a discrimination score,  $R_i$  which was defined for each probe pair as  $R_i = (PM_i - MM_i)/(PM_i + MM_i)$ , where  $PM_i$  and  $MM_i$  were the intensity of the perfect match and mis-match cells of probe pair  $i$ , respectively.

To assess the extent of variation accumulated during sample preparation, hybridization, and scanning procedures, raw intensity values from two different probe chip arrays were plotted against each other on a log scatter plot: the intensity of tension-free HPLF on the horizontal axis; that of tension-loaded HPLF, at 0.5, 1.0, 2.0 or 16 h, on the vertical axis. To confirm the microarray data, real-time reverse transcription-polymerase reaction (RT-PCR) was performed as described below for randomly selected genes.

Global normalization was performed for data obtained from the raw data. The normalized data were analyzed statistically by one-way ANOVA

( $p < 0.05$ ) and *K*-means clustering methods ( $n = 8$ ). The functional annotation of the CT genes were examined using the Agilent Databases (Agilent Technologies, Palo Alto, CA) and the Affymetrix Databases (<http://www.affymetrix.com/analysis/netaffx/xmlquery.affx>). The CT genes were classified into categories based on the biological process in the GeneSpring Gene Ontology (Agilent).

Ingenuity Systems' Pathways Knowledge Base (version 3.0: Winter'04 Release containing 20,000 genes; Ingenuity Systems, Mountain View, CA) was used to search for cellular pathways affected by cyclic tension. A detailed description of ingenuity pathways analysis (IPA) can be found on <http://www.ingenuity.com>. Data sets containing CT genes accession numbers and their corresponding expression fold-change values were imported into IPA software. Focus genes identified by the IPA program were categorized based on location, cellular components, and reported biochemical, biologic, and molecular functions using the software. The program queried the Ingenuity Systems' Pathways Knowledge Base for interactions between the focus genes and all other gene objects stored in the knowledge base, and generated a set of networks ranked by score. The score is the negative log of a  $p$  value and indicates the likelihood of the focus genes being found in the networks due to random chance. A score of 3 indicates that there is a 1/1000 chance that the focus genes are in a network due solely to chance. Therefore, scores of 3 or higher represent a 99.9% confidence level. Biological functions were then calculated and assigned to each network.

#### 2.4. Phalloidin staining

Static HPLF were cultured and either treated with 1  $\mu\text{M}$  Y27632 or treated with solvent alone (Cat. 688000; CALBIOCHEM, San Diego, CA) for 1, 2, 8 or 16 h. To detect F-actin fibers, HPLF were fixed with 3.7% formaldehyde, washed twice with PBS (pH 7.2) supplemented with 0.5% Triton X-100, and treated with 5 mg/ml of Texas Red-X phalloidin (Cat. T-7471; Molecular Probes) for 2 h. Staining signals were visualized using a fluorescence microscope (BX50; Olympus, Tokyo, Japan), and images captured with a digital camera (DP70; Olympus).

#### 2.5. Quantitative mRNA analysis of HPLF treated with Y27632

HPLF from a donor (24-year-old female) were pre-incubated with or without Y27632 for 1 h, and loaded with cyclic tension for different periods (0, 0.5,

1.0, 2.0 or 16 h). We randomly selected several CT genes in a merged genetic network, and performed real-time RT-PCR analysis. One microgram of total RNA was recovered from the tension-loaded and tension-free HPLF, and reverse-transcribed with oligo (dT)<sub>12–18</sub> primer, dNTPs, and SuperScript II (all from Invitrogen) in a total volume of 20  $\mu\text{l}$ . One microliter of this reaction was mixed with QuantiTect SYBR Green PCR Master Mix (Qiagen) and the gene-specific primers designed by Primer3 ([http://frodo.wi.mit.edu/cgi-bin/primer3/primer3\\_www.cgi](http://frodo.wi.mit.edu/cgi-bin/primer3/primer3_www.cgi)). Real-time RT-PCR was performed using the DNA Engine Opticon 2 (Bio-Rad, Hercules, CA) according to the manufacturer's instructions. The amplification conditions consisted of an initial 15 min denaturation step at 95 °C, followed by 40 cycles of denaturation at 94 °C for 15 s, annealing at 55 °C for 30 s, and elongation at 72 °C for 30 s. Four independent assays were performed for each gene. Relative expression was shown after normalization against the expression for  $\beta$ -actin mRNA. The data were analyzed statistically by Student's *t*-test. Values of  $p < 0.05$  were considered significant.

### 3. Results

#### 3.1. Identification and characterization of CT genes in HPLF

Microarray analysis was performed using HPLF subjected to cyclic tension for up to 16 h and control HPLF. A considerably higher number of transcripts exhibited signal intensities differing by >2-fold with tension-loaded versus control HPLF in the replicates. Each result was represented in log/log scatter plots to evaluate the consistency of the data. The microarray data was confirmed using real-time RT-PCR on randomly selected gene transcripts (data not shown).

We performed global normalization on the microarray data from all three donors, and identified 122 CT genes that had levels of expression significantly altered by the cyclic tension (Supplementary-1). To visualize the overall response to cyclic tension, kinetic patterns of the CT transcripts were analyzed with the *K*-means clustering method, and the all CT genes were assigned to eight clusters (Fig. 1, Supplementary-1). The clusters 2, 5, 6 and 7 included tension-induced genes while the clusters 3 and 4 included tension-suppressed genes. As a functional classification of CT genes, a list of seven different categories was established based on GeneSpring Database (Supplementary-2). All clusters included genes that could be included in two categories: intracellular signaling and cell growth/maintenance.

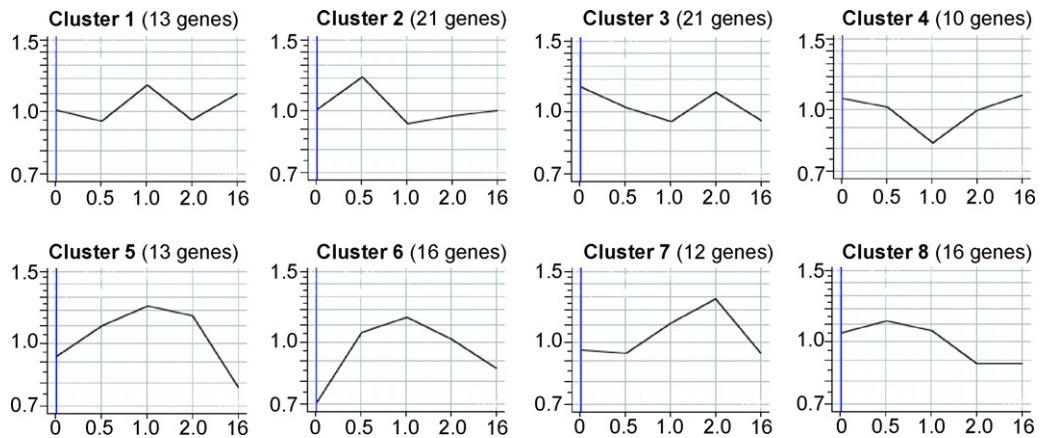


Fig. 1. *K*-means clustering of CT genes. The 122 CT genes were assigned to 8 clusters by applying *K*-means methods. Each cluster is represented by the centroid (average pattern) of the kinetics. The number of clusters and assigned genes is indicated on the top of each kinetic graph. The *x* axis represents application periods of cyclic tension (0, 0.5, 1.0, 2.0, or 16 h), and the *y* axis represents the expression value, indicated after global normalization, in logarithmical scale.

Both of these categories are composed of fundamental biological processes such as metabolism, biogenesis, cell cycle, cell growth, and cell death.

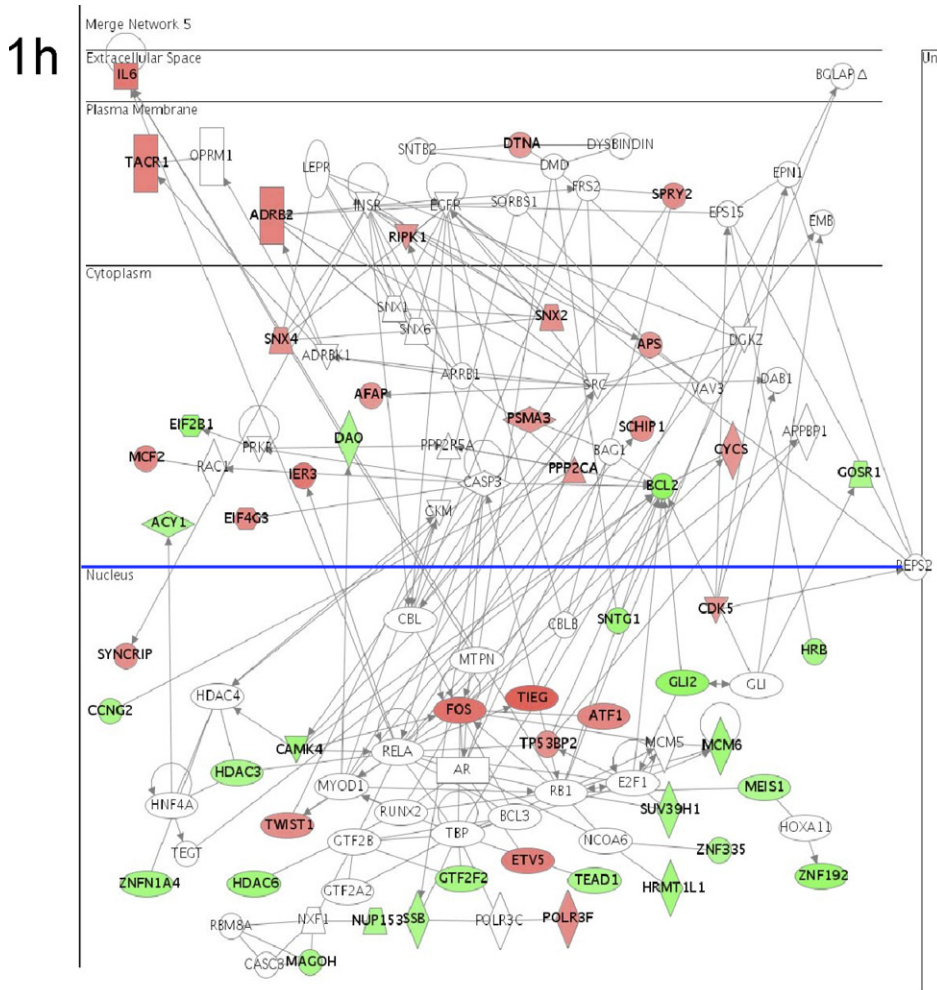
### 3.2. Identification of genetic networks affected by cyclic tension on HPLF

To examine how CT genes interact through perturbed biological networks, we performed network analysis on CT genes using Ingenuity Pathway Analysis (IPA). IPA provides a tool to construct and extract relevant information from the microarray analysis, and integrates individual genes. Of the 122 CT genes, 63 were mapped to genetic networks defined by IPA. These networks describe functional relationships among gene products based on findings presented in peer-reviewed scientific publications. IPA associated these networks with known biological pathways, and identified as significant 24 networks. Notably, the top 4 genetic networks with a score of 10 or higher and containing 10 or more focus genes represent the extensive interrelation and interaction between the genes affected by cyclic tension, which regulate unique biological processes (Table 1). Since overlapping genes were not detected in network-4, three networks were merged to form a major network containing 50 focus genes regulating cell death, cellular assembly and organization, and cellular function and maintenance (Table 1, Fig. 2, Supplementary-3). The merged network included key mediators, such as *B-cell CLL/lymphoma 2* (BCL2) and *v-fos FBJ murine osteosarcoma viral oncogene homolog* (FOS). For a better understanding of the temporal and spatial gene expression in response to mechanotransduction, we per-

formed sequential analysis using the merged pathway (Fig. 2, Supplementary-3). The analysis revealed that the cyclic tension induced a transient and self-limiting response based on alterations in RNA abundance and functional subcellular localization. After 0.5 h of cyclic tension, all nuclear transcription factors were down-regulated except FOS, which reached a maximum level as an early responsive gene. The nuclear transcription factors such as *tumor protein p53 binding protein 2* (TP53BP2), and *TGF $\beta$  inducible early growth response* (TIEG), and extra-nucleic molecules such as *adrenergic receptor  $\beta$ 2* (ADRB2) and *immediate early response* (IER3) were up-regulated 1–2 h after cyclic tension, apparently a critical event to adapt to external changes resulting from mechanical stress (Fig. 2, Supplementary-3). After 16 h of cyclic tension, the cells subjected to mechanotransduction returned to homeostasis (0 h). We identified correlations among these results through the use of the *K*-means cluster (Fig. 1). While early responsive genes, FOS and BCL2 were categorized in cluster 2, all 14 tension-suppressed genes were localized in the nucleus and categorized in cluster 3 or 4. Clusters 5, 6 and 7 included 15 tension-induced genes that were mainly localized outside the nucleus (Fig. 3).

### 3.3. Effect of Rho/ROCK pathway on CT gene expression in HPLF

To examine how the Rho/ROCK pathway participates in regulating mechanotransduction in HPLF, we analyzed the kinetics of selected CT genes in the presence or absence of Y27632, a small-molecule inhibitor of ROCK activity (Uehata et al., 1997). It has been shown



**Node Shapes**

- ◇, enzyme    △, phosphatase    ▽, kinase    ◊, peptitase    ▱, transporter
- , G-protein coupled receptor    □, nuclear receptor    ○, transcription factor
- ⬡, translation factor    ○, transmembrane receptor    □, cytokine    ○, others

**Edge Types**

- binding only    ○→○ acts on

Fig. 2. Pathway analysis of focus CT genes involved in mechanotransduction. A prototypical pathway in a tension-loaded cell was constructed from 50 focus CT genes involved in mechanotransduction. Temporal and spatial changes of the expression of CT genes were analyzed at different time periods of cyclic tension (0, 0.5, 1.0, 2.0, or 16h), and the pathway after 1h of stressing was shown (see also [Supplementary-3](#)). Genes statistically increased from baseline are colored red while decreased are green. Bold genes were identified as CT genes by the microarray analysis, and are listed in [Table 1](#). Other genes were neither on the expression array nor significantly regulated. Abbreviations of these genes can be found in [Supplementary-4](#). (For interpretation of the references to color in this figure legend, the reader is referred to the web version of the article.)

Table 1  
Genetic networks affected by cyclic tension

Network ID	Focus genes <sup>a</sup>	Score <sup>b</sup>	Top functions
1	<b>ACY1</b> , <b>ADRB2</b> , APPBP1, AR, <b>ATF1</b> , BAG1, <b>BCL2</b> , <b>CAMK4</b> , CASP3, <b>CCNG2</b> , <b>CYCS</b> , <b>EIF2B1</b> , <b>EIF4G3</b> , EMB, <b>ETV5</b> , <b>FOS</b> , GLI, <b>GLI2</b> , <b>GOSR1</b> , <b>HDAC3</b> , HDAC4, HNF4A, <b>MCF2</b> , POLR3A, POLR3C, <b>POLR3F</b> , <b>PPP2CA</b> , PPP2R5A, PRKR, <b>PSMA3</b> , RAC1, <b>RIPK1</b> , <b>SSB</b> , <b>TP53BP2</b> , <b>ZNFN1A4</b>	35	Cancer, cell death, reproductive system disease
2	BGLAP, CASC3, CRADD, DGKZ, DMD, <b>DTNA</b> , DYSBINDIN, E2F1, GTF2A1, GTF2A2, GTF2B, <b>GTF2F2</b> , HOXA11, <b>HRMT1L1</b> , <b>IER3</b> , <b>IL6</b> , <b>MAGOH</b> , <b>MCM6</b> , <b>MEIS1</b> , MTPN, NCOA6, <b>NUP153</b> , NXF1, RB1, REL, RELA, SNTB2, <b>SNTG1</b> , <b>SUV39H1</b> , TBP, <b>TEAD1</b> , <b>TIEG</b> , <b>TP53BP2</b> , <b>ZNF192</b> , <b>ZNF335</b>	22	Viral function, gene expression, cellular assembly and organization
3	<b>ADRB2</b> , ADRBK1, <b>AFAP</b> , <b>APS</b> , ARRB1, CBL, CBLB, <b>CDK5</b> , CKM, DAB1, <b>DAO</b> , EGFR, EPN1, EPS15, FRS2, <b>HDAC6</b> , <b>HRB</b> , INSR, LEPR, MYOD1, OPRM1, REPS2, RUNX2, <b>SCHIP1</b> , SNX1, <b>SNX2</b> , <b>SNX4</b> , SNX6, SORBS1, <b>SPRY2</b> , SRC, <b>SYNCRIP</b> , <b>TACR1</b> , <b>TWIST1</b> , VAV3	18	Cellular function and maintenance, amino acid metabolism, developmental disorder
4	CD34, CDKN2B, CEBPA, <b>CENPE</b> , <b>CTNNA1</b> , CTNNB1, DDIT3, DUSP1, <b>DUSP6</b> , ELK1, <b>EXO1</b> , GJA1, GTF2I, JUP, MAPK1, MLH1, MSH2, MSH6, MYB, MYBL2, MYC, ORC1L, ORC2L, ORC3L, ORC4L, <b>ORC5L</b> , ORC6L, <b>PIGC</b> , <b>PKN2</b> , PMS2, <b>PTMA</b> , TNRC6, <b>TRIB1</b> , <b>YMEIL1</b> , <b>ZNF42</b>	13	Cell cycle, DNA replication, recombination, and repair, cancer

<sup>a</sup> Bold and underlined genes are those identified by the microarray analysis. The other genes are neither on microarray nor significantly regulated. See [Supplementary-4](#) for the abbreviations of genes.

<sup>b</sup> A score of >3 was considered significant ( $p < 0.001$ ).

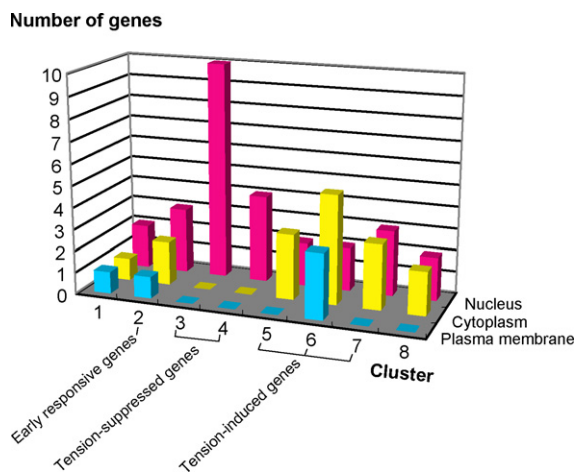


Fig. 3. Subcellular localization and *K*-means clustering of focus CT genes on IPA. Fifty focus CT genes in IPA were classified based on the subcellular localization and the *K*-means clustering. The *x* axis represents *K*-means clustering described in Fig. 1, and the *y* axis represents the number of classified genes. The early responsive genes are classified in cluster 2. The clusters 5, 6 and 7 included tension-induced genes while the clusters 3 and 4 included tension-suppressed genes. The subcellular localizations are indicated as follows: nucleus, red; cytoplasm, yellow; plasma membrane and extracellular space, blue. (For interpretation of the references to color in this figure legend, the reader is referred to the web version of the article.)

that ROCK promotes both actin–myosin contraction and actin polymerization (Kimura et al., 1996; Maekawa et al., 1999). Thus, we first examined the effect of Y27632 on polymeric (F) actin, the dominant structural constituent of the cell cortex in static HPLF. Phalloidin staining revealed that F-actin fibers appeared thinner and less dense in HPLF treated with Y27632 for 1 h, whereas the dense fibers were observed clearly in HPLF without Y27632 treatment (Fig. 4). The similar results were also observed in HPLF following treatment with Y27632 for 16 h (data not shown). These findings indicated that inactivation of ROCK led to loss of stress fibers, and ROCK activity was necessary for controlling actin cytoskeleton organization in HPLF.

To examine the alteration of CT genes by Y27632, we randomly selected 8 CT genes from the merged network (Fig. 2, [Supplementary-3](#)), and performed real-time RT-PCR analysis on the tension-loaded HPLF cultured with or without Y27632 (Fig. 5). Y27632 effectively inhibited the tension-induced *aminoacylase 1* (*ACY1*) genes expression, and also maintained the basal expression levels of tension-suppressed *activating transcription factor 1* (*ATF1*) and *golgi SNAP receptor complex member 1* (*GOSR1*) genes. However, Y27632 did not significantly alter the other tension-induced genes; *TP53BP2*, *ADRB2*, *BCL2*, *FOS*, and *caspase 3* (*CASP3*). These results suggested that mechanotransduction in HPLF

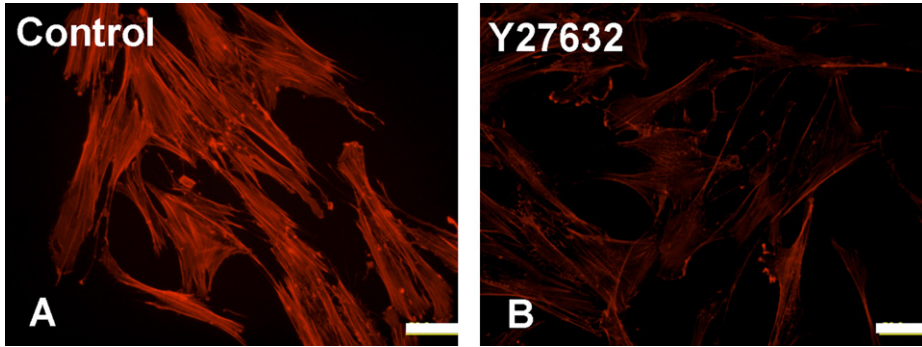


Fig. 4. Effect of Y27632 on development of actin fibers in HPLF. F-actin was stained with Texas Red-X phalloidin. Static HPLF treated with Y27632 exhibited faint F-actin fibers (B) whereas control HPLF had dense F-actin fibers (A). Three independent experiments were performed, and a typical set of results is shown. Bar equals 10 µm.

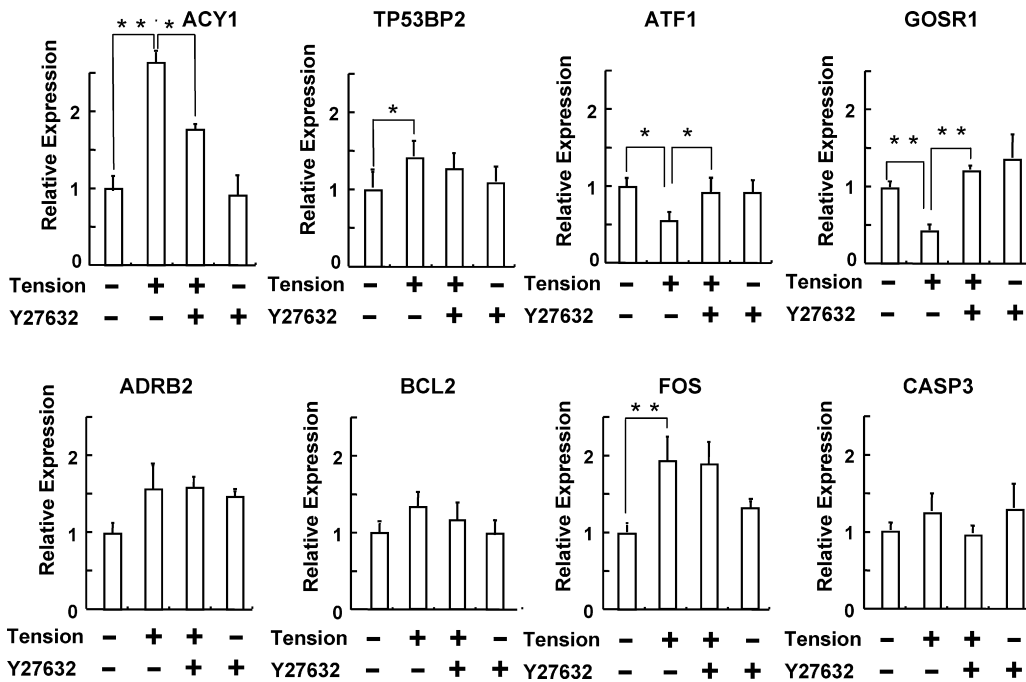


Fig. 5. Effect of Y27632 on mRNA expression of CT genes in HPLF. Real-time RT-PCR was performed using HPLF mRNA after 0.5–2 h of cyclic tension. The relative expression was valued against  $\beta$ -actin expression as a fold increase. The data were analyzed statistically using Student's *t*-test (\* $p$ <0.05; \*\* $p$ <0.01). Error bars indicate standard deviation of three independent assays for each gene. Abbreviations of these genes and PCR primer sequence can be found in Supplementary-4 and -5.

includes both Rho/ROCK-dependent and Rho/ROCK-independent pathways, and the alternative pathway may compensate for the effect of the Rho/ROCK pathway on CT gene expression.

#### 4. Discussion

In this study, we have identified 122 CT genes from HPLF using Human Genome Focus GeneChip probe array (Affymetrix). Recently, shear stress-responsive genes have been examined in human umbilical vein

endothelial cells (HUVECs) and coronary artery endothelial cells (HCAECs) using HuGene FL array (Affymetrix) (Ohura et al., 2003). In addition, ultraviolet (UV) radiation-induced genes have been detected in human skin fibroblasts using HGU95Av2 arrays (Affymetrix) (Gentile, Latonen, & Laiho, 2003). The distributions of their variability are similar to ours, suggesting that both UV radiation and cyclic tension forces are moderate to elicit changes in the gene expression in the fibroblasts. Although the HuGene FL and HGU95Av2 arrays cover 39 and 70% of the 122 CT

genes, respectively, none of the CT genes were found in the sets of either the shear stress-responsive genes, or the UV radiation-induced genes. These findings suggest that changes in fibroblast gene expression may be quite dependent on the specific type of stress.

In previous studies, 50–100 N forces were generally used as an occlusal loading (Holmes, Diaz-Arnold, & Leary, 1996; Southard, Behrens, & Tolley, 1989) probably because similar vertical forces have been measured during chewing movements in several in vivo studies (Proffit, Fields, & Nixon, 1983; Richter, 1995). The model, which is loaded with a vertical load of 100 N on the lower pre-molar, mimicks the effect of a moderate orthodontic force with the stresses across periodontal ligament within 40 kPa (Toms & Eberhart, 2003). In the present study, we applied cyclic tension at 36 kPa to the flexible-bottomed culture plates using the Flexercell Strain Unit, thus the magnitude of cyclic tension in our study is distributed within the physiological range. The application of moderate orthodontic force causes bone resorption, while the application of excessive orthodontic force results in excessive compressive force, which induces local ischemia, tissue hyalinization, and cell death in the periodontal ligament (Reitan & Rygh, 1994). In a concerted remodeling process, it is the right balance between death and renewal that decides between health and disease. Although it seems to vary in different cell types, one of candidates that modulate mechanical stress-induced apoptosis is caspase-3 (CASP3) (Earnshaw, Martins, & Kaufmann, 1999). However, cyclic tension did not significantly alter CASP3 expression in our model. This is further evidence that the cyclic tension applied mimicks physiological force.

The number of genes with altered expression may reflect the complexity of the biologic response to mechanical loading, and provide guidance in investigating the intricate processes that take place in mechanically stress-loaded cells. Therefore, the 122 CT genes were classified into seven functional categories based on the GeneSpring Database, and their expression patterns were assigned into eight clusters by the *K*-means clustering methods. As expected, most of CT genes are involved in various kinds of intra- and intercellular signaling mechanisms. The functional analysis and clustering of individual CT genes provides a means to assess overall changes and characterizations however this approach provides fewer insights into specific biological processes and signaling networks directly responsive to cyclic tension. Thus, we performed network analysis on CT genes using IPA, and sequential analysis using the network and the *K*-means clustering. We found that mechanotransduction in HPLF initiates induction of the early

responsive genes, FOS and BCL2 while other transcription factors were suppressed after 0.5 h of cyclic tension. FOS is thought to have an important role in signal transduction, cell proliferation and differentiation, and bone development (Johnson, Spiegelman, & Papaioannou, 1992; Wang et al., 1992). The role of FOS during mechanotransduction has been extensively described in bone, and those studies showed that mechanically induced bone formation is preceded by expression of FOS (Iqbal & Zaidi, 2005; Pavalko et al., 1998; Sadoshima, Takahashi, Jahn, & Izumo, 1992). Our study also confirmed that FOS is a key mediator of mechanotransduction in HPLF exposed to cyclic tension. FOS expression may initiate HPLF differentiation to regenerate periodontal ligament and surrounding hard tissues. It has been reported that BCL2 negatively regulates both apoptosis and autophagy, which is critical in tissue homeostasis, development and disease (Hockenbery, Nunez, Milliman, Schreiber, & Korsmeyer, 1990; Pattingre et al., 2005). In HPLF, the immediate expression of apoptosis-preventing BCL2 by cyclic tension may be involved in the control of cell viability.

Following the induction of early responsive genes, intra- and extra-nuclear molecules, such as TP53BP2, TIEG, ADRB2 and IER3 were up-regulated 1–2 h after cyclic tension. TP53BP2 was identified as an interacting protein with p53, BCL2 and nuclear factor  $\kappa$ B (NF- $\kappa$ B) (Iwabuchi, Bartel, Li, Marraccino, & Fields, 1994; Naumovski & Cleary, 1996; Yang et al., 1999). TP53BP2 interacts with p53 to activate proapoptotic events, and involvement in various biological processes such as carcinogenesis has been shown (Mori, Okamoto, Takahashi, Ueda, & Okamoto, 2000). Interestingly, IER3 is an apoptosis inhibitor involved in NF- $\kappa$ B-mediated cell survival (Wu, Ao, Prasad, Wu, & Schlossman, 1998), and BCL2 and IER3 have been reported to prevent the TP53BP2 mediated apoptosis (Takahashi et al., 2005). Thus, selective actions of TP53BP2 with BCL2, IER3 and NF- $\kappa$ B may determine the susceptibility of cells to triggering the apoptotic pathway in response to external force. The physiologic roles of ADRB2 and TIEG have been proposed by characterizing genetically modified mouse models (Eleftheriou et al., 2005; Subramaniam et al., 2005). The *Adrb2*-deficient mice showed that the sympathetic nervous system favors bone resorption by increasing expression in osteoblast progenitor cells of the osteoclast differentiation factor, *receptor activator of NF- $\kappa$ B ligand* (*Rankl*). On the other hand, the analysis of *Tieg*-deficient osteoblasts revealed that TIEG expression is critical for both osteoblast-mediated mineralization and osteoblast support of osteoclast differentiation. Thus, ADRB2 and TIEG may

be crucial molecules in HPLF for regulation of bone homeostasis.

Inhibition assays using Y27632 revealed that static HPLF failed to develop stress fibers as visualized by F-actin staining. Y27632 inhibits two isoforms of a serine/threonine kinase, termed ROCK-I and II, although Y27632 is not completely specific for these kinases it has a strong negative impact on ROCK-induced cellular functions (Davies, Reddy, & Caivano, 2000; Rottner, Hall, & Small, 1999). It has been recognized that inactivation of ROCKs (or ROCK-I) causes a loss of stress fibers and focal adhesion (Riento & Ridley, 2003; Yoneda, Multhaupt, & Couchman, 2005), and Rho/ROCK-dependent cytoskeletal reorganization has been reported in various cells and tissues. However inactivation of the Rho/ROCK axis has different effects on cell behavior, such as differentiation, apoptosis or tumorigenesis (Hakuma et al., 2005; McBeath, Pirone, Nelson, Bhadriraju, & Chen, 2004; Svoboda, Moessner, Field, & Acevedo, 2004), depending on the cell context and cell type analyzed. Thus, Rho/ROCK might to be included in several groups of signaling molecules that may regulate the variety of downstream signals controlling the phenotypic changes in the cells, which need to be further examined in HPLF. It has been reported that Y27632 potently stimulated bone morphogenetic protein (BMP)-2/4 expression, osteoblast differentiation, and bone nodule formation (Harmey, Stenbeck, Nobes, Lax, & Grigoriadis, 2004), suggesting a possible mechanism for bone metabolism involving periodontal ligament cells and osteocytes regulated by Rho/ROCK.

Y27632 selectively altered some CT gene expression such as ACY1, ATF1, GOSR1 however Y27632 exposure did not significantly alter the expression of other CT genes. It has been reported that the mammalian homologue of *Drosophila Diaphanous* protein 1 (Dia1) is also a crucial downstream target of Rho, that regulates actin polymerization and microtubule organization (Ishizaki et al., 2001; Palazzo, Cook, Alberts, & Gundersen, 2001). Among multiple Rho targets, it has been described that the combined action of ROCK and Dia1 are sufficient to substitute for active Rho in the process of mechanotransduction (Watanabe, Kato, Fujita, Ishizaki, & Narumiya, 1999), moreover the growth of focal adhesions can be achieved when mechanical force is applied even if ROCK activity is suppressed by Y27632 (Geiger & Bershadsky, 2001; Riveline et al., 2001). Thus, there is a possibility that the Rho–ROCK pathway can be bypassed if tension is applied externally, and that Dia1 could partially compensate for the cellular response to mechanotransduction in HPLF when ROCK is inactive (Fig. 6). Fos induced-Rho/ROCK-independent pathways

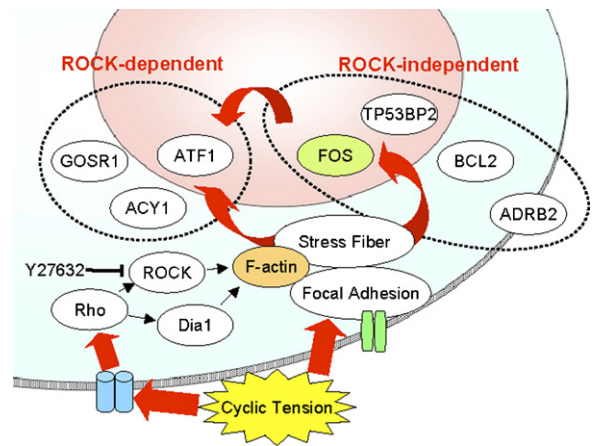


Fig. 6. Schematic representation of CT genes expression. Cyclic tension-induced focal adhesion, stress fibers and CT genes expression are mediated by activation of Rho-Dia1 or Rho–ROCK that is inhibited by Y27632. Early responsive gene, FOS expression is increased when cyclic tension is applied even if ROCK activity is suppressed by Y27632. Y27632 does not alter TP53BP2, ADRB2, and BCL2 (ROCK-independent) genes expression as well, while Y27632 effectively recover ACY1, ATF1, and GOSR1 (ROCK-dependent) genes expression to the basal level. Dia1 might partially compensate mechanotransduction in HPLF when ROCK is inactive. Rho, Ras-homolog of small GTPase; ROCK, Rho-associated kinases; Dia1, mammalian homologue of *Drosophila Diaphanous* protein 1. Abbreviations of CT genes can be found in Supplementary-4.

may tightly control HPLF survival through regulation of BCL2, TP53BP2 or IER3, and bone remodeling by ADRB2 or TIEG. To clarify these signaling pathways regulating CT gene expression, we need to further examine the kinetics of mRNA expression and phenotypes of ROCK- or *Dia1*-knockdown HPLF in the next study.

In conclusion, oligonucleotide array analysis revealed that 122 CT genes had significantly altered levels of expression in tension-loaded HPLF, and that typical kinetic patterns and functional classifications existed for the CT genes. By combining the *K*-means cluster and IPA, we found temporal and spatial alterations of CT gene expression, and the presence of several signaling pathways likely responsible for controlling the response in HPLF mechanotransduction. Some of these pathways were not dependent on Rho–ROCK activity, and thus the overall response may be compensated by other signaling pathways. The complex regulation of mechanotransduction in HPLF needs to be further analyzed to allow application of these findings to control the regeneration of periodontal ligament.

## Acknowledgements

This study was supported by a Grant-in-Aid for Scientific Research B (No. 14370710 to ST), a Grant-

in-Aid for Scientific Research A (Nos. 16209056 and 18209057), a Grant-in-Aid for Scientific Research B (No. 17390562 to FN), a Grant-in-Aid for Scientific Research C (No. 17591991 to HA), and a Grant-in-Aid for Scientific Research A1 (No. 16209063 to YA) from the Japan Society for the Promotion of Science, Kobayashi Magobe Memorial Foundation, Ryobi Teien Foundation, and Inamori Foundation (FM), and Suzuken Memorial Foundation (ST). We would like to thank Dr. Charles F. Shuler, Director of Center for Craniofacial Molecular Biology, University of Southern California, for reviewing the manuscript.

## Appendix A. Supplementary data

Supplementary data associated with this article can be found, in the online version, at doi:10.1016/j.biocel.2007.01.015.

## References

- Abeyta, M. J., Clark, A. T., Rodriguez, R. T., Bodnar, M. S., Pera, R. A. R., & Firpo, M. T. (2004). Unique gene expression signatures of independently-derived human embryonic stem cell lines. *Human Molecular Genetics*, *13*, 601–608.
- Amano, M., Chihara, K., Kimura, K., Fukata, Y., Nakamura, N., Matsuura, Y., et al. (1997). Formation of actin stress fibers and focal adhesions enhanced by Rho-kinase. *Science*, *275*, 1308–1311.
- Banes, A. J., Link, G. W., Gilbert, J. W., Tay, R. T. S., & Monbureau, O. (1990). Culturing cells in a mechanically activate environment. *American Biotechnology Laboratory*, *8*, 12–22.
- Calvano, S. E., Xiao, W., Richards, D. R., Felciano, R. M., Baker, H. V., Cho, R. J., et al. (2005). A network-based analysis of systemic inflammation in humans. *Nature*, *437*, 1032–1037.
- Chicurel, M. E., Chen, C. S., & Ingber, D. E. (1998). Cellular control lies in the balance of forces. *Current Opinion in Cell Biology*, *10*, 232–239.
- Chiquet, M., Renedo, A. S., Huber, F., & Fluck, M. (2003). How do fibroblasts translate mechanical signals into changes in extracellular matrix production? *Matrix Biology*, *22*, 73–80.
- Davies, S. P., Reddy, H., & Caivano, M. (2000). Specificity and mechanism of action of some commonly used protein kinase inhibitors. *Biochemical Journal*, *351*, 95–105.
- Earnshaw, W. C., Martins, L. M., & Kaufmann, S. H. (1999). Mammalian caspases: Structure, activation, substrates, and functions during apoptosis. *Annual Review of Biochemistry*, *68*, 383–424.
- Eleftheriou, F., Ahn, J. D., Takeda, S., Starbuck, M., Yang, X., Liu, X., et al. (2005). Leptin regulation of bone resorption by the sympathetic nervous system and CART. *Nature*, *434*, 514–520.
- Etienne-Manneville, S., & Hall, A. (2002). Rho GTPases in cell biology. *Nature*, *420*, 629–635.
- Geiger, B., & Bershadsky, A. (2001). Assembly and mechanosensory function of focal contacts. *Current Opinion in Cell Biology*, *13*, 584–592.
- Gentile, M., Latonen, L., & Laiho, M. (2003). Cell cycle arrest and apoptosis provoked by UV radiation-induced DNA damage are transcriptionally highly divergent responses. *Nucleic Acids Research*, *31*, 4779–4790.
- Hakuma, N., Kinoshita, I., Shimizu, Y., Yamazaki, K., Yoshida, K., Nishimura, M., et al. (2005). E1A/PEA3 activates the Rho/Rho-associated kinase pathway to increase the malignancy potential of non-small-cell lung cancer cells. *Cancer Research*, *65*, 10776–10782.
- Harmey, D., Stenbeck, G., Nobes, C. D., Lax, A. J., & Grigoriadis, A. E. (2004). Regulation of osteoblast differentiation by *Pasteurella Multocida* toxin (PMT): A role for Rho GTPase in bone formation. *Journal of Bone and Mineral Research*, *19*, 661–670.
- Hiratsuka, K., Kamino, Y., Nagata, T., Takahashi, Y., Asai, S., Ishikawa, K., et al. (2002). Microarray analysis of gene expression changes in aging in mouse submandibular gland. *Journal of Dental Research*, *81*, 679–682.
- Hockenbery, D., Nunez, G., Milliman, C., Schreiber, R. D., & Korsmeyer, S. J. (1990). Bcl-2 is an inner mitochondrial membrane protein that blocks programmed cell death. *Nature*, *348*, 334–336.
- Holmes, D. C., Diaz-Arnold, A. M., & Leary, J. M. (1996). Influence of post dimension on stress distribution in dentin. *The Journal of Prosthetic Dentistry*, *75*, 140–147.
- Ingber, D. E. (1997). Tensegrity: The architectural basis of cellular mechanotransduction. *Annual Review of Physiology*, *59*, 575–599.
- Ingber, D. E. (2003). Mechanobiology and diseases of mechanotransduction. *Annals of Medicine*, *35*, 564–577.
- Iqbal, J., & Zaidi, M. (2005). Molecular regulation of mechanotransduction. *Biochemical and Biophysical Research Communications*, *328*, 751–755.
- Ishizaki, T., Morishima, Y., Okamoto, M., Furuyashiki, T., Kato, T., & Narumiya, S. (2001). Coordination of microtubules and the actin cytoskeleton by the Rho effector mDia1. *Nature Cell Biology*, *3*, 8–14.
- Iwabuchi, K., Bartel, P. L., Li, B., Marraccino, R., & Fields, S. (1994). Two cellular proteins that bind to wild-type but not mutant p53. *Proceedings of the National Academy of Science of the United States of America*, *91*, 6098–6102.
- Johnson, R. S., Spiegelman, B. M., & Papaioannou, V. (1992). Pleiotropic effects of a null mutation in the *c-fos* proto-oncogene. *Cell*, *71*, 577–586.
- Kasamatsu, A., Endo, Y., Uzawa, K., Nakashima, D., Koike, H., Hashitani, S., et al. (2005). Identification of candidate genes associated with salivary adenoid cystic carcinomas using combined comparative genomic hybridization and oligonucleotide microarray analysis. *International Journal of Biochemistry & Cell Biology*, *37*, 1869–1880.
- Khan, S., & Sheetz, M. P. (1997). Force effects on biochemical kinetics. *Annual Review of Biochemistry*, *66*, 785–805.
- Kimura, K., Ito, M., Amano, M., Chihara, K., Fukata, Y., Nakafuku, M., et al. (1996). Regulation of myosin phosphatase by Rho and Rho-associated kinase (Rho-kinase). *Science*, *273*, 245–248.
- Kletsas, D., Basdra, E. K., & Papavassiliou, A. G. (2002). Effect of protein kinase inhibitors on the stretch-elicited *c-Fos* and *c-Jun* up-regulation in human PDL osteoblast-like cells. *Journal of Cellular Physiology*, *190*, 313–321.
- Maekawa, M., Ishizaki, T., Boku, S., Watanabe, N., Fujita, A., Iwamatsu, A., et al. (1999). Signaling from Rho to the actin cytoskeleton through protein kinases ROCK and LIM-kinase. *Science*, *285*, 895–898.
- McBeath, R., Pirone, D. M., Nelson, C. M., Bhadriraju, K., & Chen, C. S. (2004). Cell shape, cytoskeletal tension, and RhoA regulate stem cell lineage commitment. *Developmental Cell*, *6*, 483–495.
- McCulloch, C. A., Lekic, P., & McKee, M. D. (2000). Role of physical forces in regulating the form and function of the periodontal ligament. *Periodontology 2000*, *24*, 56–72.

- Mori, T., Okamoto, H., Takahashi, N., Ueda, R., & Okamoto, T. (2000). Aberrant overexpression of 53BP2 mRNA in lung cancer cell lines. *FEBS Letters*, *465*, 124–128.
- Myokai, F., Oyama, M., Nishimura, F., Ohira, T., Yamamoto, T., Arai, H., et al. (2003). Unique genes induced by mechanical stress in periodontal ligament cells. *Journal of Periodontal Research*, *38*, 255–261.
- Naumovski, L., & Cleary, M. L. (1996). The p53-binding protein 53BP2 also interacts with Bcl2 and impedes cell cycle progression at G2/M. *Molecular and Cellular Biology*, *16*, 3884–3892.
- Numaguchi, K., Eguchi, S., Yamakawa, T., Motley, E. D., & Inagami, T. (1999). Mechanotransduction of rat aortic vascular smooth muscle cells requires RhoA and intact actin filaments. *Circulation Research*, *85*, 5–11.
- Ohura, N., Yamamoto, K., Ichioka, S., Sokabe, T., Nakatsuka, H., Baba, A., et al. (2003). Global analysis of shear stress-responsive genes in vascular endothelial cells. *Journal of Atherosclerosis Thrombosis*, *10*, 304–313.
- Palazzo, A. F., Cook, T. A., Alberts, A. S., & Gundersen, G. G. (2001). mDia mediates Rho-regulated formation and orientation of stable microtubules. *Nature Cell Biology*, *3*, 723–729.
- Pattingre, S., Tassa, A., Qu, X., Garuti, R., Liang, X. H., Mizushima, N., et al. (2005). Bcl-2 antiapoptotic proteins inhibit Beclin 1-dependent autophagy. *Cell*, *122*, 927–939.
- Pavalko, F. M., Chen, N. X., Turner, C. H., Burr, D. B., Atkinson, S., Hsieh, Y. F., et al. (1998). Fluid shear-induced mechanical signaling in MC3T3-E1 osteoblasts requires cytoskeleton–integrin interactions. *American Journal of Physiology*, *275*, C1591–C1601.
- Proffit, W. R., Fields, H. W., & Nixon, W. L. (1983). Occlusal forces in normal and long face adults. *Journal of Dental Research*, *62*, 566–570.
- Rajagopalan, D. (2003). A comparison of statistical methods for analysis of high density oligonucleotide array data. *Bioinformatics*, *19*, 1469–1476.
- Reitan, K., & Rygh, P. (1994). Biomechanical principles and reactions. In T. H. Graber & R. L. Vanarsdall (Eds.), *Orthodontics, current principles and techniques* (pp. 96–192). Missouri: C.V. Mosby.
- Richter, E. J. (1995). In vivo vertical forces on implants. *International Journal of Oral & Maxillofacial Implants*, *10*, 99–108.
- Ridley, A. J., & Hall, A. (1992). The small GTP-binding protein rho regulates the assembly of focal adhesions and actin stress fibers in response to growth factors. *Cell*, *70*, 389–399.
- Riento, K., & Ridley, A. J. (2003). Rocks: Multifunctional kinases in cell behaviour. *Nature Reviews Molecular Cell Biology*, *4*, 446–456.
- Riveline, D., Zamir, E., Balaban, N. Q., Schwarz, U. S., Ishizaki, T., Narumiya, S., et al. (2001). Focal contacts as mechanosensors: Externally applied local mechanical force induces growth of focal contacts by an mDia1-dependent and ROCK-independent mechanism. *Journal Cell Biology*, *153*, 1175–1186.
- Rottner, K., Hall, A., & Small, J. V. (1999). Interplay between Rac and Rho in the control of substrate contact dynamics. *Current Biology*, *9*, 640–648.
- Sadoshima, J., Takahashi, T., Jahn, L., & Izumo, S. (1992). Roles of mechano-sensitive ion channels, cytoskeleton, and contractile activity in stretch-induced immediate-early gene expression and hypertrophy of cardiac myocytes. *Proceedings of the National Academy of Science of the United States of America*, *89*, 9905–9909.
- Seo, B. M., Miura, M., Gronthos, S., Bartold, P. M., Batouli, S., Brahimi, J., et al. (2004). Investigation of multipotent postnatal stem cells from human periodontal ligament. *Lancet*, *364*, 149–155.
- Southard, T. E., Behrents, R. G., & Tolley, E. A. (1989). The anterior component of occlusal force part 1. Measurement and distribution. *American Journal of Orthodontics and Dentofacial Orthopedics*, *96*, 493–500.
- Subramaniam, M., Gorny, G., Johnsen, S. A., Monroe, D. G., Evans, G. L., Fraser, D. G., et al. (2005). TIEG1 null mouse-derived osteoblasts are defective in mineralization and in support of osteoclast differentiation in vitro. *Molecular and Cellular Biology*, *25*, 1191–1199.
- Svoboda, K. K., Moessner, P., Field, T., & Acevedo, J. (2004). ROCK inhibitor (Y27632) increases apoptosis and disrupts the actin cortical mat in embryonic avian corneal epithelium. *Developmental Dynamics*, *229*, 579–590.
- Takahashi, N., Kobayashi, S., Kajino, S., Imai, K., Tomoda, K., Shimizu, S., et al. (2005). Inhibition of the 53BP2-mediated apoptosis by nuclear factor kappaB and Bcl-2 family proteins. *Genes to Cells*, *10*, 803–811.
- Toms, S. R., & Eberhart, A. W. (2003). A nonlinear finite element analysis of the periodontal ligament under orthodontic tooth loading. *American Journal of Orthodontics and Dentofacial Orthopedics*, *123*, 657–665.
- Uehata, M., Ishizaki, T., Satoh, H., Ono, T., Kawahara, T., Morishita, T., et al. (1997). Calcium sensitization of smooth muscle mediated by a Rho-associated protein kinase in hypertension. *Nature*, *389*, 990–994.
- Wang, N., Butler, J. P., & Ingber, D. E. (1993). Mechanotransduction across the cell surface and through the cytoskeleton. *Science*, *260*, 1124–1127.
- Wang, Z. Q., Ovitt, C., Grigoriadis, A. E., Mohle-Steinlein, U., Ruther, U., & Wagner, E. F. (1992). Bone and haematopoietic defects in mice lacking c-fos. *Nature*, *360*, 741–745.
- Watanabe, N., Kato, T., Fujita, A., Ishizaki, T., & Narumiya, S. (1999). Cooperation between mDia1 and ROCK in Rho-induced actin reorganization. *Nature Cell Biology*, *1*, 136–143.
- Wu, M. X., Ao, Z., Prasad, K. V., Wu, R., & Schlossman, S. F. (1998). IEX-1L, an apoptosis inhibitor involved in NF- $\kappa$ B mediated cell survival. *Science*, *281*, 998–1001.
- Yamamoto, T., Myokai, F., Nishimura, F., Ohira, T., Shiomi, N., Yamashiro, K., et al. (2003). Gene profiling in human periodontal ligament fibroblasts by subtractive hybridization. *Journal of Dental Research*, *82*, 643–647.
- Yang, J. P., Hori, M., Takahashi, N., Kawabe, T., Kato, H., & Okamoto, T. (1999). NF- $\kappa$ B subunit p65 binds to 53BP2 and inhibits cell death induced by 53BP2. *Oncogene*, *18*, 5177–5186.
- Yoneda, A., Multhaupt, H. A., & Couchman, J. R. (2005). The Rho kinases I and II regulate different aspects of myosin II activity. *Journal of Cell Biology*, *170*, 443–453.

# Microarray analysis of IL-1 $\beta$ -stimulated chemokine genes in synovial fibroblasts from human TMJ

Naomi Ogura<sup>1,2</sup>, Miwa Akutsu<sup>1</sup>, Makiko Tobe<sup>1,2</sup>, Hiroyuki Sakamaki<sup>1,2</sup>, Yoshimitsu Abiko<sup>2,3</sup>, Toshiro Kondoh<sup>1,2</sup>

<sup>1</sup>Department of Maxillofacial Surgery, Nihon University School of Dentistry at Matsudo, Chiba; <sup>2</sup>Research Institute of Oral Science, Nihon University School of Dentistry at Matsudo, Chiba; <sup>3</sup>Department of Biochemistry and Molecular Biology, Nihon University School of Dentistry at Matsudo, Chiba, Japan

**BACKGROUND:** Interleukin (IL)-1 $\beta$  is thought to play a key role in several pathologic conditions of the temporomandibular joint (TMJ). Gene expression profile of synovial fibroblasts stimulated with IL-1 $\beta$  was studied by oligonucleotide microarray analysis to elucidate candidate genes associated with intracapsular pathologic conditions of TMJ.

**METHODS:** RNA was isolated from synovial fibroblasts from five patients after IL-1 $\beta$  treatment. Gene expression profiling was performed with a GeneChip. Changes in gene expression were determined by comparing IL-1 $\beta$ -treated cells with untreated cells.

**RESULTS:** A total of 121 genes showed a greater than threefold difference in average intensity between untreated and IL-1 $\beta$ -treated synovial fibroblasts in five experiments. Five chemokines were among the 10 most upregulated genes, and the most upregulated gene was CCL20. The 121 IL-1 $\beta$ -responsive genes included 12 chemokines whose mRNA levels were confirmed by real-time PCR.

**CONCLUSION:** These data should provide useful information about the pathologic conditions of TMJ, especially in support of diagnosis and therapeutic approaches to TMJ.

*J Oral Pathol Med* (2007) 36: 223–8

**Keywords:** chemokine; interleukin-1 $\beta$ ; oligonucleotide microarray; synovial fibroblasts; temporomandibular joint

## Introduction

Synovitis, which often accompanies intracapsular pathologic conditions such as disk displacement (DD)/

internal derangement (ID) and osteoarthritis (OA) of the temporomandibular joint (TMJ), is characterized by chronic inflammatory changes, including hyperplasia of the synovial lining (1, 2), growth of small new blood vessels (1), and infiltration of inflammatory cells (1, 3–5). In addition, synovial cells produce a number of putative mediators of inflammation (6, 7).

Interleukin (IL)-1 $\beta$  is a proinflammatory cytokine that affects cell proliferation (8), inflammatory responses (9), and matrix remodeling (10). Elevated expression of IL-1 $\beta$  in the joint is known to result in activation of inflammatory and degradative pathways in synovial cells, which in turn contribute to the progression of rheumatoid arthritis (RA; 8, 11). Under pathologic conditions of the TMJ, levels of IL-1 $\beta$  are elevated in synovial fluids obtained from patients with OA and RA (12). Studies have also indicated that IL-1 $\beta$  in synovial fluid is associated with pain in the TMJ (13, 14). However, the involvement of synovial cells under pathologic conditions in the TMJ is poorly understood, as synovial cells have been difficult to cultivate in quantities sufficient for study.

Our group has isolated synovial cells from the human diseased TMJ and examined how regulation of IL-1 $\beta$  affects the underlying inflammatory status (15–17). We hypothesized that identification of IL-1 $\beta$ -responsive genes in synovial fibroblasts could help develop models for the inflammatory condition of the TMJ. However, obtaining an overview of the molecular and cellular responses of synovial fibroblasts to IL-1 $\beta$  has been difficult, in part because classic approaches for studying inflammatory factors have focused on identification and analysis of specific postulated factors on an individual basis. DNA microarray techniques have recently been developed to facilitate comprehensive expression analysis of large numbers of defined genes (18–20). Microarray analysis is an efficient method for exploring the functions of uncharacterized genes, as the expression pattern of uncharacterized genes can be compared with the expression pattern of characterized genes.

Correspondence: Toshiro Kondoh, Department of Maxillofacial Surgery, Nihon University School of Dentistry at Matsudo, 2-870-1, Sakaecho-Nishi, Matsudo, Chiba 271-8587, Japan. Tel: +81 47 360 9394, Fax: +81 47 360 9394, E-mail: kondo.toshiro@nihon-u.ac.jp  
Accepted for publication November 21, 2006

Microarray analysis can also be used to search for differentially expressed genes, which may include diagnostic and therapeutic markers.

In order to understand how IL-1 $\beta$  can induced the intracapsular pathologic condition of the TMJ, we examined the gene expression profiles of non-induced and IL-1 $\beta$ -induced synovial fibroblasts from the human TMJ using an oligonucleotide microarray approach.

## Materials and methods

### Cell culture

Human synovial tissue was obtained from five patients with ID who underwent arthroscopy of the TMJ (three females and two males; age range: 17–27 years). Patients gave complete informed consent for the surgery and for the use of their tissue in research. Isolation and primary cultures of synovial fibroblasts were performed according to the guidelines established by the Institutional Review Board of Nihon University School of Dentistry at Matsudo (EC03-003).

Synovial fibroblasts from the TMJ were prepared as previously described (15). For the experiments, we used synovial fibroblasts from the sixth to eighth passages.

### Total RNA extraction

Synovial fibroblasts were incubated with or without 1 unit/ml IL-1 $\beta$  for 4 h. Total cellular RNA from synovial fibroblasts (TMJ 1–5) was extracted using RNeasy kits (Qiagen, Valencia, CA, USA), and was then stored at  $-80^{\circ}\text{C}$  until used.

### GeneChip expression analysis

For gene expression profiling, we used the Affymetrix GeneChip Human Genome Focus Array (Affymetrix, Santa Clara, CA, USA) according to Affymetrix protocols. Briefly, double-stranded cDNA was generated from 7  $\mu\text{g}$  of total RNA using a T7-oligo (dT) primer and the Superscript Choice System kit (Invitrogen, Carlsbad, CA, USA). cDNA was then purified with a GeneChip Sample Clean-up Module (Affymetrix). Biotin-labeled cRNA was synthesized by *in vitro* transcription using the BioArray high-yield RNA transcript labeling system (ENZO, Farmingdale, NY, USA). cRNA was then purified using a GeneChip Sample Clean-up Module. Biotin-labeled cRNA was added to the fragmentation buffer (Affymetrix), and was heated for 35 min at  $95^{\circ}\text{C}$ . Fragmented cRNA (10  $\mu\text{g}$ ) was hybridized to the Human Genome Focus Array (8793 genes) for 16 h at  $45^{\circ}\text{C}$ . Arrays were subjected to washing and staining with R-phycoerythrin streptavidin (SAPE, Molecular Probes, Eugene, OR, USA) using GeneChip Fluidics Station 400 (Affymetrix).

In order to amplify the signals, the arrays were further stained with goat biotinylated antistreptavidin antibody (Vector Laboratories, Burlingame, CA, USA), followed by SAPE. After scanning (scanner from Affymetrix), the oligonucleotide hybridization data were exported for gene expression value analysis using AFFYMETRIX MICROARRAY SUITE (version 5.0). The hybridization intensity for each gene was calculated with a probe set containing

24 specific probes for perfect matches and mismatches. The expression of each gene was also categorized as 'present', 'absent', or 'marginal'. For quality control, cRNA samples were hybridized to the test microarray chip (Test 3; Affymetrix) in order to ensure equal hybridization to 5'- and 3'-oligonucleotides of the genes chosen for standardization (GAPDH and  $\beta$ -actin) before hybridization with Focus Array.

### Data analysis

Raw data from 10 GeneChips were loaded into GENESPRING software (version 6.2; Agilent Technologies, Waldbronn, Germany). Data were normalized using the median raw data from each array as a reference. Changes in gene expression were determined by comparing controls (average normalized intensity of untreated cells) with IL-1 $\beta$  treatment (average normalized intensity of IL-1 $\beta$ -treated cells).

### Real-time PCR

cDNA was synthesized using a GeneAmp RNA PCR kit (Perkin-Elmer, Norwalk, CT, USA). Real-time PCR was performed using a DyNAmo SYBR Green qPCR kit (Finnzymes, Espoo, Finland). The PCR mixture contained 20 pmol of forward and reverse primers and 2  $\mu\text{l}$  of cDNA. Amplification was performed using a DNA Engine Opticon 1 (MJ Research, San Francisco, CA, USA), with pre-heating at  $95^{\circ}\text{C}$  for 10 min, followed by 40 cycles of  $94^{\circ}\text{C}$  for 15 s,  $57^{\circ}\text{C}$  for 30 s, and  $72^{\circ}\text{C}$  for 30 s. Amplicons were detected directly by measuring the increase in fluorescence caused by the binding of SYBR Green I dye to gene-specific, amplified, double-stranded DNA (SYBR fluorescence systems in real-time PCR can be used to semiquantitatively analyze mRNA expression with on-line monitoring). Following the completion of PCR amplification, the temperature was raised from the annealing temperature to  $95^{\circ}\text{C}$  for melting curve analysis.

The initial template concentration was derived from the cycle number at which the fluorescent signal crossed a threshold ( $C_T$ ) in the exponential phase of PCR. The number of transcripts was determined based on the threshold cycles of chemokines and GAPDH.  $\Delta C_T$  ( $C_T$ -chemokine minus  $C_T$ -GAPDH) indicates the relative amount of chemokine transcripts.  $\Delta\Delta C_T$  ( $\Delta C_T$ -treated minus  $\Delta C_T$ -control) represents the relative  $n$ -value compared with the control. The quantity  $2^{-n}$  represents the difference in chemokine expression between IL-1 $\beta$ -treated cells and controls. Chemokine primer sequences are given in Table 1.

## Results

The expression of 8793 genes on the Human Genome Focus Array was compared between controls (average values of five non-treated cells from five patients) and IL-1 $\beta$ -treated cells (average values of IL-1 $\beta$ -treated cells from five patients). A total of 121 genes showed a greater than threefold difference in intensity between control and IL-1 $\beta$ -treated synovial fibroblasts; 111 were upregulated and 10 were downregulated.

**Table 1** Primers for chemokine

Chemokine	Primers	bp
CCL20 (MIP-3)	F: 5'-GCA AGC AAC TTT GAC TGC TG-3' R: 5'-CAA GTC CAG TGA GGC ACA AA-3'	342
CXCL3 (GRO- $\gamma$ )	F: 5'-TAA ATG ACA GGG TGG GGA AC-3' R: 5'-GCA TTA TGC CCT ACA AGC AA-3'	225
CCL7 (MCP-3)	F: 5'-CCT GGA CAA GAA AAC CCA AA-3' R: 5'-TTC AAA ACC CAC CAA AAT CC-3'	245
CXCL2 (GRO- $\beta$ )	F: 5'-CCC TGC CTT ACA GGA ACA GAA-3' R: 5'-TCC CTG CCG TCA CAT TGA TCT-3'	403
CXC10 (IP-10)	F: 5'-TGC AAG CCA ATT TTG TCC ACG TGT TG-3' R: 5'-GCA GCT GAT TTG GTG ACC ATC ATT GG-3'	302
CXCL1 (GRO- $\alpha$ )	F: 5'-TGC AGG GAA TTC ACC CCA AG-3' R: 5'-CAG GGC CTC CTT CAG GAA CA-3'	229
CXCL8 (IL-8)	F: 5'-ATC ACT TCC AAG CTG GCC GTG GCT-3' R: 5'-TCT CAG CCC TCT TCA AAA ACT TCT C-3'	289
CCL8 (MCP-2)	F: 5'-TGC AAA ATC CTG GTG ATG TG-3' R: 5'-AGG AGC ACT GAT TGC CAA AG-3'	166
CX3CL1 (fractalkine)	F: 5'-GAG TGG GTC CAA TGC ACT TT-3' R: 5'-CAC AGA CGT TGG TGA TGA GG-3'	241
CXCL6 (GCP-2)	F: 5'-CAA TGA TCT GTG CTC TGC AA-3' R: 5'-CCA ACA TGA CAC ACA GGA AAA-3'	218
CCL5 (RANTES)	F: 5'-TAC ACC AGT GGC AAG TGC TC-3' R: 5'-GAA GCC TCC CAA GCT AGG AC-3'	199
CCL2 (MCP-1)	F: 5'-CCA ATT CTC AAA CTG AAG CTC GCA-C3' R: 5'-GTT AGC TGC CAG ATT CTT GGG TTG TG-3'	372
GAPDH	F: 5'-ATC ACC ATC TTC CAG GAG-3' R: 5'-ATC GAC TGT GGT CAT GAG-3'	315

CCL, CC motif chemokine ligand; CXCL, CXC motif chemokine ligand; CX3CL, CX3C motif chemokine ligand; MIP, macrophage inflammatory protein; GRO, growth-regulated oncogene; MCP, monocyte chemoattractant protein; IP, interferon-inducible protein; IL, interleukin; GDP, granulocyte chemotactic protein; RNATES, regulated upon activation, normal T expressed and secreted; GAPDH, glyceraldehyde-3-phosphate dehydrogenase.

**Table 2** Upregulated genes by treatment with IL-1 $\beta$

Rank <sup>a</sup>	Gene	GenBank	Fold change <sup>b</sup> (IL-1 $\beta$ /control)	Gene title Affy
1	CCL20	NM_004591	413.6	Chemokine (C-C motif) ligand 20
2	CXCL3	NM_002090	60.8	Chemokine (C-X-C motif) ligand 3
3	BCL2A1	NM_004049	41.0	BCL2-related protein A1
4	PTGS2	NM_000963	38.9	Prostaglandin-endoperoxide synthase 2
5	CXCL2	M57731	36.3	Chemokine (C-X-C motif) ligand 2
6	IL-8	AF043337	35.6	Interleukin 8
7	CSF3	NM_000759	29.4	Colony-stimulating factor 3 (granulocyte)
8	CCL7	NM_006273	21.0	Chemokine (C-C motif) ligand 7
9	IL-1 $\beta$	M15330	20.5	Interleukin 1, $\beta$
10	IL-6	NM_000600	19.9	Interleukin 6

<sup>a</sup>Ranking of upregulated gene by IL-1 $\beta$ .

<sup>b</sup>Average normalized intensity of IL-1 $\beta$ -stimulated cell in TMJ 1-5/average normalized intensity of control cell in TMJ 1-5.

Table 2 lists the top 10 upregulated genes. The gene most strongly upregulated by IL-1 $\beta$  (rank 1) was CCL20 (MIP-3 $\alpha$ ), a member of the chemokine superfamily. In fact, five chemokines were among the top 10 upregulated genes; CXCL3 (GRO- $\gamma$ ; rank 2), CXCL2 (GRO- $\beta$ ; rank 5), IL-8 (CXCL8; rank 6), and CCL7 (MCP-3; rank 8). The remaining five genes in the top 10 were BCL2A1 (BCL-related protein A1), PTGS2 (prostaglandin-endoperoxide synthetase 2), CSF3 (granulocyte colony-stimulating factor; G-CSF), IL-1B (IL-1 $\beta$ ), and IL-6.

The 121 IL-1 $\beta$ -responsive genes, which showed a greater than threefold difference between control and IL-1 $\beta$ -treated synovial fibroblasts, were categorized

based on the ontology of their molecular function (Fig. 1). The category with the most genes was signal transduction (34 genes; 32 upregulated and two down-regulated), followed by inflammatory response (20 genes; 20 upregulated), proliferation (15 genes; 13 upregulated and two downregulated), and chemotaxis (12 genes; 12 upregulated). Inflammatory response (20 of 139 genes, 14.4%) and chemotaxis (12 of 88 genes, 13.6%) accounted for the largest percentage of IL-1 $\beta$ -responsive genes among those identified on HG Focus Array. All of the 12 chemotaxis genes were also categorized as inflammatory response genes, such as chemokine superfamily members.

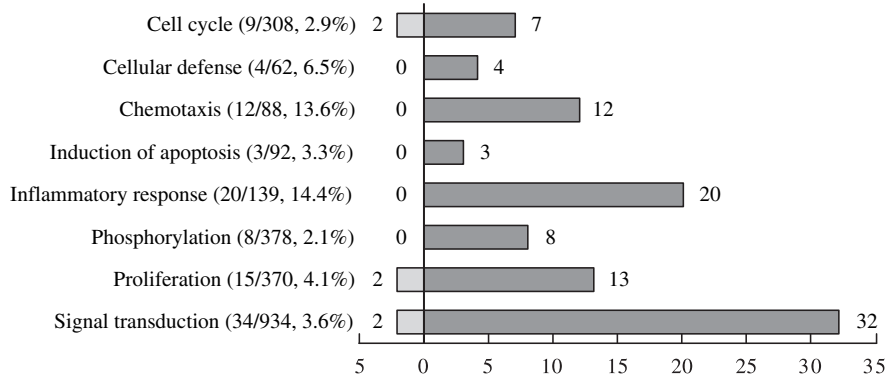


**Figure 1** Ontology for IL-1 $\beta$ -responsive genes. The categories of each gene are indicated (number of IL-1 $\beta$ -responsive genes/number of genes identified on HG Focus Array, percentage of IL-1 $\beta$ -responsive genes).

**Table 3** Levels of IL-1 $\beta$ -responsive chemokines mRNA in synovial fibroblasts from TMJ

Chemokine	GenBank	Fold (IL-1 $\beta$ /control)		Chemoattract target cells
		GeneChip	Real-time PCR	
CCL20 (MIP-3 $\alpha$ )	NM_004591	545.2	224.6	Memory T cell, immature dendritic cell
CXCL3(GRO- $\gamma$ )	NM_002090	61.6	158.3	Neutrophil, endothelial cell
CCL7 (MCP-3)	NM_006273	47.0	86.4	Monocyte, Th1 cell, eosinophil basophil, NK cell, dendritic cell
CXCL2(GRO- $\beta$ )	NM_002089	34.5	83.7	Neutrophil, melanoma cell
CXC10 (IP-10)	NM_001565	13.8	87.5	Monocyte, Th1 cell, NK cell
CXCL1 (GRO- $\alpha$ )	NM_001511	11.7	72.4	Neutrophil, lymphocyte, monocyte
CXCL-8(IL-8)	NM_000584	11.3	77.4	Neutrophil, CD8 <sup>+</sup> T cell, NK cells, monocyte
CCL8(MCP-2)	NM_005623	9.9	50.8	CD4 <sup>+</sup> T cell, CD8 <sup>+</sup> T cell, monocyte, eosinophil, basophil, NK cell
CX3CL1 (fractalkine)	NM_002996	9.5	8.9	NK cell, intraepithelial lymphocyte, CD8 <sup>+</sup> T cell, CD4 <sup>+</sup> T cell, monocytes
CXCL6(GCP-2)	NM_002993	6.4	19.3	Neutrophil
CCLS(RANTES)	NM_002985	4.0	8.3	Eosinophil, T cell, monocyte, basophil
CCL2(MCP-1)	NM_002982	3.5	7.2	Monocyte, T cell, basophil

CCL, CC motif chemokine ligand; CXC, CXC motif chemokine ligand; CX3CL, CX3C motif chemokine ligand; MIP, macrophage inflammatory protein; GRO, growth-related gene product; MCP, monocyte chemoattractant protein; IP, interferon-inducible protein; IL, interleukin; GDP, granulocyte chemotactic protein; RANTES, regulated upon activation, normal T expressed and secreted.

We focused on genes that encode chemokine superfamily members, as this gene family exhibits the most significant responses to IL-1 $\beta$  (Table 2 and Fig. 1). The 12 chemokines included five CC motif chemokines, six CXC motif chemokines, and one CX3C motif chemokines (Table 3). Figure 2 shows scatter plots of the 121 IL-1 $\beta$ -responsive genes and the 12 indicated chemokines. CCL20, CCL2, IL-8, CXCL1, CXCL2, and CXCL3 exhibited high expression in IL-1 $\beta$ -treated cells. Table 3 shows the IL-1 $\beta$ -induced fold-change using microarray and real-time PCR analysis in the TMJ 5 sample. Although the fold-change between the control and IL-1 $\beta$ -treated synovial fibroblasts determined by real-time PCR differed from that found on microarray, the rank order of the IL-1 $\beta$  response was similar between microarray and real-time PCR (Table 3).

### Discussion

Changes in the expression and production of inflammatory factors have an impact on both homeostasis and the pathologic condition of the TMJ. We hypothesized that identification of IL-1 $\beta$ -responsive genes in synovial

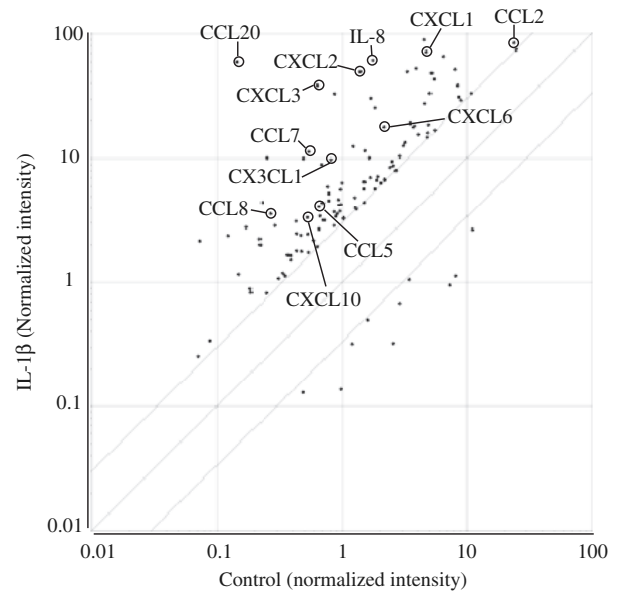


**Figure 2** Chemokines in scatter plots of IL-1 $\beta$ -responsive genes. Normalized intensity was calculated from five experiments using samples TMJ 1–5.

fibroblasts could help develop models for the inflammatory condition of the TMJ. Cell culture systems provide a well-established means for initial identification of cytokine-responsive genes. Of the cells from patients with intracapsular pathology of the TMJ, we decided to analyze the cells that produced the lowest levels of cytokines under untreated conditions, as we were unable to obtain synovial cells from healthy individuals.

We performed oligonucleotide microarray analysis in order to examine the consistency of gene regulation in synovial fibroblasts treated with IL-1 $\beta$ . Among the 8793 genes tested, a total of 121 exhibited a greater than threefold change in intensity between control and IL-1 $\beta$ -treated synovial fibroblasts, and these genes were categorized based on their molecular functions. Many of the upregulated genes can be categorized as 'signal transduction' or 'inflammatory response' genes. It has previously been suggested that IL-1 $\beta$  contributes to the production of inflammatory factors by modulating the expression of signal transduction.

Numerous chemokine superfamily members, which were categorized inflammatory response and chemotaxis genes, were also among the top 10 IL-1 $\beta$ -responsive genes identified in this study. Chemokines are considered key players in the diapedesis of leukocytes from the vasculature into tissues in inflammatory diseases (21–23). Inflammatory arthropathies are characterized histologically by infiltration of inflammatory cells and enlargement of the synovial lining layer (24, 25). Accumulation of neutrophils, activated T cells, and macrophages in inflamed synovial tissues may lead to significant structural damage to joints with RA (11, 24, 25). Inflammatory cells have also been detected in synovial tissue and in fluid from patients with intracapsular pathologies of the TMJ (1, 3, 5). The mechanisms leading to cellular infiltration of the synovium and joint degeneration have been elucidated to a degree by studying the release of degradative enzymes (26), various products of oxidative metabolism (27), and inflammatory cytokines (24). The following sequence of events is consistent with these findings: (i) chemokines produced by synovial fibroblasts stimulate chemotaxis of neutrophils, macrophages, and T lymphocytes; (ii) these inflammatory cells produce inflammatory cytokines such as IL-1 $\beta$ , matrix degradative enzymes, and various products of oxidative metabolism; (iii) the enzymes and oxidative metabolites cause degradation of the extracellular matrix; (iv) the inflammatory cytokines stimulate synovial fibroblasts to produce more chemokines. Furthermore, the subset of CXC-type chemokines that contain the sequence Glu-Leu-Arg (the 'ELR' motif), CXCL1, 2, 3, 6, 8, are also thought to promote angiogenesis (28). Thus, induction of the ELR-CXCs may lead to both recruitment of inflammatory cells and new small vessels in synovial tissues. Although chemotaxis is a necessary function of homeostasis, inappropriate infiltration of inflammatory cells may cause joint degeneration.

The other genes among the top 10 responsive genes were BCL2A1 (Bfl-1/A1 protein), PTGS2 (COX2), CSF3 (G-CSF), IL-1B, and IL-6. Many reports have

demonstrated that prostaglandin E2 synthesized by COX2, G-CSF, IL-1 $\beta$ , and IL-6 is increased in synovial tissues and fluids with severe inflammation, such as in RA or OA (29–31). Bfl-1/A1 protein is a member of the Bcl-2 family, which also includes Bcl-2 and Bcl-x (L), and suppresses apoptosis (32). This factor may be associated with hyperplasia of the synovial lining.

The development and application of genome-scale technologies for studying the IL-1 $\beta$  response may help to understand inflammation and develop new treatments. This study looked at changes in the gene expression of chemokines in response to IL-1 $\beta$  in synovial fibroblasts from the human TMJ using microarray. We also compared the gene expression levels detected by microarray and real-time PCR methods. Although the fold-change between control and IL-1 $\beta$ -treated synovial fibroblasts measured by real-time PCR differed slightly from that on microarray analysis, the rank order of IL-1 $\beta$ -responsive genes was similar, thus suggesting that gene chip analysis is a valid and powerful tool for analyzing the expression of a large number of molecules.

We used microarray analysis to identify differentially expressed genes in order to characterize synovial fibroblasts. As expected, synovial fibroblasts express vimentin, prolyl 4-hydroxylase, and type I collagen, which are fibroblast markers. In contrast, the expression of HLA class II antigens were not detected (data not shown). We observed no significant differences in the gene expression levels of cell markers between control and IL-1 $\beta$ -treated cells. These data were consistent with the notion that synovial fibroblasts are fibroblasts-like cells with no role in antigen presentation.

In conclusion, our comparative gene expression profile analysis has revealed interesting features of synovial fibroblasts from human TMJ. Upon IL-1 $\beta$  stimulation, synovial fibroblasts expressed high levels of several chemokines, suggested that IL-1 $\beta$  promotes the recruitment of leukocytes to the inflammation sites in TMJ synovium. These findings demonstrated that synovial fibroblasts in TMJ should be considered as important as its surrounding cells or tissue in the initiation or progression of inflammatory TMJ. In addition, we also suggest that the present data will be useful for the identification of candidates for genes with key roles in the initiation and progression of pathologic intracapsular conditions of the TMJ.

## References

1. Carls FR, von Hochstetter A, Makek M, Engelke W. Diagnostic accuracy of TMJ arthroscopy in correlation to histological findings. *J Craniomaxillofac Surg* 1995; **23**: 75–80.
2. Dijkgraaf LC, Liem RSB, de Bont LGM. Synovial membrane involvement in osteoarthritic temporomandibular joints. A light microscopic study. *Oral Surg Oral Med Oral Pathol Oral Radiol Endod* 1997; **83**: 373–86.
3. Gynther GW, Holmlund AB, Reinholt FP, Lindblad S. Temporomandibular joint involvement in generalized osteoarthritis and rheumatoid arthritis: a clinical,

- arthroscopic, histologic, and immunohistochemical study. *Int J Oral Maxillofac Surg* 1997; **26**: 10–6.
4. Gynther GW, Dijkgraaf LC, Reinholt FP, Holmlund AB, Liem RSB, de Bont LGM. Synovial inflammation in arthroscopically obtained biopsy specimens from the temporomandibular joint: a review of the literature and a proposed histologic grading system. *J Oral Maxillofac Surg* 1998; **56**: 1281–6.
  5. Kardel R, Ulfgrén A-K, Reinholt FP, Holmlund A. Inflammatory cell and cytokine patterns in patients with painful clicking and osteoarthritis in the temporomandibular joint. *Int J Oral Maxillofac Surg* 2003; **32**: 390–6.
  6. Chin JE, Winterrowd GE, Krzesicki RF, Sanders ME. Role of cytokines in inflammatory synovitis. The coordinate regulation of intercellular adhesion molecule 1 and HLA class I and class II antigens in rheumatoid synovial fibroblasts. *Arthritis Rheum* 1990; **33**: 1776–86.
  7. Richards CD, Agro A. Interaction between oncostatin M, interleukin 1 and prostaglandin E<sub>2</sub> in induction of IL-6 expression in human fibroblasts. *Cytokine* 1994; **6**: 40–7.
  8. Bucala R, Ritchlin C, Winchester R, Cerami A. Constitutive production of inflammatory and mitogenic cytokines by rheumatoid synovial fibroblasts. *J Exp Med* 1991; **173**: 569–74.
  9. Dinarello CA, Ikejima T, Warner SJC, et al. Interleukin 1 induces interleukin 1. I. Induction of circulating interleukin-1 in rabbits *in vivo* and in human mononuclear cells *in vitro*. *J Immunol* 1987; **139**: 1902–10.
  10. Vincenti MP, Brinckerhoff CE. Early response genes induced in chondrocytes stimulated with the inflammatory cytokine interleukin-1 $\beta$ . *Arthritis Res* 2001; **3**: 381–8.
  11. Sweeney SE, Firestein GS. Rheumatoid arthritis: regulation of synovial inflammation. *Int J Biochem Cell Biol* 2004; **36**: 372–8.
  12. Rooney M, Symons JA, Duff GW. Interleukin 1 beta in synovial fluid is related to local disease activity in rheumatoid arthritis. *Rheumatol Int* 1990; **10**: 217–9.
  13. Alstergren P, Ernberg M, Kvarnström M, Kopp S. Interleukin-1 $\beta$  in synovial fluid from the arthritic temporomandibular joint and its relation to pain, mobility, and anterior open bite. *J Oral Maxillofac Surg* 1998; **56**: 1059–65.
  14. Takahashi T, Kondoh T, Fukuda M, Yamazaki Y, Toyosaki T, Suzuki R. Proinflammatory cytokines detectable in synovial fluids from patients with temporomandibular disorders. *Oral Surg Oral Med Oral Pathol Oral Radiol Endod* 1998; **85**: 135–41.
  15. Ogura N, Tobe M, Sakamaki H, et al. Interleukin-1 $\beta$  induces interleukin-6 mRNA expression and protein production in synovial cells from human temporomandibular joint. *J Oral Pathol Med* 2002; **31**: 353–60.
  16. Tobe M, Ogura N, Abiko Y, Nagura H. Interleukin-1 $\beta$  stimulates interleukin-8 production and gene expression in synovial cells from human temporomandibular joint. *J Oral Maxillofac Surg* 2002; **60**: 741–7.
  17. Ogura N, Tobe M, Sakamaki H, et al. Interleukin-1 $\beta$  increases RANTES gene expression and production in synovial fibroblasts from human temporomandibular joint. *J Oral Pathol Med* 2004; **33**: 629–33.
  18. Allander SV, Illei PB, Chen Y, et al. Expression profiling of synovial sarcoma by cDNA microarrays. Association of ERBB2, IGFBP2, and ELF3 with epithelial differentiation. *Am J Pathol* 2002; **161**: 1587–95.
  19. Wang P-L, Ohura K, Fujii T, et al. DNA microarray analysis of human gingival fibroblasts from healthy and inflammatory gingival tissues. *Biochem Biophys Res Commun* 2003; **305**: 970–3.
  20. Sana TR, Janatpour MJ, Sathe M, McEvoy LM, McClanahan TK. Microarray analysis of primary endothelial cells challenged with different inflammatory and immune cytokines. *Cytokine* 2005; **29**: 256–69.
  21. Robinson E, Keystone EC, Schall TJ, Gillett N, Fish EN. Chemokine expression in rheumatoid arthritis (RA): evidence of RANTES and macrophage inflammatory protein (MIP)-1 $\beta$  production by synovial T cells. *Clin Exp Immunol* 1995; **101**: 398–407.
  22. Lisignoli G, Toneguzzi S, Pozzi C, et al. Chemokine expression by subchondral bone marrow stromal cells isolated from osteoarthritis (OA) and rheumatoid arthritis (RA) patients. *Clin Exp Immunol* 1999; **116**: 371–8.
  23. König A, Krenn V, Toksoy A, Gerhard N, Gillitzer R. Mig, GRO $\alpha$  and RANTES messenger RNA expression in lining layer, infiltrates and different leucocyte populations of synovial tissue from patients with rheumatoid arthritis, psoriatic arthritis and osteoarthritis. *Virchows Arch* 2000; **436**: 449–58.
  24. Steiner G, Tohidast-Akrad M, Witzmann G, et al. Cytokine production by synovial T cells in rheumatoid arthritis. *Rheumatology* 1999; **38**: 202–13.
  25. Patterson AM, Schmutz C, Davis S, Gardner L, Ashton BA, Middleton J. Differential binding of chemokines to macrophages and neutrophils in the human inflamed synovium. *Arthritis Res* 2002; **4**: 209–14.
  26. Dreier R, Grässel S, Fuchs S, Schaumburger J, Bruckner P. Pro-MMP-9 is a specific macrophage product and is activated by osteoarthritic chondrocytes via MMP-3 or a MT-MMP/MMP-13 cascade. *Exp Cell Res* 2004; **297**: 303–12.
  27. Borsiczky B, Szabó Z, Jaberansari MT, Mack PPO, Röth E. Activated PMNs lead to oxidative stress on chondrocytes. *Acta Orthop Scand* 2003; **74**: 190–5.
  28. Strieter RM, Polverini PJ, Kunkel SL, et al. The functional role of the ELR motif CXC in chemokine-mediated angiogenesis. *J Biol Chem* 1995; **270**: 27348–57.
  29. Attur MG, Patel IR, Patel RN, Abramson SB, Amin AR. Autocrine production of IL-1 $\beta$  by human osteoarthritis-affected cartilage and differential regulation of endogenous nitric oxide, IL-6, prostaglandin E<sub>2</sub>, and IL-8. *Proc Assoc Am Physicians* 1998; **110**: 65–72.
  30. Yano K, Nakagawa N, Yasuda H, Tsuda E, Higashio K. Synovial cells from a patient with rheumatoid arthritis produce osteoclastogenesis inhibitory factor/osteoprotegerin: reciprocal regulation of the production by inflammatory cytokines and basic fibroblast growth factor. *J Bone Miner Metab* 2001; **19**: 365–72.
  31. Lawlor KE, Campbell IK, Metcalf D, et al. Critical role for granulocyte colony-stimulating factor in inflammatory arthritis. *Proc Natl Acad Sci U S A* 2004; **101**: 11398–403.
  32. D'Sa-Eipper C, Subramanian T, Chinnadurai G. bfl-1, a bcl-2 homologue, suppresses p53-induced apoptosis and exhibits potent cooperative transforming activity. *Cancer Res* 1996; **56**: 3879–82.

## Acknowledgements

We gratefully acknowledge the assistance of Asayo Imaoka regarding GeneChip technology. This study was supported by a Grant-in-Aid for Scientific Research (c) (17592111) from the Japan Society for the Promotion of Science, and by a Grant for Research at the Frontier of Science from the Ministry of Education, Science, Sports and Culture (2001).

This article was downloaded by:[Nihon University]  
On: 16 April 2008  
Access Details: [subscription number 773310727]  
Publisher: Informa Healthcare  
Informa Ltd Registered in England and Wales Registered Number: 1072954  
Registered office: Mortimer House, 37-41 Mortimer Street, London W1T 3JH, UK



## IUBMB Life

Publication details, including instructions for authors and subscription information:

<http://www.informaworld.com/smpp/title~content=t713723531>

### Effects of reactive oxygen species (ROS) on antioxidant system and osteoblastic differentiation in MC3T3-E1 cells

Masato Arai<sup>a</sup>; Yasuko Shibata<sup>a</sup>; Kamolpan Pugdee<sup>a</sup>; Yoshimitsu Abiko<sup>a</sup>; Yorimasa Ogata<sup>a</sup>

<sup>a</sup> Department of Periodontology, Nihon University School of Dentistry at Matsudo, Chiba, Japan

Online Publication Date: 01 January 2007

To cite this Article: Arai, Masato, Shibata, Yasuko, Pugdee, Kamolpan, Abiko, Yoshimitsu and Ogata, Yorimasa (2007) 'Effects of reactive oxygen species (ROS) on antioxidant system and osteoblastic differentiation in MC3T3-E1 cells', IUBMB Life, 59:1, 27 - 33

To link to this article: DOI: 10.1080/15216540601156188

URL: <http://dx.doi.org/10.1080/15216540601156188>

PLEASE SCROLL DOWN FOR ARTICLE

Full terms and conditions of use: <http://www.informaworld.com/terms-and-conditions-of-access.pdf>

This article maybe used for research, teaching and private study purposes. Any substantial or systematic reproduction, re-distribution, re-selling, loan or sub-licensing, systematic supply or distribution in any form to anyone is expressly forbidden.

The publisher does not give any warranty express or implied or make any representation that the contents will be complete or accurate or up to date. The accuracy of any instructions, formulae and drug doses should be independently verified with primary sources. The publisher shall not be liable for any loss, actions, claims, proceedings, demand or costs or damages whatsoever or howsoever caused arising directly or indirectly in connection with or arising out of the use of this material.

## Research Communication

# Effects of Reactive Oxygen Species (ROS) on Antioxidant System and Osteoblastic Differentiation in MC3T3-E1 Cells

Masato Arai, Yasuko Shibata, Kamolparn Pugdee, Yoshimitsu Abiko and Yorimasa Ogata

Department of Periodontology, Nihon University School of Dentistry at Matsudo, Chiba, Japan

---

### Summary

Oxidative stress regulates cellular functions in multiple pathological conditions, including bone formation by osteoblastic cells. However, little is known about the cellular mechanisms responsible for the effects of oxidative stress on osteoblast functions in senescence. To clarify the inhibitory effects of oxidative stress on osteoblastic mineralization, we examined the relationship between the antioxidant system and bone formation in MC3T3-E1 cells. After a single exposure to H<sub>2</sub>O<sub>2</sub> within range of a non-toxic concentration for cells, the mineralization level was diminished half. Under the same conditions, gene expression of the transcription factor Nrf2, which regulates antioxidant enzymes, was up-regulated. In addition, gene expression for the osteogenic markers Runx2, ALP, and BSP was lower than that in non-treated cells, whereas expression of the osteocalcin gene was up-regulated following H<sub>2</sub>O<sub>2</sub> exposure. These results suggest that reduced mineralization by MC3T3-E1 cells after H<sub>2</sub>O<sub>2</sub> exposure is the result of an up-regulated antioxidant system and altered osteogenic gene expression.

IUBMB *Life*, 59: 27–33, 2007

---

**Keywords** Osteoblastic differentiation; reactive oxygen species (ROS); senescence; antioxidant; Nrf2.

### INTRODUCTION

Reactive oxygen species (ROS), such as hydrogen peroxide (H<sub>2</sub>O<sub>2</sub>), hydroxyl radicals, and superoxide, are generated under various physiological conditions and believed to contribute to the etiology of atherosclerosis, cerebellar ischemia,

and the process of aging (1–5). Further, oxidative stress induced by ROS has been implicated in the induction of certain types of cell injury (6, 7). However, a recently proposed hypothesis states that ROS plays an important role in the regulation of cell proliferation and metabolism (8–10).

In bone tissues, both formation and maintenance are regulated by bone-forming osteoblasts and bone-resorbing osteoclasts (11–13), while an imbalance between those two cell types leads to the pathogenesis and etiology of certain bone metabolic diseases, including osteoporosis and osteopetrosis (14). Recent evidence has shown that ROS and antioxidant enzymes might be involved in the pathogenesis of bone loss such as osteoporosis (15, 16). In addition, Ozgocmen et al. (17) reported that antioxidant enzyme activities that serve as oxidative stress markers, such as superoxide dismutase (SOD), glutathione peroxidase (GSH-Px), and lipid peroxidation end-product malondialdehyde (MDA), might be important indicators of bone loss in postmenopausal women. In experimental studies, the effects of ROS on genes involved in osteoblast proliferation and differentiation remain unclear, in part because of the sometimes conflicting results observed with different stages of cultured osteoblastic cells and various oxygen tensions. Also, the process of osteoblast differentiation leading to bone mineralization is a poorly understood series of temporally and spatially coordinated events that occur within weeks or months. A significant end-point in this process is creation of a mineralized matrix that consists mainly of collagen, non-collagenous proteins, and hydroxyapatite. Extracellular aging, which is caused by accumulation of molecular damage by oxidation, glycation, and crosslinking of long-living extracellular proteins, is a major cause of several important human aging pathologies in bone tissue. We have shown that oxidized fibronectin (FN) induces the reduction of nodule formation with decreases in alkaline phosphatase (ALP) activity and levels of secretion of type I collagen in rat calvarial osteoblasts *in vitro* (18, 19). However, there is scant

---

Received 27 October 2006; accepted 6 December 2006

Address correspondence to: Yorimasa Ogata, Department of Periodontology, Nihon University School of Dentistry at Matsudo, 2-870-1, Sakaecho-Nishi, Matsudo, Chiba 271-8587, Japan. Tel: +81 47 360 9362. Fax: +81 47 360 9362.

E-mail: ogata.yorimasa@nihon-u.ac.jp

information regarding antioxidant systems in osteoblastic differentiation.

The sensitive cellular response to mild oxidative stress induces activation of several antioxidant enzymes that play an important role in the protection of cells against ROS and facilitate the prevention of oxidative stress-induced metabolism (20). In addition, the transcription factor nuclear factor E2 p45-related factor 2 (Nrf2) is one of the critical transcription factors involved in the regulation of antioxidant enzymes (21, 22). Nrf2 forms heterodimers with small Maf proteins for selective recognition of the antioxidant-responsive element (ARE) or electrophile-responsive element on target genes (21–23).

Recently, a study by Hinoi et al. (24) using MC3T3-E1 cells stably transfected with an nrf2 expression vector indicated that Nrf2 negatively regulates osteoblast differentiation through inhibition of runt-related transcription factor 2 (Runx2)-dependent transcriptional activity. In the present study, we attempted to reassess the effects of antioxidant systems on osteoblast differentiation, and also determined gene expressions for antioxidant-related and osteogenic marker molecules using hydrogen peroxide ( $H_2O_2$ )-treated MC3T3-E1 cells. To determine the effects of oxidative stress on MC3T3-E1 cells, we treated the cells directly with  $H_2O_2$ , as we have observed that  $H_2O_2$  stress inhibits differentiation of MC3T3-E1 cells. Using identical conditions, we found that a single exposure to  $H_2O_2$  led to an up-regulated antioxidant system and down-regulated the gene expression of osteogenic marker molecules in MC3T3-E1 cells.

## MATERIALS AND METHODS

### Cell Culture and $H_2O_2$ Treatment

MC3T3-E1 cells were purchased from Cell Bank (Riken BioResource Center, Ibaraki, Japan) and cultured in  $\alpha$ -MEM, plus L-glutamine, ribonucleosides, and deoxyribonucleosides, Invitrogen Co. CA) containing 10% fetal bovine serum (FBS) supplemented with antibiotics (50  $\mu$ g/ml gentamycin sulfate, 0.3  $\mu$ g/ml amphotericin B, 100 units/ml penicillin G potassium) at 37°C in a  $CO_2$  incubator (5%  $CO_2$ /95% air). MC3T3-E1 cells were subcultured at approximately 80% confluence in every 3 days in 75-cm<sup>2</sup> flasks.

To investigate the effects of ROS as an *in vitro* cellular senescence, we prepared the  $H_2O_2$ -treated MC3T3-E1 cells by the method of Chen et al. (25) with slight modification. MC3T3-E1 cells were plated at a high density ( $1 \times 10^5$  cells/ml, 0.5 ml/well) to provide near confluence in a 24 well plate. After 2 days, the cells were treated with  $\alpha$ -MEM containing  $H_2O_2$  and cultured for 3 h. Subsequently, they were washed with fresh  $\alpha$ -MEM to omit  $H_2O_2$ . To observe osteoblastic differentiation,  $\alpha$ -MEM containing 10% FBS, antibiotics, 50  $\mu$ g/ml of ascorbic acid, and 5 mM of

$\beta$ -glycerophosphate ( $\beta$ -GP) were used. The culture medium was changed to fresh every 3 days throughout the 50 day experimental period. The viability of MC3T3-E1 cells after  $H_2O_2$  treatment in each concentration was assessed using Alamar Blue assay (Biosource International, CA). Alamar Blue was added to each well in an amount equal to 10% of the culture volume and incubated for 3 h. The supernatants were extracted and absorbance was measured at wavelengths of 570 nm and 600 nm.

### Determination of Mineralization Levels

To determine the degree of calcification in MC3T3-E1 cells, cultured cells were stained with Alizarin red S. Calcification levels were determined using a calcium assay kit (Calcium C, Wako, Osaka, Japan). To quantitate the ability of bone-nodule formation, mineralized bone nodules were visible as white nodules after fixing and were further confirmed by modified von Kossa staining (26). The contents of each well were fixed for 15 min in 10% neutral buffered formalin, then a 5% silver nitrate solution (45 min) and 3% sodium thiosulphate (5 min) were used for von Kossa staining.

### Real time-PCR

Cultured MC3T3-E1 cells, with or without exposure to  $H_2O_2$ , were homogenized using TRIzol reagent (Invitrogen Co., Carlsbad, CA), after which total RNA was isolated using a FastPrepFP 120 Instrument (BIO 101 Inc., Vista, CA). Samples (1  $\mu$ g) of total RNA were then reverse transcribed, followed by olig-dT primer and MuLV reverse transcriptase (final volume; 20  $\mu$ l), and then 5- $\mu$ l aliquots from the diluted cDNA (1/100-fold) were used as templates for real-time PCR. To assess the effects of  $H_2O_2$  on the transcription of genes (listed in Table 1), PCR amplification was performed using SYBR Green real-time PCR master mix (TOYOBO Co., LTD, Osaka, Japan) with an ABI Prism 7700 and Sequence Detection System software (Applied Biosystems, Foster City, CA). The expression level of each gene was observed as the cycle number by real-time PCR, with their levels normalized to that of the housekeeping enzyme glyceraldehyde-3-phosphate dehydrogenase (GAPDH).

## RESULTS

### Effects of $H_2O_2$ on Mineralization of MC3T3-E1 Cells

Before attempting to clarify the effects of  $H_2O_2$  on the process of osteoblast differentiation, we tried to confirm the  $H_2O_2$  effects on cell viability of MC3T3-E1 cells. In order to investigate the effect of osteoblastic differentiation in cellular senescence caused by oxidative stress, we modified the experimental condition by Chen et al. (25) and referred to the study of Fatokun et al. (27). We assessed the viability of MC3T3-E1 cells using Alamar Blue assay. As shown in Table 2, the concentration of  $H_2O_2$  more than 600  $\mu$ M result

**Table 1**  
Primers used for real time-PCR

Protein name	GenBank ID	Primers
NQO1	NM_008706	up; 5'-ctccaagcagcctgtttgacc-3' down; 5'-tcccatcctcgtggagcaaag-3'
Nrf2	U70475	up; 5'-ttagtacgacgacagaaggac-3' down; 5'-ccagttgaaactgagcgaag-3'
MafF	NM_010755	up 5'-gtggatcccttaccgacaaag-3' down; 5'-catcagcgttcatccga-3'
MafG	NM_010756	up; 5'-taaagtccaagacggatgct-3' down; 5'-agaggagaaaggaaggaaa-3'
MafK	NM_010757	up; 5'-agctcatcatgctaagaacagg-3' down; 5'-gacagggcccgggttatg-3'
Keap1	NM_016679	up; 5'-accagggcaagatctacgtc-3' down; 5'-ggccatggatttgagtctg-3'
Runx2	NM_009820	up; 5'-ctcagtgatttagggcgatt-3' down; 5'-aggggtaagactggtcatagg-3'
OC	MMBGPR	up; 5'-agctatcagaccagatggtc-3' down; 5'-ttttggagctgctgtgacatc-3'
BSP	NM_008318	up; 5'-taccagcttatgaggacgaa-3' down; 5'-gcatttgcggaaatcactctg-3'
ALP	NM_007431	up; 5'-ccatgtagattacgctcaca-3' down; 5'-Atggaggattccagatacagg-3'
GAPDH	M33197	up; 5'-atcaccatcttccaggag-3' down; 5'-atggactgtggtcatgag-3'

The primers sets were designed using the primer searching software Genetyx-Mac Version 13.0.5. The suitability of each primer set was confirmed using cDNA samples from first strand cDNA, as described in 'Materials and Methods'. The optimum temperature for amplification was used to perform real-time PCR, after confirming the melting curve of each primer set.

**Table 2**  
Viability of MC3T3-E1 cells treated with H<sub>2</sub>O<sub>2</sub>

H <sub>2</sub> O <sub>2</sub> (μM)	A570-A600	Cell viability (%)
0	0.390 ± 0.031	100
200	0.396 ± 0.031	101.5
300	0.390 ± 0.031	100.0
400	0.390 ± 0.004	100.0
500	0.376 ± 0.036	96.4
600	*0.265 ± 0.049	67.9
700	**0.190 ± 0.033	48.7

MC3T3-E1 cells were treated with various concentrations of H<sub>2</sub>O<sub>2</sub> for 3 h and cell viability was assessed using AlamarBlue assay. Data are shown as the mean ± SD from three different cultures. Significant differences compared to control are shown at the following probability level. \**P* < 0.05, \*\**P* < 0.01.

in decrease of the viability significantly, but the lower concentration of H<sub>2</sub>O<sub>2</sub> less than 500 μM did not have a significant effect on MC3T3-E1 cells on each culture period in

our experimental condition. Therefore, we used a single exposure of 400 μM of H<sub>2</sub>O<sub>2</sub> in the following experiments.

We attempted to examine the H<sub>2</sub>O<sub>2</sub> effects on the mineralization of long cultured MC3T3-E1 cells. After a single treatment with H<sub>2</sub>O<sub>2</sub>, MC3T3-E1 cells were cultured for 50 days with α-MEM supplemented with 10% FBS, 5 mM of β-GP, and 50 μg/ml of ascorbic acid. To determine the level of mineralization, an Alizarin red S assay, a calcium assay, and von Kossa staining were used. At 14-day, it has observed that H<sub>2</sub>O<sub>2</sub> induced the inhibitory effect on calcification in MC3T3-E1 cells (Fig. 1A). Next, we determined the alteration of calcium levels in long cultured MC3T3-E1 during 50 days using a calcium assay kit. The cultured cells were washed with Phosphate buffered saline (PBS) and calcium in the matrix was dissolved with 0.5 M HCl. As shown in Figure 1B, the calcium levels in H<sub>2</sub>O<sub>2</sub>-treated MC3T3-E1 cells reached a maximum at 30-day, while those in non-treated MC3T3-E1 cells remained increased throughout the 50 days experimental period. Calcification levels in the H<sub>2</sub>O<sub>2</sub>-treated MC3T3-E1 cells were half of those in the non-treated cells at all stages. In addition, nodule formation in H<sub>2</sub>O<sub>2</sub>-treated MC3T3-E1 cells after 7, 14, 21, 30, 40, and 50 days was also reduced as compared with the non-treated cells, as shown by von Kossa staining (Fig. 1C).

#### Effects of H<sub>2</sub>O<sub>2</sub> on Gene Expression of Antioxidant Enzymes

The antioxidant enzyme NAD(P)H:quinone oxidoreductase (NQO1) is known to detoxify quinones and generate antioxidant forms of ubiquinone. NQO1 is highly inducible by a number of stimuli, including electrophilic metabolites and oxidative stress (20, 28), and is considered to be a stress response indicator. To confirm the results of antioxidant system activity in MC3T3-E1 cells after treatment with H<sub>2</sub>O<sub>2</sub>, we performed real time PCR analysis for the gene expression of NQO1. Total RNA was extracted from both H<sub>2</sub>O<sub>2</sub>-treated and non-treated MC3T3-E1 cells on days 1, 3, and 7. Each real-time PCR result was quantified and normalized to the expression level of GAPDH. As shown in Figure 2, NQO1 gene expression was strongly induced by H<sub>2</sub>O<sub>2</sub> at first day. The increased gene expression of NQO1 remained high even at day 7, in spite of a single exposure of H<sub>2</sub>O<sub>2</sub>.

Nrf2 is responsible for the induction of NQO1 in response to oxidative stress (21–23). Next, we determined the gene expression for Nrf2, Keap1, Maf-F, Maf-G, and Maf-K using real time-PCR analysis. As shown in Table 3, Nrf2 gene expression was increased, whereas the up-regulation of Keap1 was not observed using the same cDNA samples (1/100-fold).

#### Effects of H<sub>2</sub>O<sub>2</sub> on Gene Expression for Osteogenic Marker Enzymes

The effects of H<sub>2</sub>O<sub>2</sub> on the gene expression of ALP, bone sialoprotein (BSP), osteocalcin (OC), and Runx2 were determined using real-time and the end-point PCR assays.

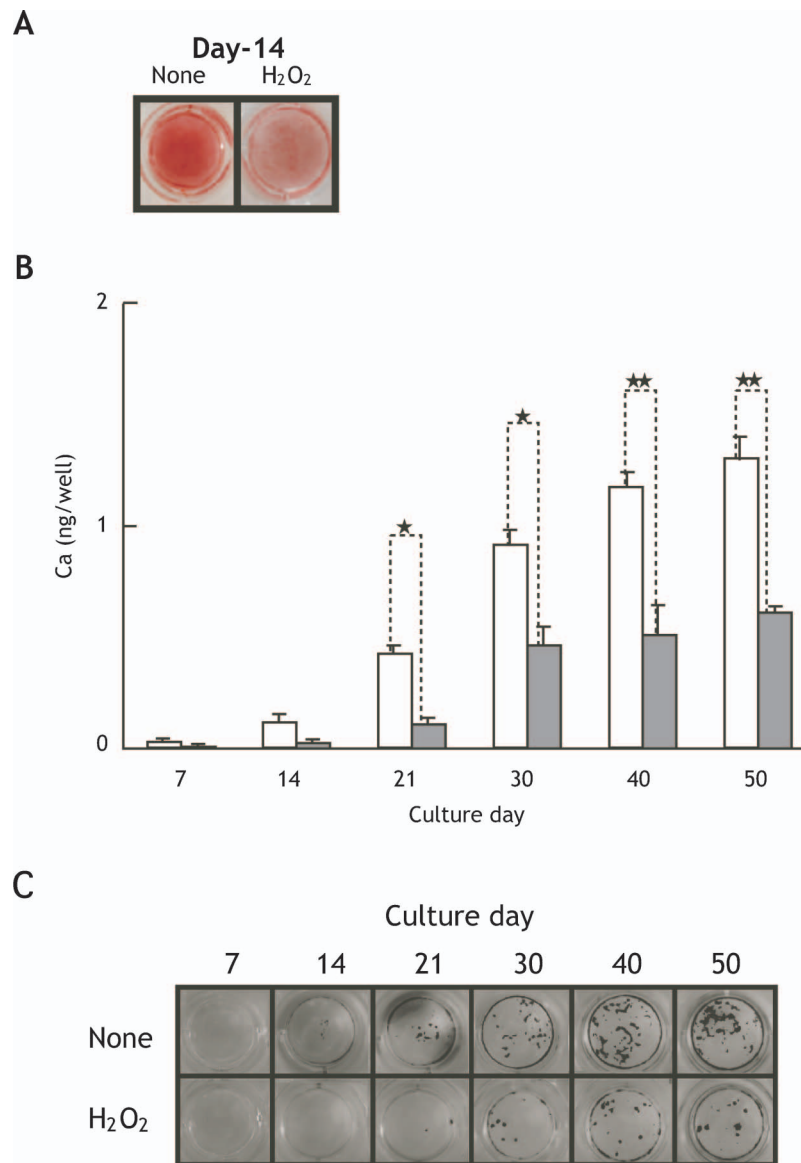


**Figure 1.** Effects of H<sub>2</sub>O<sub>2</sub> on calcification of MC3T3-E1 cells. MC3T3-E1 cells were treated with 400  $\mu$ M of H<sub>2</sub>O<sub>2</sub> for 3 h. The medium was immediately changed to fresh  $\alpha$ -MEM to remove H<sub>2</sub>O<sub>2</sub>, then the cells were cultured for the indicated numbers of days. (A) H<sub>2</sub>O<sub>2</sub>-treated and non-treated MC3T3-E1 cells were cultured for 14 days and stained with Alizarin red S. (B) To quantitate calcium levels, the cells were washed twice with PBS. Calcium in the matrix was dissolved with 0.5 M HCl, assay reagent was added, and then the sample was measured at a wavelength of 598 nm. White and gray columns mean the results in the non-treated and H<sub>2</sub>O<sub>2</sub>-treated MC3T3-E1 cells, respectively. \* $P < 0.05$ , \*\* $P < 0.01$ ; significant difference as compared to the non-treated. Data are shown as the means  $\pm$  SE ( $n = 5$ ). (C) Effects of H<sub>2</sub>O<sub>2</sub> on nodule formation of MC3T3-E1 cells. Von Kossa staining was used for determining mineralization.

The results of end-point PCR for ALP, BSP, Runx2, OC, Nrf2 and GAPDH after PCR of 38, 35, 45, 32, 35 and 35 cycles, respectively, are shown in Figure 3. In H<sub>2</sub>O<sub>2</sub>-treated MC3T3-E1 cells, ALP, BSP, Runx2 showed lower levels of expression than in non-treated cells. Notable, the gene expression for Runx2 was very low and strongly inhibited by H<sub>2</sub>O<sub>2</sub> treatment. In contrast, that of OC was up-regulated by

H<sub>2</sub>O<sub>2</sub> exposure from day 1. Nrf2 mRNA level was also increased by H<sub>2</sub>O<sub>2</sub>.

## DISCUSSION

Oxidative stress regulates cellular functions in multiple pathological conditions, including bone formation by

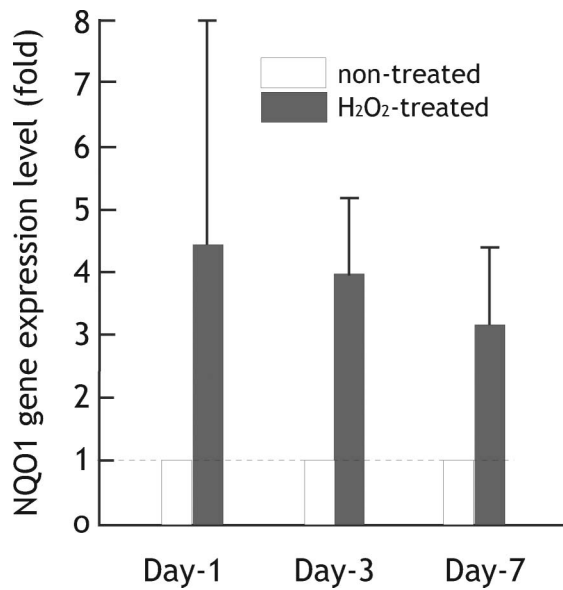


**Figure 2.** Increased and maintained gene expression of NQO1. Gene expression levels in H<sub>2</sub>O<sub>2</sub>-treated MC3T3-E1 cells were compared with those of non-treated MC3T3-E1 cells. MC3T3-E1 cells were treated with 400  $\mu$ M of H<sub>2</sub>O<sub>2</sub> for 3 h, then the medium was immediately changed to fresh  $\alpha$ -MEM with 5 mM of  $\beta$ -GP and 50  $\mu$ g/ml of ascorbic acid. The expression level of each gene was observed as the cycle number by real-time PCR, with their levels normalized to that of the housekeeping enzyme GAPDH. The solid column indicates the fold increases of gene expression levels for H<sub>2</sub>O<sub>2</sub>-treated MC3T3-E1 cells compare with non-treated cells (open column).

**Table 3**

Effects of H<sub>2</sub>O<sub>2</sub> on antioxidant related-gene expression on day 7

Genes	Control	H <sub>2</sub> O <sub>2</sub>	Fold increase
GAPDH	1.0	1.0	
NQO1	235.9 $\pm$ 77.4	572.9 $\pm$ 93.7	2.43
Nrf2	231.2 $\pm$ 66.2	510.4 $\pm$ 120.0	2.21
MafF	0.75 $\pm$ 0.34	2.58 $\pm$ 1.02	3.44
MafG	n.d.	n.d.	–
MafK	n.d.	n.d.	–
Keap1	n.d.	n.d.	–

Five microliters of 1/100-fold diluted cDNA was used as a template for real-time PCR; n.d. = 'not detectable' in this condition for 40 cycles.

osteoblastic cells. To clarify the effects of H<sub>2</sub>O<sub>2</sub> on the process of osteoblast differentiation leading to bone mineralization, a significant end point in this process to create a mineralized matrix in MC3T3-E1 cells was determined. We treated the

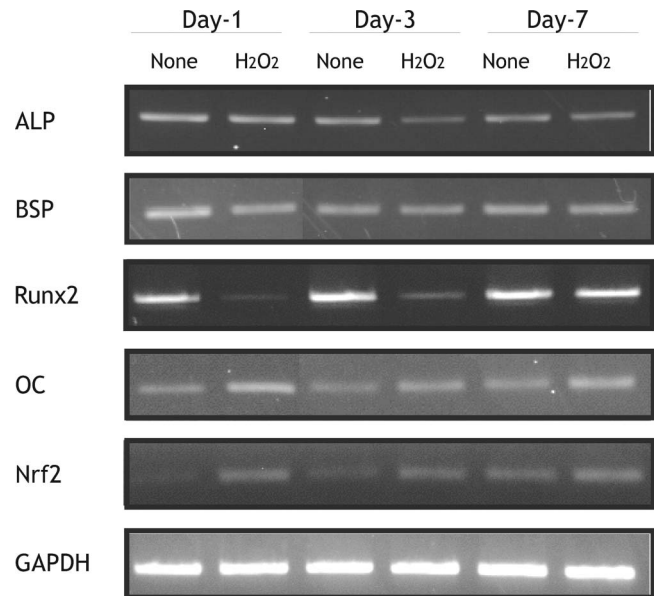


**Figure 3.** End-point RT-PCR analysis of osteogenic marker molecules. Ethidium bromide staining patterns for the amplified PCR products using agarose gel electrophoresis are shown. cDNA samples (1/100-fold) were used as templates. Amplification was done with 38, 35, 45, 32, 35, and 35 cycles for ALP, BSP, Runx2, OC, Nrf2, and GAPDH, respectively.

cells directly with H<sub>2</sub>O<sub>2</sub> and found that their differentiation was inhibited (Fig. 1). To clarify the effects of oxidative stress on mineralization by MC3T3-E1 cells, we examined the relationship between the antioxidant system and bone formation in MC3T3-E1 cells. After a single exposure to H<sub>2</sub>O<sub>2</sub>, the levels of calcification in H<sub>2</sub>O<sub>2</sub>-treated MC3T3-E1 cells were half that in non-treated cells at all culture stages. We considered that if H<sub>2</sub>O<sub>2</sub> could induce cell death signaling in MC3T3-E1 cells, then the surviving cells in the plates would proliferate first, thus delaying the start of differentiation toward the end-point of mineralization. As a result, calcification levels were expected to reach the same levels of the control cells after a long culture period. However, even though 500  $\mu$ M of H<sub>2</sub>O<sub>2</sub> have no effect on cell viability in our experimental conditions (Table 2), the calcification level in H<sub>2</sub>O<sub>2</sub>-treated MC3T3-E1 cells (400  $\mu$ M of H<sub>2</sub>O<sub>2</sub>) was inhibited throughout the present 50 days experimental period (Fig. 1).

In previous studies, Nrf2 has been shown to be an essential component of ARE-binding transcriptional machinery (29–31), and played an important role in regulating the expression of many mammalian detoxifying and antioxidant enzymes under oxidative or electrophilic stress in various Nrf2-deficient mice experiments. On the other hand, it was also reported that Nrf2 might negatively regulate osteoblast

differentiation through inhibition of Runx2-dependent transcriptional activity in *nrf2*-overexpressed MC3T3-E1 cells (24). In that study, the expression levels of Maf-G and Maf-F were expressed in a constitutive manner during cultivation from 3 to 28 days in *nrf2*-overexpressed MC3T3-E1 cells, with sustained expression seen with Runx2 mRNA for a period of up to 28 days. In contrast, in our experiment, the gene expression of Maf-F was up-regulated (Table 3) by a single treatment with H<sub>2</sub>O<sub>2</sub>. Maf-F may partner with Nrf2 in H<sub>2</sub>O<sub>2</sub>-stimulated MC3T3-E1 cells in antioxidant systems, because gene expression for Maf-G and Maf-K was not detectable after 40 cycles in our experimental condition. We found that a single treatment with H<sub>2</sub>O<sub>2</sub> induced the gene expression of Nrf2 and Maf-F in MC3T3-E1 cells (Table 3).

A previous study found that stable over expression of Nrf2 significantly impaired Runx2-dependent stimulation of OC promoter activity and recruitment of Runx2 on the OC promoter without affecting the expression of Runx2 mRNA (24). Further, Nrf2 bound to the ARE-like sequence of the OC promoter. As a result, they suggested that Nrf2 might negatively regulate cellular differentiation through inhibition of Runx2-dependent transcriptional activity in osteoblasts. In the present H<sub>2</sub>O<sub>2</sub>-treated MC3T3-E1 cells, the gene expression of Runx2 was inhibited (Fig. 3). We reasonably expected that OC gene expression would be decreased by H<sub>2</sub>O<sub>2</sub>-induced Runx2 reduction because of the mild ROS stimuli. Unexpectedly, OC gene expression was increased by the single exposure to H<sub>2</sub>O<sub>2</sub> as compared with non-treated MC3T3-E1 cells (Fig. 3). It is suggested that the increased gene expression of Nrf2 and Maf-F, which are known to up-regulate genes for antioxidant molecules, might have induced the high expression level of the OC gene in the H<sub>2</sub>O<sub>2</sub>-treated MC3T3-E1 cells.

A gene expression profile during all phases of MC3T3-E1 cell differentiation (proliferation, matrix accumulation, and terminal differentiation indicated by mineralization) previously reported demonstrated the gene expression of OC after 14 days (32). In the present H<sub>2</sub>O<sub>2</sub>-treated MC3T3-E1 cells, OC gene expression level was already high on day 1 and remained strongly induced on days 3 and 7, despite inhibition of the gene expression of Runx2 (Fig. 3). We considered that the induction of OC gene expression during the early stages might have caused an alteration of differentiation and/or mineralization in MC3T3-E1 cells.

Our results indicated that a single exposure to H<sub>2</sub>O<sub>2</sub>-induced inhibition of mineralization by the following processes: (1) ROS inhibited the gene expression of osteogenic marker molecules in osteoblasts, particularly, Runx2, (2) the antioxidant system was maintained for a long period in H<sub>2</sub>O<sub>2</sub>-treated MC3T3-E1 cells, and (3) Nrf2/MafF might alter the gene expression profile of some osteogenic marker proteins. Therefore, this particular antioxidant system may be a novel target with great benefits for the discovery and

development of innovative strategies useful for therapy and treatment of a variety of diseases associated with cellular damage caused by ROS, such as bone loss associated with aging.

## ACKNOWLEDGEMENTS

This research was supported in part by a Grant from the Academic Frontier Project for Private Universities, a matching fund subsidy from MEXT (Ministry of Education, Culture, Sports, Science and Technology), 2001–2005, and Grants-in-Aid for Scientific Research (A1; 16209063). We gratefully acknowledge the collaboration with of Dr T. Sato, Dr Y. Otsuka-Tanaka, and Dr J. Mega in this study.

## REFERENCES

- Ames, B. N., and Shigenaga, M. K. (1992) Oxidants are a major contributor to aging. *Ann. NY Acad. Sci.* **663**, 85–96.
- Jenner, P. (1994) Oxidative damage in neurodegenerative disease. *Lancet* **344**, 796–798.
- Halliwell, B., and Gutteridge, J. M. (1990) Role of free radicals and catalytic metal ions in human disease: an overview. *Methods Enzymol.* **186**, 1–85.
- Key, L. L. Jr, Wolf, W. C., Gundberg, C. M., and Ries, W. L. (1994) Superoxide and bone resorption. *Bone* **15**, 431–436.
- Beckman, K. B., and Ames, B. N. (1998) The free radical theory of aging matures. *Physiol. Rev.* **78**, 547–581.
- Hyslop, P. A., Hinshaw, D. B., Halsey, W. A. Jr, Schraufstatter, I. U., Sauerheber, R. D., Spragg, R. G., Jackson, J. H., and Cochrane, C. G. (1988) Mechanisms of oxidant-mediated cell injury. The glycolytic and mitochondrial pathways of ADP phosphorylation are major intracellular targets inactivated by hydrogen peroxide. *J. Biol. Chem.* **263**, 1665–1675.
- Schraufstatter, I., Hyslop, P. A., Jackson, J. H., and Cochrane, C. G. (1988) Oxidant-induced DNA damage of target cells. *J. Clin. Invest.* **82**, 1040–1050.
- Slater, A. F., Stefan, C., Nobel, I., van den Dobbelsteen D. J., and Orrenius, S. (1995) Signalling mechanisms and oxidative stress in apoptosis. *Toxicol. Lett.* **82**, 149–153.
- Shackelford, R. E., Kaufmann, W. K., and Paules, R. S. (2000) Oxidative stress and cell cycle checkpoint function. *Free Radic. Biol. Med.* **28**, 1387–1404.
- Allen, R. G., and Tresini, M. (2000) Oxidative stress and gene regulation. *Free Radic. Biol. Med.* **28**, 463–499.
- Rodan, G. A. (1992) Introduction to bone biology. *Bone* **13** (Suppl. 1), S3–6.
- Meghji, S. (1992) Bone remodeling. *Br. Dent. J.* **172**, 235–242.
- Noda, M. (2006) Current topics in pharmacological research on bone metabolism: regulation of bone mass by the function of endogenous modulators of bone morphogenetic protein in adult stage. *J. Pharmacol. Sci.* **100**, 211–214.
- Seeman, E. (2003) Reduced bone formation and increased bone resorption: rational targets for the treatment of osteoporosis. *Osteoporos. Int.* **14** (Suppl. 3), S2–8.
- Maggio, D., Barabani, M., Pierandrei, M., Polidori, M. C., Catani, M., Mecocci, P., Senin, U., Pacifici, R., and Cherubini, A. (2003) Marked decrease in plasma antioxidants in aged osteoporotic women: results of a cross-sectional study. *J. Clin. Endocrinol. Metab.* **88**, 1523–1527.

16. Yalin, S., Bagis, S., Polat, G., Dogruer, N., Cenk Aksit S., Hatungil, R., and Erdogan, C. (2005) Is there a role of free oxygen radicals in primary male osteoporosis? *Clin. Exp. Rheumatol.* **23**, 689–692.
17. Ozgocmen, S., Kaya, H., Fadillioglu, E., Aydogan, R., and Yilmaz, Z. (2006) Role of antioxidant systems, lipid peroxidation, and nitric oxide in postmenopausal osteoporosis. *Mol. Cell. Biochem. Epub.*
18. Suzuki, H., Hayakawa, M., Kobayashi, K., Takiguchi, H., and Abiko, Y. (1997) H<sub>2</sub>O<sub>2</sub>-derived free radicals treated fibronectin substratum reduces the bone nodule formation of rat calvarial osteoblast. *Mech. Ageing Dev.* **98**, 113–125.
19. Hosoya, S., Suzuki, H., Yamamoto, M., Kobayashi, K., and Abiko, Y. (1998) Alkaline phosphatase and type I collagen gene expressions were reduced by hydroxyl radical-treated fibronectin substratum. *Mol. Genet. Metab.* **65**, 31–34.
20. Anwar, A., Siegel, D., Kepa, J. K., and Ross, D. (2002) Interaction of the molecular chaperone Hsp70 with human NAD(P)H:quinone oxidoreductase 1. *J. Biol. Chem.* **277**, 14060–14067.
21. Itoh, K., Ishii, T., Wakabayashi, N., and Yamamoto, M. (1999) Regulatory mechanisms of cellular response to oxidative stress. *Free Radic. Res.* **31**, 319–324.
22. Lee, J.-S., and Surh, Y.-J. (2005) Nrf2 as a novel molecular target for chemoprevention. *Cancer Lett.* **224**, 171–184.
23. Onodera, K., Shavit, J. A., Motohashi, H., Katsuoka, F., Akasaka, J., Engel, J. D., and Yamamoto, M. (1999) Characterization of the murine *mafF* gene. *J. Biol. Chem.* **274**, 21162–21169.
24. Hinoi, E., Fujimori, S., Wang, L., Hojo, H., Uno, K., and Yoneda, Y. (2006) Nrf2 negatively regulates osteoblast differentiation via interfering with Runx2-dependent transcriptional activation. *J. Biol. Chem.* **281**, 18015–18024.
25. Chen, J.-H., Stoeber, K., Kingsbury, S., Ozanne, S. E., Williams, G. H., and Hales, C. N. (2004) Loss of proliferative capacity and induction of senescence in oxidatively stressed human fibroblasts. *J. Biol. Chem.* **279**, 49439–49446.
26. Drury, R. A. B., and Wallington, E. A. (1980) In *Modified von Kossa Method in Carleton's Histological Technique* (5th ed.), pp. 217–218, Oxford University Press, Oxford.
27. Fatokun, A. A., Stone, T. W., and Smith, R. A. (2006) Hydrogen peroxide-induced oxidative stress in MC3T3-E1 cells: the effects of glutamate and protection by purines. *Bone* **39**, 542–551.
28. Ross, D. (2005) Functions and distribution of NQO1 in human bone marrow: potential clues to benzene toxicity. *Chem. Biol. Interact.* **153–154**, 137–146.
29. Ma, Q., Kinneer, K., Bi, Y., Chan, J. Y., and Kan, Y. W. (2004) Induction of murine NAD(P)H:quinone oxidoreductase by 2,3,7,8-tetrachlorodibenzo-p-dioxin requires the CNC (cap 'n' collar) basic leucine zipper transcription factor Nrf2 (nuclear factor erythroid 2-receptor) and Nrf2 signal transduction. *Biochem. J.* **377** (Pt 1), 205–213.
30. Itoh, K., Chiba, T., Takahashi, S., Ishii, T., Igarashi, K., Katoh, Y., Oyake, T., Hayashi, N., Satoh, K., Hatayama, I., Yamamoto, M., and Nabeshima, Y. (1997) An Nrf2/small Maf heterodimer mediates the induction of phase II detoxifying enzyme genes through antioxidant response elements. *Biochem. Biophys. Res. Commun.* **236**, 313–322.
31. Nguyen, T., Yang, C. S., and Pickett, C. B. (2004) The pathways and molecular mechanisms regulating Nrf2 activation in response to chemical stress. *Free Radic. Biol. Med.* **37**, 433–441.
32. Beck, G. R. Jr, Zerler, B., and Moran, E. (2001) Gene array analysis of osteoblast differentiation. *Cell Growth Differ.* **12**, 61–83.

## Effect of F-spondin on cementoblastic differentiation of human periodontal ligament cells <sup>☆</sup>

Masae Kitagawa <sup>a,b</sup>, Yasusei Kudo <sup>a</sup>, Shinji Iizuka <sup>a</sup>, Ikuko Ogawa <sup>b</sup>, Yoshimitsu Abiko <sup>c</sup>,  
Mutsumi Miyauchi <sup>a</sup>, Takashi Takata <sup>a,\*</sup>

<sup>a</sup> Department of Oral and Maxillofacial Pathobiology, Graduate School of Biomedical Sciences, Hiroshima University, Japan

<sup>b</sup> Center of Oral Clinical Examination, Hiroshima University Hospital, Hiroshima, 734-8553, Japan

<sup>c</sup> Department of Biochemistry, School of Dentistry at Matsudo, Nihon University, 270-8587, Japan

Received 21 August 2006

Available online 1 September 2006

---

### Abstract

Cementum is a mineralized tissue produced by cementoblasts covering the roots of teeth that provides for the attachment of periodontal ligament to roots and surrounding alveolar bone. To study the mechanism of proliferation and differentiation of cementoblasts is important for understanding periodontal physiology and pathology including periodontal tissue regeneration. However, the detailed mechanism of the proliferation and differentiation of human cementoblasts is still unclear. We previously established human cementoblast-like (HCEM) cell lines. We thought that comparing the transcriptional profiles of HCEM cells and human periodontal ligament (HPL) cells derived from the same teeth could be a good approach to identify genes that influence the nature of cementoblasts. We identified F-spondin as the gene demonstrating the high fold change expression in HCEM cells. Interestingly, F-spondin highly expressing HPL cells showed similar phenotype of cementoblasts, such as up-regulation of mineralized-related genes. Overall, we identified F-spondin as a promoting factor for cementoblastic differentiation.

© 2006 Elsevier Inc. All rights reserved.

**Keywords:** F-spondin; Cementoblast; Periodontal ligament; Differentiation

---

Cementum is a mineralized tissue produced by cementoblasts covering the roots of teeth that provides for the attachment of periodontal ligament to roots and surrounding alveolar bone [1]. Cementum contributes to the regeneration of the connective tissue attachment to root surface, denuded due to periodontal disease. Therefore, it is very important for studying the detailed mechanisms proliferation and differentiation of human cementoblasts to understand periodontal physiology and pathology, including periodontal tissue regeneration. Several attempts have been made to obtain makers of cementoblasts [2–5]. Recent studies have shown new makers of cementum or

cementum-periodontal ligament such as cementum-derived attachment protein (CAP) [2] and cementum-derived protein (CP-23) [5]. However, the detailed role of these molecules has not been revealed in the differentiation of cementoblasts.

We recently have established human cementoblast-like (HCEM) cell lines and human periodontal ligament (HPL) cell lines from same teeth by *hTERT* transfection to examine the molecule involving with the differentiation of cementoblasts [6]. HCEM cell lines obtained from teeth root lining cells showed high alkaline phosphatase (ALP) activity, calcified nodule formation, and the expression of mineralized related genes, including type I collagen (COL1), ALP, runt-related transcription factor 2 (Runx2), osteocalcin (OCN), bone sialoprotein (BSP), and CP-23. On the other hand, HPL cells from middle part of periodontal ligament showed low ALP and mineralization activity, and

---

<sup>☆</sup> This work was supported in part by Grants-in-Aid from the ministry of education, science and culture of Japan.

\* Corresponding author. Fax: +81 82 257 5619.

E-mail address: [ttakata@hiroshima-u.ac.jp](mailto:ttakata@hiroshima-u.ac.jp) (T. Takata).

did not express OCN and BSP which are maker of genes showing the mature differentiation of cementoblasts. Here we compared the transcriptional profiles of HCEM cells and HPL cells by microarray analysis in order to identify the genes that differ in their expression. We identified F-spondin as the gene demonstrating the high fold change expression in HCEM cells. F-spondin is an extracellular matrix protein required for pathfinding of commissural axons during floor plate development [7,8]. In the present study, to know the role of F-spondin for cementoblastic differentiation, we transfected F-spondin into HPL cells, and examined the expression of the mineralized related genes, COLI, ALP, Runx2, OCN, BSP, and CP-23 in vitro.

## Methods

These studies were performed in compliance with regulations administered by the experimentation committee of the Graduate School of Biomedical Sciences, Hiroshima University.

**Cell culture.** HCEM cells which we previously established [6] and human osteoblasts (NHOst, OTT4, and Ost) provided by Dr. Tahara (Hiroshima University) were cultured in Minimum Essential Medium Alpha ( $\alpha$ -MEM, Invitrogen, Grand Island, NY) with 10% fetal bovine serum (FBS) plus penicillin G solution (10 U/ml) and streptomycin (10 mg/ml) in a humidified atmosphere of 5% CO<sub>2</sub> at 37 °C. NHOst and Ost are normal human osteoblast cells, OTT4 is immortalized human osteoblast cell lines with *SV40-T* and *hTERT*. HPL cells were cultured in Dulbecco's Modified Eagle's Medium (DMEM, Nissui Pharmaceutical Co. Ltd.).

**Gene array analysis.** The human focus array using the system containing 8500 genes probes was used for comparing the transcriptional profiles between HCEM cells and HPL cells. This array contains a broad range of genes derived from publicly available, well-annotated mRNA sequences. Total RNA was isolated from cultures of confluent cells using the RNeasy Mini Kit (Qiagen, K.K., Tokyo, Japan) according to the manufacturer's instructions. Preparations were quantified and their purity was determined by standard spectrophotometric methods.

**Reverse transcription-polymerase chain reaction (RT-PCR).** Total RNA was isolated from cultures of confluent cells using the RNeasy Mini Kit (Qiagen) according to the manufacturer's instructions. Preparations were quantified and their purity was determined by standard spectrophotometric methods. cDNA was synthesized from 1  $\mu$ g total RNA according to the Rever Tra Dash (Toyobo Biochemicals, Tokyo, Japan). The oligonucleotide RT-PCR primers for human F-spondin, rat F-spondin, chemokine orphan receptor (CMKOR1), phosphotriesterase related (PTER), solute carrier family member1 (SLC14A1), and matrix metalloproteinase (MMP) 13 are listed in Table 1. Primers for COLI,

ALP, Runx2, OCN, BSP, CP-23, and glyceraldehyde-3-phosphate (GAPDH) were described previously [6]. Aliquots of total cDNA were amplified with 1.25 U rTaq-DNA polymerase (Qiagen), and amplifications were performed in a PC701 thermal cycler (Astec, Fukuoka, Japan) for 28–30 cycles after an initial 30 s denaturation at 94 °C, annealed for 30 s at 55–60 °C, and extended for 1 min at 72 °C in all primers. The amplification reaction products were resolved on 1.5% agarose/TAE gels (Nacalai Tesque, Inc., Kyoto, Japan), electrophoresed at 100 mV, and visualized by ethidium-bromide staining.

**Generation of F-spondin highly expressing HPL cells.** Packaging GP-293 cells (Clontech, Palo Alto, CA) were transfected with retroviral plasmid encoding a rat F-spondin cDNA according to the manufacturer's instructions. A plasmid pMT21-FP5, encoding rat F-spondin cDNA, was kindly provided by Dr. Klar (Hebrew University). After 48 h of transfection, the virus-containing medium was collected and supplemented with 8  $\mu$ g/ml polybrene (Sigma, St. Louis, MO). Then, the culture medium of the target cells was replaced with this viral supernatant for 24 h. This infection process was repeated a second time after a 12 h recovery in normal medium. The stable clones were obtained by puromycin selection (1  $\mu$ g/ml) in the culture medium.

And clones were examined expressions of F-spondin by RT-PCR and Western blot. Four F-spondin-expressing clones were chosen for the subsequent experiments. A rat F-spondin cDNA was also cloned into pBICEP-CMV-2 (Sigma) and was transfected into 293T cells.

**Western blot analysis.** Subconfluent cells, in 90 mm culture dishes, were used for Western blot analysis. Western blotting was carried out as we described previously [9]. Thirty  $\mu$ g/ml of protein was solubilized in Laemmli sample buffer by boiling, and subjected to 10% sodium dodecyl sulfate-polyacrylamide gel electrophoresis (SDS-PAGE), followed by electroblotting onto a nitrocellulose filter. The filter was blocked for 1 h at 4 °C with phosphate-buffered saline (PBS) buffer containing 5% nonfat dried milk powder. Western blot analysis was performed using an anti-SPON1 polyclonal antibody (ProSci, Flint Place Poway, CA), anti-FLAG M2 monoclonal antibody (Sigma), and  $\beta$ -actin monoclonal antibody (Sigma) dissolved in PBS containing 5% nonfat dried milk powder and incubating for 60 min at room temperature. Incubation with a secondary peroxidase-coupled goat anti-IgY Fc antibody (ProSci) and a secondary peroxidase-coupled goat anti-mouse antibody was performed under the same conditions. For detection of the immunocomplex, the ECL Western blotting detection system (Amersham, Buckinghamshire, UK) was used.

**Tissue samples.** Tissue samples of periodontal tissues including tooth were retrieved from the Surgical Pathology Registry of Hiroshima University Hospital, after approval by the Ethical Committee of our institutions. 3.7% buffered-formalin fixed, decalcified for 3 days, and paraffin-embedded tissues were used for immunohistochemical examination.

**Immunohistochemical staining.** To examine expression of F-spondin in seven human periodontal tissues cases, the 4.5  $\mu$ m sections were stained immunohistochemically with an anti-SPON1 antibody (Prosci). Endogenous peroxidase was quenched by incubating with 0.3% H<sub>2</sub>O<sub>2</sub> in methanol for 30 min. Nonspecific staining was blocked using Dako Protein Block

Table 1  
Oligonucleotide primer sequences utilized in the RT-PCR

RT-PCR primer set		Sequence	GenBank Accession numbers
F-spondin (human)	F	5'-ggaattgttcgagaagaca-3'	NM_006108
	R	5'-gggtttgttgggtgactcat-3'	
F-spondin (rat)	F	5'-gccgaagcttatgagctatctcccgcg-3'	NM_172067
	R	5'-gccgctcgagctaacaaagggtgcacgttgc-3'	
CMKOR1	F	5'-acgtgggtgctctcttctgtg-3'	NM_020311
	R	5'-agcatcaagacccgaagcta-3'	
PTER	F	5'-ttagccgagacacagacagc-3'	NM_030664
	R	5'-cgatcttcacagccctcttc-3'	
SLC14A1	F	5'-cacgagtcatttctgctga-3'	NM_015865
	R	5'-acacaaggatagggtgcag-3'	
MMP13	F	5'-ctgagaggctccgagaaatg-3'	NM_002427
	R	5'-ggctcttgagtggtcaaga-3'	

Serum Free (Dako, Carpinteria, CA). The sections were incubated with the primary antibody (1:500) for overnight at 4 °C, and then incubated with a secondary peroxidase-coupled goat anti-IgY Fc antibody (ProSci) for 30 min. For visualization, they were treated with Liquid DAB (3,3'-diaminobenzidine) Chromogen Syatem (Dako) according to the manufacturer's protocol.

**Measurement of ALP Activity.** The quantitative analysis of ALP activity was performed biochemically by Bessey-Lowry enzymologic method using nitrophenyl phosphate as a substrate [10]. Cells were plated in 24-well culture plates ( $1 \times 10^5$  cells per well) and cultured in DMEM containing 10% FBS, penicillin G sodium (10 U/ml) and streptomycin sulfate (10 mg/ml) for confluent that cells were plated for 1week. The cells were washed with PBS and homogenized ultrasonically in 0.5 ml of 10 mM Tris-HCl buffer (pH 7.4) containing 25 mM MgCl<sub>2</sub>. Aliquots of the homogenates were used for quantification of ALP activity.

**Collagen assay.** The measurement of collagen concentration was performed using Sircol™ Collagen Assay kit (Biocolor, Northern Ireland) according to the manufacturer's instruction. Cells were plated in 24-well culture plates ( $1 \times 10^5$  cells per well), and cultured in DMEM containing 10% FBS, penicillin G sodium (10 U/ml) and streptomycin sulfate (10 mg/ml) for confluent that cells were plated for 1 week. The culture media were used for measurement of collagen concentration.

**Statistical analysis.** The results of cell growth analysis and quantitative ALP activity were shown as means  $\pm$  SE and analyzed for significance

using Wilcoxon's test for non-paired examination. *P* values of less than 0.05 were judged to be statistically significant.

**Results**

*Identification of F-spondin as a cementoblast-specific highly expressed gene*

We previously established a HCEM cell line from root surface and a HPL cell line from middle part of periodontal ligament of the same extracted human teeth [6]. In the present study, therefore, we thought that to compare the transcriptional profiles of HCEM cells and HPL cells could be a good approach to identify genes that influence the nature of cementoblasts (Fig. 1A). By microarray analysis, several genes were selectively highly expressed in HCEM (Fig. 1A). Among these genes, one of the highly expressed genes was F-spondin. High expression of F-spondin in HCEM cells, but not in HPL cells, was confirmed by RT-PCR (Fig. 1B). As cementoblasts share many characteristics to

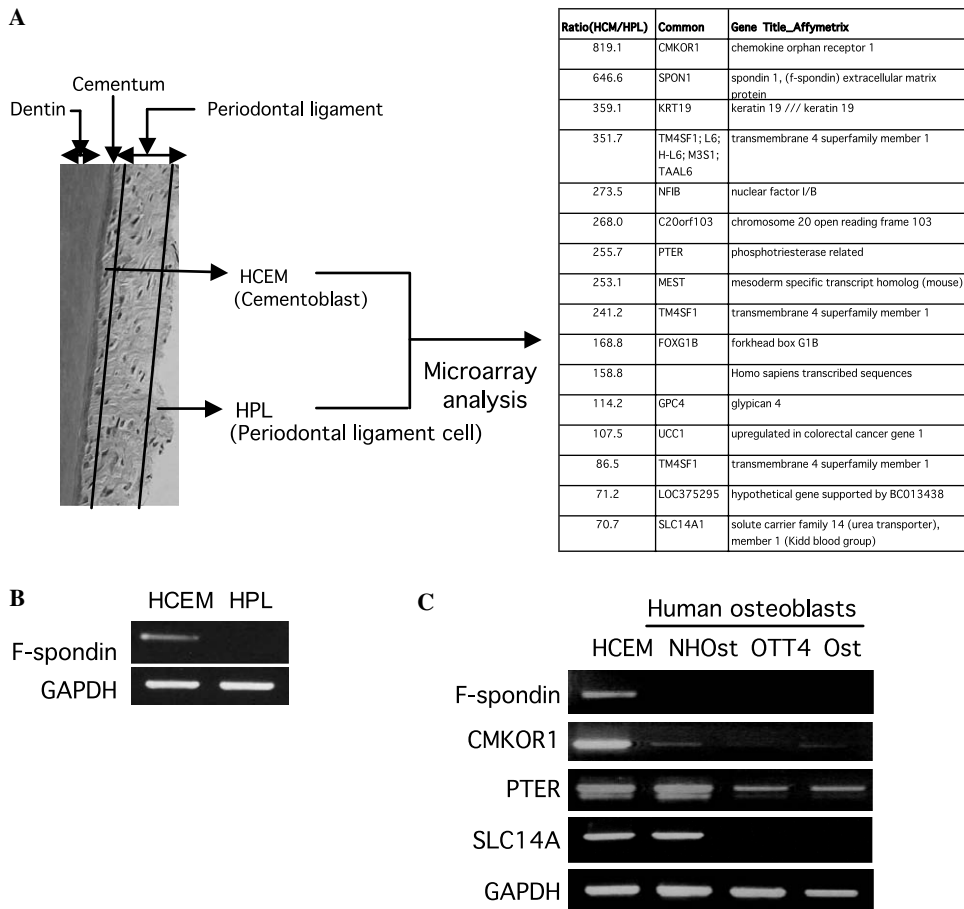


Fig. 1. F-spondin is identified as a cementoblast specific gene. (A) Human cementoblast-like (HCEM) cells and human periodontal ligament (HPL) cells were established from the same extracted teeth by using modified enzymatic digestion methods. The transcriptional profiles of HCEM cells and HPL cells were compared by microarray analysis. Highly expressed genes in HCEM cells are listed. Among these genes, F-spondin was identified the gene demonstrating the high fold change expression in HCEM cells. (B) The expression of F-spondin mRNA by RT-PCR. F-spondin mRNA expression is observed in HCEM cells, but not in HPL cells. (C) The expression of F-spondin mRNA is not observed in human osteoblast cell lines (NHOst, OTT4 and Ost). The expression of CMKOR1, PTER, and SLC14A1 is observed in both HCEM and NHOst.

osteoblasts, we examined the expression of F-spondin in HCEM and human osteoblasts (NHOst, OTT4, and Ost). Interestingly, HCEM expressed F-spondin mRNA, but osteoblasts did not (Fig. 1C). On the other hand, CMKOR1, PTER, and SLC14A1 were detected in both HCEM and NHOst (Fig. 1C). Thus, F-spondin is specifically expressed in cementoblasts among the cells, which compose the periodontal tissue.

#### *F-spondin expression in human periodontal tissue*

To confirm the specific expression of F-spondin in cementoblasts by immunohistochemical analysis, we first checked the accuracy of the antibody by Western blotting. F-spondin antibody specifically recognized F-spondin expression in FLAG-F-spondin transfected 293T cells (Fig. 2A). Then, we immunohistochemically examined its expression in seven normal periodontal tissues. As expected, F-spondin obviously expressed in the root lining cells (Fig. 2B).

#### *High expression of F-spondin promotes the differentiation of HPL cells in vitro*

To know the role of F-spondin for cementoblastic differentiation, we stably transfected F-spondin into HPL cells, which are the poorly differentiated cells in comparison with cementoblasts. We obtained 4 stable clones of F-spondin highly expressing HPL cells (HPL-spondin) (Fig. 3A). High expression of F-spondin changed the morphology, showing short spindle shapes in comparison with control cells (Fig. 3B). Next, we examined the expression of mRNA for COLI, ALP, Runx2, OCN, BSP, and CP-23 by RT-PCR in F-spondin highly expressing HPL cells. In addition, we examined collagen assay and ALP activity by biochemical methods. Higher expression of ALP,

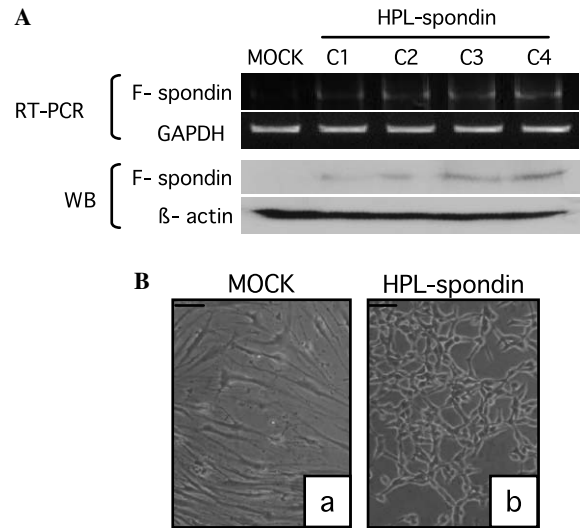


Fig. 3. High expression of F-spondin in HPL cells. (A) Stable clones of F-spondin highly expressing HPL-cells (HPL-spondin) expressed F-spondin mRNA and protein. GAPDH and  $\beta$ -actin were used for loading control in RT-PCR and Western blot analysis. (B) HPL-spondin cells show shorter spindle shapes (b) in comparison with control cells (a). (scale bar = 100  $\mu$ m).

OCN, and BSP, and lower expression of COLI were observed in F-spondin highly expressing HPL-cells in comparison with control cells (Fig. 4A). Both HPL-spondin cells and control cells expressed Runx2 and CP-23 mRNA at the same levels (Fig. 4A). The findings that increased expression of ALP mRNA and decreased expression of COLI mRNA in F-spondin highly expressing HPL cells were confirmed by collagen assay (Fig. 4B) and ALP activity (Fig. 4C), respectively. To know the reason why type I collagen decreased in HPL-spondin, we examined MMP13 expression. It is known that MMP13 is involved in type I and II collagen degradation and expressed in both terminal

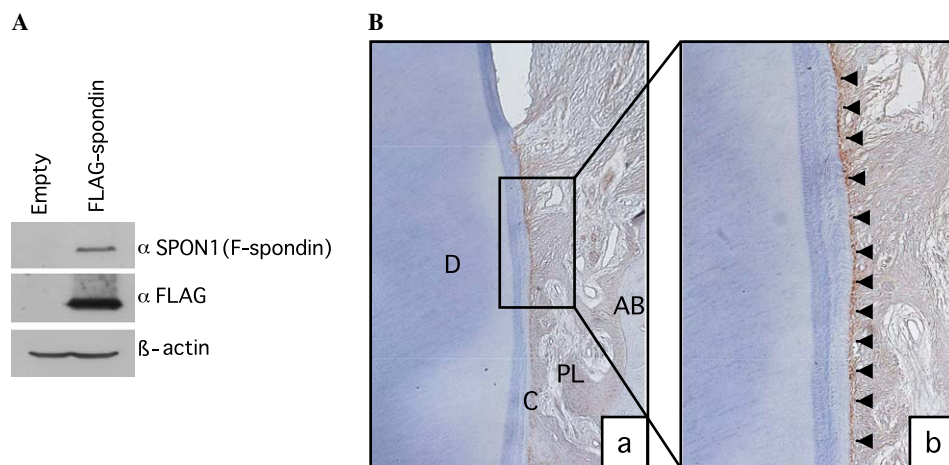


Fig. 2. F-spondin expression in human periodontal tissues. (A) Checking the accuracy of the anti-SPON1 antibody by Western blot. F-spondin antibody specifically recognizes F-spondin in FLAG-F-spondin transfected 293T cells. (B) Immunohistochemical staining with the anti-SPON1 antibody in human periodontal tissue. High expression of F-spondin was observed in cell located along the root surface (triangles). C, cementum; D, dentin; PL, periodontal ligament; AB, alveolar bone. Original magnification  $\times 40$  (a),  $\times 200$  (b).

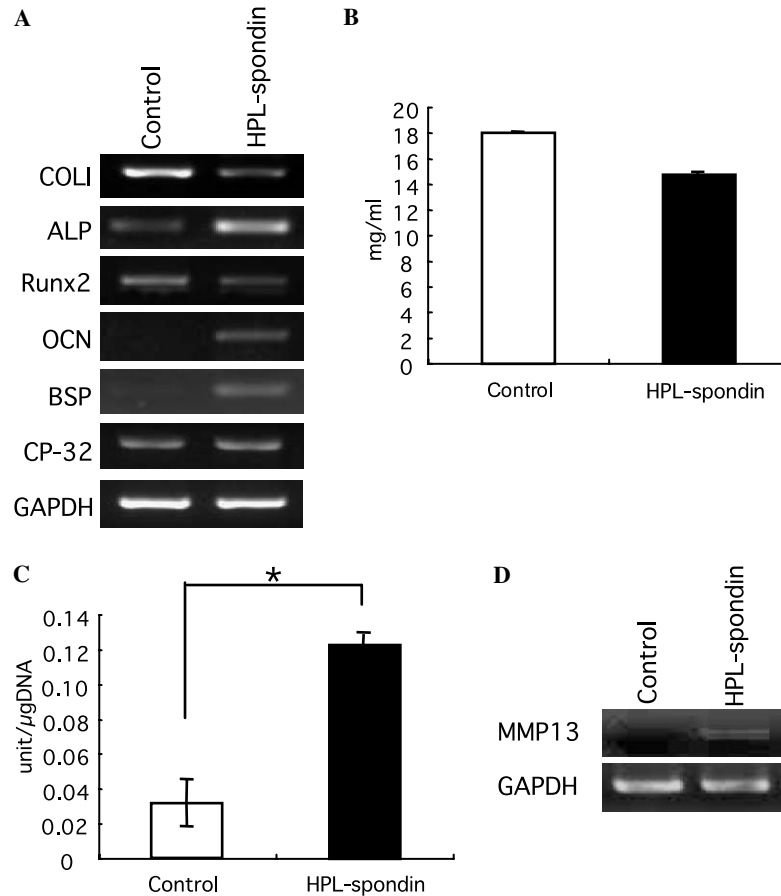


Fig. 4. F-spondin promotes the differentiation of HPL cells in vitro. (A) Expression of mRNA for COL1, ALP, Runx2, OCN, BSP, and CP-23 by RT-PCR in HPL-spondin. Higher expression of ALP, OCN, and BSP, and lower expression of COL1 are observed in HPL-spondin in comparison with control cells. Both HPL-spondin and control cells express Runx2 and CP-23 mRNA at the same levels. (B) Measurement of collagen concentration. Collagen concentration tends to decrease in HPL-spondin by collagen assay. (C) ALP activity by biochemical methods. Increased ALP activity is observed in HPL-spondin cells in comparison with control cells. \*Significant difference ( $P < 0.05$ ). (D) Expression of MMP13 mRNA by RT-PCR. HPL-spondin cells express MMP13 mRNA at higher level in comparison with control cells.

hypertrophic chondrocytes and osteoblasts [11,12]. Interestingly, HPL-spondin cells expressed MMP13 mRNA at higher level in comparison with control cells (Fig. 4D).

## Discussion

The periodontium is a complex structural and functional unit consisting of four different components, i.e., gingiva, alveolar bone, periodontal ligament, and cementum [13]. Cementum plays an important role of the attachment of periodontal ligament to roots. The progenitor cells in bone marrow spaces migrate into the perivascular area of the periodontal ligament and move to the bone and tooth surface, and then differentiate into osteoblasts or cementoblasts [14,15]. In similar to osteoblasts, cementoblasts express noncollagenous bone matrix proteins, COL1, ALP, Runx2, OCN, BSP, and so on [15,16]. Recently, CAP and CP-23 have been identified as new makers for cementum or cementum-periodontal ligament [2,5]. However, we still do not know the detailed mechanism of cementoblastic or osteoblastic differentiation from progen-

itor cells in bone marrow spaces. To study the detailed mechanism of cementoblastic differentiation and proliferation of cementoblasts, we recently established a human cementoblast-like cell line, HCEM, from root lining cells and a human periodontal ligament cell line, HPL, from middle part of periodontal ligament of the same teeth by using enzymatic digestion method [6].

In the present study, to identify the molecules playing the role for cementoblastic differentiation, we compared gene expression profiles between HCEM and HPL by microarray analysis. As HCEM and HPL were established from same teeth, we thought that comparing the gene expression profiles between them could be a good approach for identifying the gene of cementoblastic differentiation. Here we found several genes highly expressed in HCEM cells in comparison with HPL cells, but most genes except for F-spondin expressed in osteoblasts by RT-PCR (Fig. 1A and C). Therefore, in the present study, we focused on F-spondin. In fact, the expression of F-spondin mRNA was observed only in cementoblast, but not in osteoblasts and periodontal ligament cells (Fig. 1B and C).

Moreover, F-spondin expression was observed only in the cells on the root surface (cementoblasts) by immunohistochemistry (Fig. 2B). These findings suggest that F-spondin may be a specific molecule for cementoblasts among the periodontal tissues.

F-spondin is an extracellular matrix protein and promotes neurite outgrowth of dorsal root ganglion cells [8,17] and spinal cord neurons in cell culture [18]. F-spondin promotes the differentiation of neural precursor cells to cells with the characteristics of neurons [19]. This is the first report on the function of F-spondin in cementoblasts. It is considered that periodontal ligament consists of different cell populations in various differentiation stages according to the position in periodontal ligament. We previously reported that cell populations with larger growth potential were generally located in the middle position of periodontal ligament and cell populations with higher ALP and mineralization activities toward the surface of the root in rat periodontal ligament [20]. Therefore, we transfected F-spondin into HPL cells which are more poor cell population than HCEM cells. Interestingly, high expression of F-spondin changed the morphology (Fig. 3C) and increased the expressions of ALP, OCN, and BSP mRNA, and ALP activity (Fig. 4A and C) in HPL cells, suggesting that F-spondin may influence the differentiation of HPL cells. As cementoblasts and osteoblasts expressed ALP, OCN, and BSP, which play an important role for the mineralization [10], F-spondin promoted the differentiation of HPL cells toward the mineralization. Moreover, both HPL-spondin cells and control cells expressed CP-23 mRNA (Fig. 4A). CP-23 was expressed in mature cementum, cementoblasts, and periodontal ligament cells but not osteoblasts [21]. Therefore, F-spondin promoted cementoblastic differentiation not osteoblastic differentiation. We also found that high expression of F-spondin decreased the expression of COL1 mRNA and collagen concentration (Fig. 4A and B). This finding may be caused by increased expression of MMP13, because MMP13 is known to be a collagenase of type I collagen and to increase in the process of osteoblastic differentiation [22].

By microarray analysis, we could find a lot of genes that highly expressed in HCEM. For instance, CMKOR1, PTER, and SLC14A1 are also highly expressed in HCEM. Nuclear Factor I (NFIB), which is site specific DNA-binding protein [23], is also listed. In the future, we will examine if these genes are involved in cementoblastic differentiation. In summary, in the present study, we demonstrated a critical role of F-spondin for cementoblastic differentiation. Our findings provide new and important information for understanding the mechanism of cementoblastic differentiation. We suggest that F-spondin could be used for a novel molecular target for periodontal regeneration therapy.

#### Acknowledgments

We thank Dr. A. Klar for providing F-spondin vector. We also thank Dr. H. Tahara for providing human osteo-

blasts and Ms. A. Imaoka for supporting by microarray. This work was supported by in part by Grants-in-Aid from the Ministry of Education, Science and Culture of Japan to M.K. (18791350), Y.A. (A1-16209063) and T.T. (B1-1739048600).

#### References

- [1] A.R. Ten Cate, The periodontium: Oral Histology: Development, Structure and Function, Mosby, St. Louis, 2003, 276–279.
- [2] H. Arzate, S.W. Olson, R.C. Page, A.M. Gown, A.S. Narayanan, Production of a monoclonal antibody to an attachment protein derived from human cementum, *FASEB J.* 6 (1992) 2990–2995.
- [3] M. Saito, M. Iwase, S. Maslan, N. Nozaki, M. Yamauchi, K. Hanada, O. Takahashi, S. Sato, T. Kawase, T. Teranaka, A.S. Narayanan, Expression of cementum-derived attachment protein in bovine tooth germ during cementogenesis, *Bone* 29 (2001) 242–248.
- [4] R. Hara, M. Wato, A. Tanaka, Maker of cemento-periodontal ligament junction associated with periodontal regeneration, *J. Periodont. Res.* 40 (2005) 231–238.
- [5] M.A. Alvarez-Perez, S. Narayanan, M. Zeichner-David, B.R. Carmona, H. Arzate, Molecular cloning, expression and immunolocalization of a novel human cementum-derived protein (CP-23), *Bone* 38 (2006) 409–419.
- [6] M. Kitagawa, H. Tahara, S. Kitagawa, H. Oka, Y. Kudo, S. Sato, I. Ogawa, M. Miyauchi, T. Takata, Characterization of established cementoblast-like cell lines from human cementum lining cells in vitro and in vivo. *Bone*. in press.
- [7] Y. Feinstein, A. Klar, The neuronal class 2 TSR proteins F-spondin and midin: a small family with divergent biological activities, *Int.J. Biochem. Cell Biol.* 36 (2004) 975–980.
- [8] A. Klar, M. Baldassare, T.M. Jessekl, F-spondin: a gene expressed at high levels in the floor plate encodes a secreted protein that promotes neural cell adhesion and neurite extension, *Cell* 69 (1992) 95–110.
- [9] S. Kitajima, Y. Kudo, I. Ogawa, T. Bashir, M. Kitagawa, M. Miyauchi, M. Pagano, T. Takata, Role of Cks1 overexpression in oral squamous cell carcinomas: cooperation with Skp2 in promoting p27 degradation, *Am. J. Pathol.* 165 (2004) 2147–2155.
- [10] O.A. Bessey, O.H. Lowry, M.J. Brock, A method for the rapid determination of alkaline phosphatase with five cubic millimeter of serum, *J. Biol. Chem.* 164 (1946) 321–329.
- [11] N. Ortega, D. Behonick, D. Stickens, Z. Werb, How proteases regulate bone morphogenesis, 995 (2003) 109–116.
- [12] D. Stickens, D.J. Bshonick, N. Orthalie, B. Heyer, B. Hartenstein, Y. Yu, A.J. Fosang, M. Schorpp-Kistner, P. Angel, Z. Werb, Altered endochondral bone development in matrix metalloproteinase 13-deficient mice, *Development* 131 (2004) 5883–5895.
- [13] D.D. Bosshardt, Are cementoblasts a subpopulation of osteoblasts or a unique phenotype? *J. Dent. Res.* 84 (2005) 390–406.
- [14] C.A.G. McCulloch, A.H. Melcher, Cell density and cell generation in the periodontal ligament of mice, *Am. J. Anat.* 167 (1983) 43–58.
- [15] C.A.G. McCulloch, E. Nemeth, B. Lowenberg, A.H. Melcher, Paravascular cells in endosteal spaces of alveolar bone contribute to periodontal ligament cell population, *Anat. Rec.* 219 (1987) 233–242.
- [16] J.A. D'Errico, R.L. MacNeil, T. Takata, J. Berry, C. Strayhorn, M.J. Somerman, Expression of bone associated markers by tooth root lining cells, in situ and in vitro, *Bone* 20 (1997) 117–126.
- [17] T. Burstyn-Cohen, A. Frumkin, Y.T. Xu, S.S. Scherer, A. Klar, Accumulation of F-spondin in injured peripheral nerve promotes the outgrowth of sensory axons, *J. Neuron* 23 (1998) 8875–8885.
- [18] T. Burstyn-Cohen, V. Tzarfaty, A. Frunrkin, Y. Feinstein, E. Stoecki, A. Klar, F-spondin is required for accurate pathfinding of commissural axons at the floor plate, *Neuron* 23 (1999) 233–246.
- [19] D. Schubert, A. Klar, M. Park, R. Dargusch, W.H. Fischer, F-spondin promotes nerve precursor differentiation, *J. Neurochem.* 10 (2005), 1111/j.1471-4159.

- [20] T. Kaneda, M. Miyauchi, T. Takekoshi, S. Kitagawa, M. Kitagawa, H. Shiba, H. Kurihara, T. Takata, Characteristics of periodontal ligament subpopulations obtained by sequential enzymatic digestion of rat periodontal ligament, *Bone* 38 (2006) 420–426.
- [21] H. Arzate, S.W. Olson, R.C. Page, A.M. Gown, A.S. Narayanan, Production of a monoclonal antibody to an attachment protein derived from human cementum, *FASEB J.* 6 (1992) 2990–2995.
- [22] J.P. Tuckermann, K. Pittois, N.C. Partridge, J. Merregaert, P. Angel, Collagenase-3 (MMP-13) and integral membrane protein 2a (Itm2a) are marker genes of chondrogenic/osteoblastic cells in bone formation: sequential temporal, and spatial expression of Itm2a, alkaline phosphatase, MMP-13, and osteocalcin in the mouse, *J. Bone. Miner. Res.* 15 (2000) 1257–1265.
- [23] R.M. Gronostajski, Roles of the NFI/CTF gene family in transcription and development, *Gene* 249 (2000) 31–45.

## An inhibitory effect of A20 on NF- $\kappa$ B activation in airway epithelium upon influenza virus infection

Akira Onose<sup>a</sup>, Shu Hashimoto<sup>a,\*</sup>, Shinichi Hayashi<sup>a</sup>, Shuichiro Maruoka<sup>a</sup>, Fumio Kumasawa<sup>a</sup>, Kenji Mizumura<sup>a</sup>, Itsuro Jibiki<sup>a</sup>, Ken Matsumoto<sup>a</sup>, Yasuhiro Gon<sup>a</sup>, Tomoko Kobayashi<sup>a</sup>, Noriaki Takahashi<sup>a</sup>, Yasuko Shibata<sup>b</sup>, Yoshimitsu Abiko<sup>b</sup>, Toshikatsu Shibata<sup>c</sup>, Kazufumi Shimizu<sup>c</sup>, Takashi Horie<sup>a</sup>

<sup>a</sup> Division of Respiratory Medicine, Department of Internal Medicine, Nihon University School of Medicine, 30-1 Oyaguchikamimachi, Itabashi-ku, Tokyo 173-8610, Japan

<sup>b</sup> Department of Biochemistry and Molecular Biology, Nihon University School of Dentistry at Matsudo, Japan

<sup>c</sup> Department of Microbiology, Nihon University School of Medicine, Japan

Received 22 September 2005; received in revised form 15 March 2006; accepted 27 March 2006

Available online 20 May 2006

### Abstract

Influenza is a major disease in humans. The reemergence of avian influenza A viruses has indicated that hyperinflammatory responses are closely related to the severity of disease. Influenza virus infection induces nuclear transcription factor kappaB (NF- $\kappa$ B) activation. NF- $\kappa$ B and NF- $\kappa$ B-dependent gene products promote lung inflammation and injury. Therefore, it is important to investigate the means to attenuate NF- $\kappa$ B activation. A20 is a cytoplasmic zinc finger protein that inhibits NF- $\kappa$ B activity. However, little is known about the role of A20 in influenza virus infection. Here, we have examined the role of A20 in influenza virus infection-induced NF- $\kappa$ B promoter activation in human bronchial epithelial cells. The results showed that (1) A20 protein and mRNA are inducible and expressed in the lung from mice and human bronchial epithelial cells upon influenza virus infection; (2) NF- $\kappa$ B promoter activation was induced in bronchial epithelial cells upon influenza virus infection; and (3) overexpression by transient transfection of A20 attenuated NF- $\kappa$ B promoter activation in bronchial epithelial cells. These results indicate that A20 may function as a negative regulator of NF- $\kappa$ B-mediated lung inflammation and injury upon influenza virus infection, thereby protecting the host against inflammatory response to influenza virus infection.

© 2006 Elsevier B.V. All rights reserved.

**Keywords:** A20; Influenza virus; NF- $\kappa$ B; Bronchial epithelium; Inflammation

### 1. Introduction

Influenza virus infection is an acute respiratory infection and one of the most pandemic infectious diseases (Thompson et al., 2003). Highly pathogenic avian influenza virus subtypes H5N1 and H7N7 caused acute respiratory illness including fetal disease (Shortridge, 2003). New strains of influenza A viruses emerge in humans. Vaccine and anti-neuraminidase inhibitors are widely used for the prevention and treatment of influenza

virus infection, but it is not logically possible to prepare vaccines against all strains of influenza virus, especially unexpected outbreak of non-human subtypes of influenza A viruses (Webby and Webster, 2003; Cheng et al., 2004; Gubareva et al., 2000). The most severe complications are viral pneumonia and lung injury (Yuen et al., 1998; Peiris et al., 2004; Tran et al., 2004; Fouchier et al., 2004). During the development of viral pneumonia and lung injury, influenza virus infection-associated proinflammatory responses are involved in the pathogenesis of viral pneumonia and lung injury (Peiris et al., 2004; Guan et al., 2004; Cheung et al., 2002; Van Reeth, 2000). Therefore, it is important to clarify how to attenuate and terminate proinflammatory responses.

\* Corresponding author. Tel.: +81 3 3972 8111; fax: +81 3 3972 2893.

E-mail address: [shuh@med.nihon-u.ac.jp](mailto:shuh@med.nihon-u.ac.jp) (S. Hashimoto).

Activation of the nuclear transcription factor kappa-B (NF- $\kappa$ B) is a hallmark of inflammatory processes induced by various stimuli, including viral pathogens (Fan et al., 2001; Santoro et al., 2003). NF- $\kappa$ B activation during viral infection has been interpreted as a protective response of the host against viral infection (Santoro et al., 2003). NF- $\kappa$ B regulates anti-viral cytokine, interferon (IFN) and tumor necrosis factor (TNF)- $\alpha$  against influenza virus infection (Santoro et al., 2003; Seo and Webster, 2002; Julkunen et al., 2000). In contrast, recent data have indicated that NF- $\kappa$ B activity is associated with influenza virus infectivity and propagation (Nimmerjahn et al., 2004; Wurzer et al., 2004). Therefore, it is important to investigate the regulatory mechanism in NF- $\kappa$ B activity induced upon influenza virus infection. Preliminary data on comprehensive analysis of gene expression in human bronchial epithelial cells upon influenza virus infection have shown that A20 mRNA expression is up-regulated in bronchial epithelial cells upon influenza virus infection.

The cytoplasmic zinc finger protein A20 is encoded by an immediate early response gene and originally identified as a TNF- $\alpha$  and interleukin (IL)-1-inducible gene product in endothelial cells (Song et al., 1996). A20 acts as an inhibitor of NF- $\kappa$ B activation and NF- $\kappa$ B-dependent gene expression (Gon et al., 2004; Hu et al., 1998). The expression of A20 is itself under the control of NF- $\kappa$ B (Krikos et al., 1992), suggesting that A20 is involved in a negative feedback regulation of NF- $\kappa$ B activation and NF- $\kappa$ B-dependent gene expression. Therefore, it is possible that A20 may be a negative regulator of influenza virus infection-induced inflammatory responses. However, the role of A20 in inflammatory responses has not been clarified. In order to do so, we examined the role of A20 in NF- $\kappa$ B activation in human airway epithelial cells upon influenza virus infection in this study.

## 2. Materials and methods

### 2.1. Virus, mice and cells

Influenza virus A/Udon/307/72 (H3N2) and A/PR/8/34 (H1N1) were grown as previously described (Kujime et al., 2000). Five- to six-week-old C57/BL mice were purchased from Oriental Co., Inc. (Tokyo, Japan). Mice were housed in pathogen free conditions in accordance with the animal care guidelines of Nihon University School of Medicine. Bronchial epithelial cell lines, NCI-H<sub>292</sub>, and human embryonic kidney cell lines, HEK293, were obtained from American Type Culture as previously described (Gon et al., 2004).

### 2.2. Affymetrix gene chip analysis

Serum-starved bronchial epithelial cells were infected with influenza virus (A/Udon/307/72) at multiplicity of infection (moi) of 5 and cultured for 6 h. Total RNA was isolated from the harvested cells using RNeasy Mini Kit (Qiagen, Valencia, CA). Preparations of biotin-labeled cRNAs and hybridization to the HU-U95A Gene Chip set (Affymetrix, Santa Clara, CA)

were performed according to the manufacturer's instructions. Prior to the hybridization to the HU-U95A Gene Chip, cRNAs were first hybridized to the Test 3 chip to confirm that differences in housekeeping genes between the samples were less than 10%.

### 2.3. A20 mRNA and protein expression

For analysis of A20 mRNA expression in bronchial epithelial cells, serum-starved bronchial epithelial cells were infected with influenza virus (A/Udon/307/72) at moi of 5 and cultured. A20 mRNA and G6PDH mRNA expression were determined at the time indicated after influenza virus infection. For analysis of A20 mRNA and protein expression in the lung from mice, the mice were intranasally inoculated with 50  $\mu$ l of 10<sup>4</sup> PFU of influenza virus (A/PR/8/34) or 50  $\mu$ l of PBS (control mice). The mice were anesthetized and sacrificed, and the lungs were removed at the desired times as indicated after infection. For quantitative PCR analysis of mRNA expression, total mRNA was isolated from BEC and homogenized lung from mice using an RNA gents total RNA isolation system (Promega, Madison, WI) and reverse transcribed with Improm-II reverse transcriptase (Promega). Primers for each A20 were designed using Primer Express 2.0 software (Applied Biosystems, Foster City, CA). The following oligonucleotides were used: human A20 sense, 5'-CTGCCAGGAATGCTACAGATAC-3'; human A20 anti-sense, 5'-GTGGAACAGCTCGGATTTTCAG-3'; mouse A20 sense, 5'-AAGCTTCTAAAGGAGTACTTGATAGTGATG-3'; mouse A20 anti-sense, 5'-CAATTTTGCAGCGTTGATCAG-3'. Quantitative RT-PCR was carried out by an ABI PRISM 7300 sequence detection system using SYBR Green PCR Master Mix (Applied Biosystems). Immunohistochemical analysis of A20 protein expression was performed using immunoperoxidase technique as previously described (Koura et al., 2000). The primary antibody was rabbit anti-human A20 polyclonal antibody (Santa Cruz, Santa Cruz, CA) and nonimmune normal rabbit IgG was used as a negative control. Counterstaining was performed with haematoxylin.

### 2.4. Western blot analysis of I $\kappa$ B phosphorylation and total I $\kappa$ B

Serum-starved bronchial epithelial cells were infected with influenza virus (A/Udon/307/72) at moi of 5 and were then cultured for desired times as indicated after infection with influenza virus. Western blotting analysis of I $\kappa$ B $\alpha$  phosphorylation and degradation was performed using rabbit polyclonal antibody to phosphorylated I $\kappa$ B (Promega) and rabbit polyclonal antibody to I $\kappa$ B (Promega).  $\beta$  Tubulin was used as a housekeeping protein.

### 2.5. Plasmids, transfection and luciferase reporter assay

For analysis of NF- $\kappa$ B luciferase activity, serum-starved bronchial epithelial cells, which had been transiently transfected by NF- $\kappa$ B-Luc reporter plasmid, were infected with influenza virus (A/Udon/307/72) at moi of 5 and were then cultured for the desired time as indicated. For analysis of the effect of A20,

serum-starved bronchial epithelial cells were transiently transfected with the pcDNA3-A20 expression vectors (Miller et al., 1997) using FuGENE6 (Roche Diagnostics Corp., Indianapolis, IN). The total amount of cDNA was kept constant by supplementation with empty vector, pcDNA3 (Invitrogen, Carlsbad, CA). Every transfection included 500 ng of NF- $\kappa$ B-Luc reporter plasmid (Stratagene, La Jolla, CA) together with 5 ng of pRL-SV40-Renilla for normalization of transfection efficiency. After 24 h with the transfection, bronchial epithelial cells were infected with influenza virus (A/Udon/307/72) at moi of 5 and NF- $\kappa$ B reporter activity was determined at the desired times as indicated after infection with influenza virus as previously described (Jibiki et al., 2003).

### 2.6. Virus protein synthesis

Influenza virus protein synthesis was determined by Western blotting using the polyclonal anti-influenza virus serum as previously described (Maruoka et al., 2003). Briefly, HEK293 cells were transiently transfected with pcDNA3-Myc-A20 (2  $\mu$ g) or pcDNA3 (2  $\mu$ g) as control. At 24 h after transfection, the cells were infected with influenza virus (A/Udon/307/72) at moi of 5 for the desired times as indicated. At the end of cultivation, cells were then lysed and immunoblotted with antibodies to polyclonal anti-influenza virus (1:1000 dilution for overnight at 4) and anti-myc antibody (9E10) as previously described (Maruoka et al., 2003). Anti-rabbit-horseradish peroxidase antibody was used as a second antibody (1:2000 dilution for 1 h at room temperature). The antibody-antigen complexes were detected using the ECL system (Amersham-Pharmacia Biotech). The appropriate expressions of Myc-A20 were confirmed in the lysate.

### 2.7. Statistical analysis

Statistical significance was analyzed by using analysis of variance (ANOVA). *P* value of less than 0.05 was considered significant.

## 3. Results

### 3.1. Comprehensive gene expression in bronchial epithelial cells upon influenza virus infection

For each gene on the chip-reading software makes an expression call, such as “present”, “absent” or “marginal” according to the difference between fluorescence intensity in perfectly matched sequences and mismatched sequences containing a single base pair mutation. To minimize the number of false positive results, we excluded the sequences whose expression call of sample infected with influenza virus was determined as “absent”. We were able to detect 5998 genes among the 12,000 genes represented in the chip. We made three criteria for the list that show genes induced by influenza virus infection: (1) the intensity of expression was with at least a 10-fold increase by influenza virus infection, (2) mean expression intensity, determined by the average difference between

Table 1

GeneBank accession no.	Gene description	Uninfected intensity	IV infected intensity	Fold increase
AF008445	Phospholipid scramblase	446	10,992	24.6
M30818	Interferon-induced cellular resistance mediator protein (MxB)	735	16,876	23.0
X04602	Interleukin BSF-2 (B-cell differentiation factor)	61	1392	22.8
M33882	p78 protein mRNA (MxA)	874	19,923	22.8
U52513	RIG-G mRNA	873	19,595	22.4
X02875	Oligo A synthetase E	892	18,356	20.6
U72882	Interferon-induced leucine zipper protein (IFP35)	986	18,048	18.3
M13755	Interferon-induced 17-kDa/15-kDa protein	909	14,383	15.8
M55153	Transglutaminase (TGase)	759	10,685	14.1
M24594	Interferon-inducible 56-kDa protein	1090	15,211	14.0
U59877	Low-Mr GTP-binding protein (RAB31) mRNA	629	7332	11.7
M87434	71-kDa 2 5 oligoadenylate synthetase (p69 2-5A synthetase)	1063	11,878	11.2
D90070	ATL-derived PMA-responsive (APR) peptide	195	2166	11.1
S82240	RhoE=26-kDa GTPase homolog	157	1738	11.1
U18671	Stat2 gene	424	4641	10.9
U77643	K12 protein precursor	1475	15,632	10.6
U15932	Dual-specificity protein phosphatase mRNA	1065	11,256	10.6
M59465	Tumor necrosis factor- $\alpha$ inducible protein A20 mRNA	353	3717	10.5
U51010	Nicotinamine <i>N</i> -methyltransferase	951	9826	10.3
X13839	Vascular smooth muscle $\alpha$ -actin	81	829	10.2

fluorescence in perfectly matched sequences and mismatched sequences, in the sample infected with influenza virus, was greater than 100 (because low intense results were sometimes inaccurate), and (3) expression difference between untreated cells and influenza virus infected cells was statistically significant. Table 1 represents the mRNA expression level indicated as the average difference in only medium treated or influenza virus infected cells. When using these criteria, influenza virus infection was found to up-regulate the expressions of 32 genes. Among these genes, A20 is a remarkable gene that inhibits NF- $\kappa$ B activity. Therefore, the study was conducted to examine the effect of A20 in NF- $\kappa$ B activity induced upon influenza virus infection.

### 3.2. A20 mRNA expression in human bronchial epithelial cells and lung

To verify the data on A20 mRNA expression obtained by Gene Chip analysis, we quantitatively examined A20 mRNA expression in bronchial epithelial cells and the lung from mice upon influenza virus infection using quantitative RT-PCR.

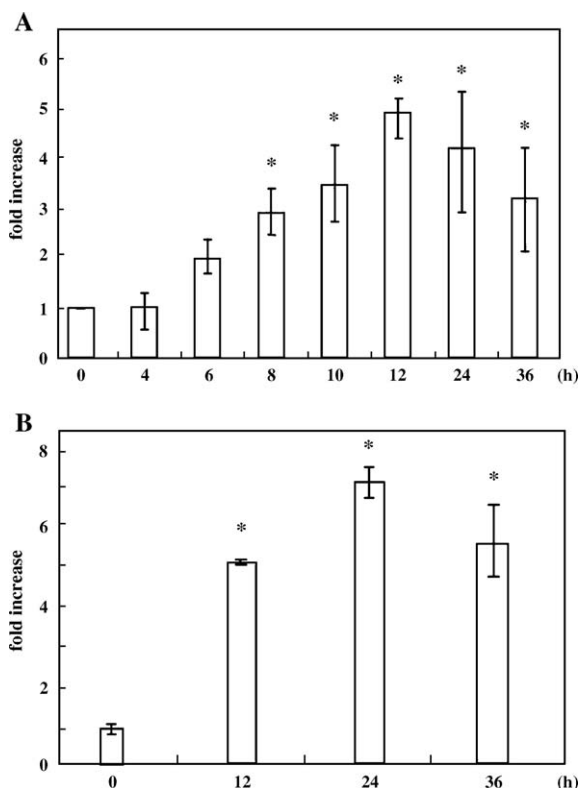


Fig. 1. A20 mRNA expression in human bronchial epithelial cells and in lung homogenates from mice. A20 mRNA expression in bronchial epithelial cells (A) and in the lungs from mice (B) were analyzed at times as indicated after influenza virus infection by quantitative RT-PCR amplification. The results are expressed as means  $\pm$  S.D. of three different experiments. \* indicates  $P < 0.05$  compared with mRNA levels in influenza virus-uninfected bronchial epithelial cells (A). \* indicates  $P < 0.05$  compared with mRNA levels in the lung from influenza virus-uninfected mice (B).

A20 mRNA expression in bronchial epithelial cells increased at 8 h, sustained from 8 to 12 h, and thereafter decreased at 24 h (Fig. 1A). A20 mRNA expression in the homogenized lung from mice increased at 12 h and was maximal at 24 h and thereafter decreased at 36 h (Fig. 1B). These results indicate that A20 mRNA is inducible and expressed in the lung from mice and bronchial epithelial cells in a time-dependent manner.

### 3.3. A20 protein expression in the lung

To verify the data on A20 mRNA expression at the levels of protein expression and identify the cellular source of A20, we performed immunohistochemistry on lung tissue from mice upon influenza virus A/PR/8 infection. We stained lung tissue specimens with anti-A20 antibody. Representative results are shown in Fig. 2. A20 is positively stained in the bronchial epithelial cells and alveolar epithelial cells of lung specimens from influenza virus-infected mice by anti-A20 antibody (Fig. 2A), but not in those from influenza virus-uninfected mice (Fig. 2C). The lung tissue specimens of lung from either influenza virus infected or uninfected mice were not stained with control antibody, normal rabbit IgG (Fig. 2B and D).

### 3.4. Influenza virus infection induces I $\kappa$ B phosphorylation and NF- $\kappa$ B activation in human bronchial epithelial cells

In the next series of experiments, we examined the effect of A20 on NF- $\kappa$ B activity. To this end, we first examined NF- $\kappa$ B signaling in bronchial epithelial cells upon influenza virus infection. Among the many proteins exhibiting I $\kappa$ B function, I $\kappa$ B $\alpha$  is the only inhibitor that, in response to cell stimulation, dissociates from the NF- $\kappa$ B heterodimer complex, with kinetics matching that of the translocation of NF- $\kappa$ B to the nucleus. It has therefore been suggested that the inducible activation of NF- $\kappa$ B is regulated mainly by the dissociation of NF- $\kappa$ B an I $\kappa$ B $\alpha$  (Traenckner et al., 1995). In order to examine influenza virus infection-induced NF- $\kappa$ B signaling, we examined I $\kappa$ B phosphorylation and I $\kappa$ B degradation, and NF- $\kappa$ B promoter activation in bronchial epithelial cells upon influenza virus infection. As shown in Fig. 3A, amounts of phosphorylated I $\kappa$ B in influenza virus-infected bronchial epithelial cells increased at 4 h after influenza virus infection, were maximal at 8 h and thereafter slightly decreased at 10 h (Fig. 3A, upper panel, P-I $\kappa$ B $\alpha$ ). Amounts of total I $\kappa$ B protein decreased along with time of culture periods, indicating an increase in amounts of phosphorylated I $\kappa$ B proteins inversely correlated with a decrease in amounts of total I $\kappa$ B proteins (Fig. 3A, middle panel, I $\kappa$ B $\alpha$ ). Almost equal amounts of tubulin protein were blotted with anti-tubulin antibody regardless of the time of culture periods (Fig. 3A, lower panel,  $\beta$ -tubulin). Next, the cells that had been transiently transfected by NF- $\kappa$ B-Luc reporter plasmid were infected with influenza virus and then NF- $\kappa$ B-dependent luciferase gene activity was determined at various times as indicated after infection with influenza virus. NF- $\kappa$ B reporter activity in influenza virus-infected cells increased at 4 h, was maximal at 8 h and thereafter returned to the basal levels at 24 h (Fig. 3B).

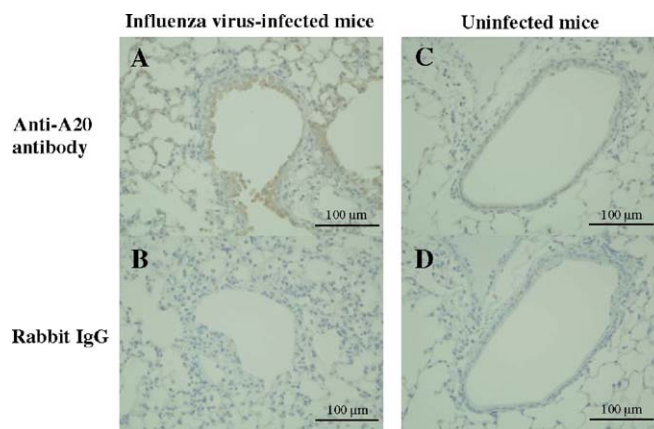


Fig. 2. A20 expression in the lung tissue specimens from mice. Mice were intranasally inoculated with influenza virus or PBS (control mice) and the lungs were removed on day 4. The lung specimens from influenza virus-infected mice (A and B) and control mice (C and D) were stained with anti-A20 antibody (A and C) or control rabbit IgG (B and D). Original magnification:  $\times 400$ . The results are representative of each group.

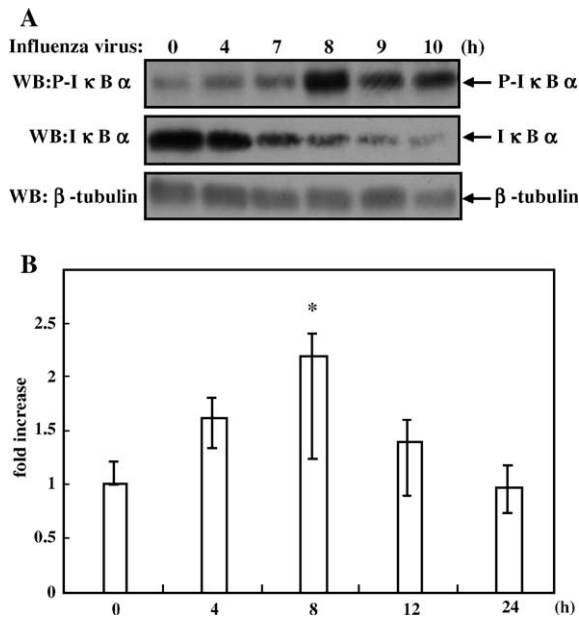


Fig. 3. Influenza virus infection induces IκB phosphorylation and NF-κB activation in human bronchial epithelial cells. IκBα phosphorylation (P-IκBα), IκBα degradation (IκBα) and β-tubulin protein expression were analyzed at times as indicated after influenza virus infection (A). NF-κB-dependent luciferase gene activity was determined at times as indicated after influenza virus infection (B). The results are expressed as means±S.D. of three different experiments. \* indicates  $P < 0.05$  compared with NF-κB activity in influenza virus-uninfected cells.

3.5. Transfection of A20 attenuates influenza virus infection-induced NF-κB promoter activation

Finally, we examined the effect of A20 in influenza virus infection-induced NF-κB promoter activation. The bronchial epithelial cells were transiently transfected by the A20 expression vector. Transient transfection of A20 attenuated

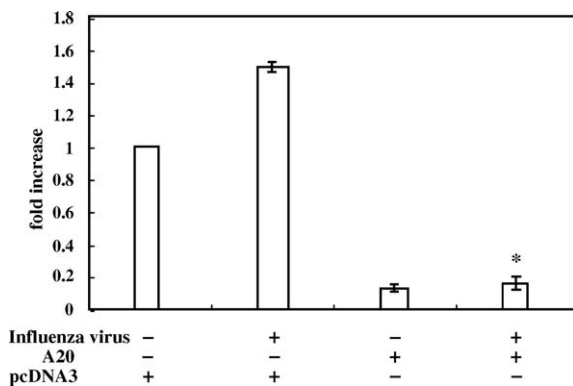


Fig. 4. NF-κB activity is depressed in the A20-transfected human bronchial epithelial cells. Bronchial epithelial cells were transiently co-transfected with the human NF-κB-Luc reporter plasmid as well as either the pcDNA-A20 expression vector or the empty pcDNA3 vector. After 24 h with the transfection, bronchial epithelial cells were infected with influenza virus and NF-κB reporter activity was determined at the desired times as indicated after influenza virus infection. The results are expressed as means±S.D. of three different experiments. \* indicates  $P < 0.05$  compared with NF-κB promoter activity in empty pcDNA3 vector-transfected cells.

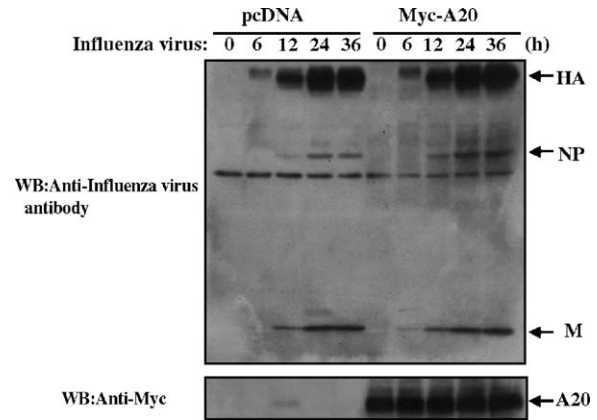


Fig. 5. Influenza virus protein synthesis in A20-transfected HEK293. Influenza virus protein synthesis was analyzed by Western blotting using polyclonal anti-influenza virus antibody as described in Materials and methods. The results are representative of two independent experiments.

NF-κB promoter activation in bronchial epithelial cells infected with influenza virus (Fig. 4).

3.6. Influenza virus protein synthesis in A20-transfected cells

Transient transfection of A20 into bronchial epithelial cells resulted in the inhibition of NF-κB promoter activation upon influenza virus infection. If influenza virus growth is inhibited in A20-transfected bronchial epithelial cells compared to that in control vector-transfected bronchial epithelial cells, the inhibited NF-κB activation might result from the inhibited replication of influenza virus. To test this possibility, influenza virus protein expression in A20-transfected HEK293 versus control vector-transfected HEK293 was compared. The amounts of three major influenza virus protein expression, including HA, NP and M1 in A20-transfected HEK293, were comparable to those in control vector-transfected HEK293, indicating that influenza virus replication is not inhibited in A20-transfected (Fig. 5). These results indicated that A20 does not inhibit influenza virus replication in these experimental conditions. The total number of cells and cell viability determined by trypan blue exclusion dye at the end of the culture period of each experiment (indicated in Figs. 1–5) did not differ with culture conditions (data not shown).

4. Discussion

In this study, in order to clarify the potentially protective role of A20 in lung inflammation and injury upon influenza virus infection, we examined the inducible expression of A20 protein and mRNA in the lung from mice and in bronchial epithelial cells and the role of A20 in NF-κB promoter activation in bronchial epithelial cells. The results showed that A20 expression was induced in the lung from mice and bronchial epithelial cells, and overexpression of A20 attenuated NF-κB promoter activation in bronchial epithelial cells upon influenza virus infection. These results indicate that A20 may function as a negative regulator for inflammatory response in influenza virus infection.

There are two major means to control influenza virus infection: the inhibition of virus propagation and virus infection-associated harmful events, including pulmonary inflammation and injury. A20 is a cytoplasmic zinc finger protein originally identified as a TNF $\alpha$ - and IL-1-inducible gene product in endothelial cells (Song et al., 1996). Subsequently, A20 expression is induced in a variety of cell types upon various stimuli (Krikos et al., 1992; Becker et al., 2000; Opiari et al., 1990; Jaattela et al., 1996). A20 negatively regulates NF- $\kappa$ B signaling (Gon et al., 2004). However, the role of A20 in influenza virus infection-induced NF- $\kappa$ B activity in bronchial epithelial cells has not been determined. Here, we have shown that A20 is inducible and expressed in the lung from mice and in bronchial epithelial cells upon influenza virus infection. To clarify the role of A20 in NF- $\kappa$ B activity, we transiently transfected A20 into bronchial epithelial cells and examined the role of overexpressed A20 in NF- $\kappa$ B promoter activation in bronchial epithelial cells upon influenza virus infection. The results have shown that overexpression of A20 results in the attenuation of influenza virus infection-induced NF- $\kappa$ B promoter activation.

We must carefully interpret our results when extrapolating *in vitro* data of the inhibitory effect of A20 on NF- $\kappa$ B activation to the *in vivo*. Airway epithelial cells produce IFN- $\beta$  and TNF- $\alpha$  that exert anti-viral activity at the early stage of influenza virus infection (Santoro et al., 2003; Seo and Webster, 2002; Julkunen et al., 2000). They serve as the key player in the host defense against influenza virus infection. The promoter of IFN- $\beta$  gene and TNF- $\alpha$  gene contains an NF- $\kappa$ B-binding site and NF- $\kappa$ B regulates IFN- $\beta$  and TNF- $\alpha$  expression (Santoro et al., 2003; Seo and Webster, 2002; Julkunen et al., 2000). Accumulated cells including macrophages, T and B lymphocytes, natural killer cells and neutrophils at the site of viral infection are capable of producing IFN- $\alpha\gamma$ , TNF- $\alpha$ , IL-1 and IL-18 (Kujime et al., 2000; Tamura and Kurata, 2004). These cytokines promote the development of Th1-type responses that are a prerequisite for antiviral immunity. NF- $\kappa$ B regulates the gene expression of these cytokines. Thus, NF- $\kappa$ B plays a defensive role against influenza virus infection.

In the contrast, NF- $\kappa$ B is suggested to be harmful to the host defense against influenza virus infection (Nimmerjahn et al., 2004; Wurzer et al., 2004; Ichiyama et al., 2004). NF- $\kappa$ B activity enhances virus propagation (Wurzer et al., 2004). Alveolar type II epithelial cells with low NF- $\kappa$ B activity were resistant to influenza A virus infection, whereas the cells with high NF- $\kappa$ B activity became susceptible to infection (Nimmerjahn et al., 2004). These studies indicate that the infectivity of influenza virus is dependent on active NF- $\kappa$ B pathways. Influenza virus-associated encephalopathy is suggested to be a proinflammatory disease and affected patients exhibit high morbidity and mortality. The levels of proinflammatory cytokines, such as IL-6 in serum and NF- $\kappa$ B activity in peripheral blood mononuclear cells, are closely associated with disease severity (Ichiyama et al., 2004). Avian influenza A virus infection causes unusual severity of disease in humans. It has been indicated that hyperproduction of NF- $\kappa$ B-dependent cytokines including TNF- $\alpha$  and IP-10 may contribute to the unusual severity of

human influenza H5N1 disease (Yuen et al., 1998; Peiris et al., 2004; Tran et al., 2004; Fouchier et al., 2004). In the murine model of viral pneumonia and lung injury upon influenza virus infection, MIP-2 that is a murine counterpart of human IL-8 increased in the lung tissue on day 2 after infection with influenza virus accompanied with increased number of neutrophils in the lung (Ochiai et al., 1993). Neutralization of MIP-2 activity with anti-MIP-2 antibody or immunoglobulin prevents and attenuates lung injury and myocarditis upon influenza virus infection (Kishimoto et al., 2004). Therefore, an inhibition of IL-8 production is an important strategy to attenuate and minimize pulmonary inflammation upon influenza virus infection. Taken together, NF- $\kappa$ B activity might be harmful and should be down-regulated when it is inappropriately and excessively activated. Thus, NF- $\kappa$ B plays the host defense and also promotes proinflammatory responses against influenza virus infection.

Vaccine is the key to controlling a pandemic and antiviral drugs are effective in treating human influenza virus disease (Palese, 2004). Recently, short interfering RNAs (siRNA) specific for highly conserved region influenza genes have been shown to inhibit influenza virus A replication in the lung from mice infected with influenza A virus (Tompkins et al., 2004). In addition to developing new antiviral drugs and vaccines, the means to control hyperinflammatory responses in the host has been expected. The inhibition of NF- $\kappa$ B by A20 may or may not be advantageous to the host defense mechanism against influenza virus infection. Recent data have indicated that A20 is critical to limiting inflammatory responses and host damages in multiple tissues (Lee et al., 2000; Heyninck and Beyaert, 2005). In this study, we showed the negative regulatory role of A20 in NF- $\kappa$ B activity in airway epithelial cell upon influenza virus infection. A20 may be advantageous to the host defense against influenza virus infection. However, the precise role of A20 remains to be clarified.

## Acknowledgement

This study was financially supported in part by a grant-in-aid for High-Tech Research Center from the Japanese Ministry of Education, Science, Sports and Culture to Nihon University, General Scientific Research from the Ministry of Education of Japan, and grants-in-aid for General Scientific Research from the Ministry of Education of Japan (14570568, 15390260), and by Culture to Nihon University and Interdisciplinary General Joint Research Grant for Nihon University.

## References

- Becker, M.N., Diamond, G., Verghese, M.W., Randell, S.H., 2000. CD14-dependent lipopolysaccharide-induced beta-defensin-2 expression in human tracheobronchial epithelium. *J. Biol. Chem.* 275, 29731–29736.
- Cheng, V.C., Tang, B.S., Wu, A.K., Chu, C.M., Yuen, K.Y., 2004. Medical treatment of viral pneumonia including SARS in immunocompetent adult. *J. Infect.* 49, 262–273.
- Cheung, C.Y., Poon, L.L., Lau, A.S., Luk, W., Lau, Y.L., Shortridge, K.F., Gordon, S., Guan, Y., Peiris, J.S., 2002. Induction of proinflammatory cytokines in human macrophages by influenza A (H5N1) viruses: a mechanism for the unusual severity of human disease? *Lancet* 360, 1831–1837.

- Fan, J., Ye, R.D., Malik, A.B., 2001. Transcriptional mechanisms of acute lung injury. *Am. J. Physiol., Lung Cell. Mol. Physiol.* 281, L1037–L1050.
- Fouchier, R.A., Schneeberger, P.M., Rozendaal, F.W., Broekman, J.M., Kemink, S.A., Munster, V., Kuiken, T., Rimmelzwaan, G.F., Schutten, M., Van Doornum, G.J., Koch, G., Bosman, A., Koopmans, M., Osterhaus, A.D., 2004. Avian influenza A virus (H7N7) associated with human conjunctivitis and a fatal case of acute respiratory distress syndrome. *Proc. Natl. Acad. Sci. U. S. A.* 101, 1356–1361.
- Gon, Y., Asai, Y., Hashimoto, S., Mizumura, K., Jibiki, I., Machino, T., Ra, C., Horie, T., 2004. A20 inhibits toll-like receptor 2- and 4-mediated interleukin-8 synthesis in airway epithelial cells. *Am. J. Respir. Cell Mol. Biol.* 31, 330–336.
- Guan, Y., Poon, L.L., Cheung, C.Y., Ellis, T.M., Lim, W., Lipatov, A.S., Chan, K.H., Sturm-Ramirez, K.M., Cheung, C.L., Leung, Y.H., Yuen, K.Y., Webster, R.G., Peiris, J.S., 2004. H5N1 influenza: a protean pandemic threat. *Proc. Natl. Acad. Sci. U. S. A.* 101, 8156–8161.
- Gubareva, L.V., Kaiser, L., Hayden, F.G., 2000. Influenza virus neuraminidase inhibitors. *Lancet* 355, 827–835.
- Heynink, K., Beyaert, R., 2005. A20 inhibits NF-kappaB activation by dual ubiquitin-editing functions. *Trends. Biochem. Sci.* 30, 1–4.
- Hu, X., Yee, E., Harlan, J.M., Wong, F., Karsan, A., 1998. Lipopolysaccharide induces the antiapoptotic molecules, A1 and A20, in microvascular endothelial cells. *Blood* 92, 2759–2765.
- Ichihama, T., Morishima, T., Isumi, H., Matsufuji, H., Matsubara, T., Furukawa, S., 2004. Analysis of cytokine levels and NF-kappaB activation in peripheral blood mononuclear cells in influenza virus-associated encephalopathy. *Cytokine* 27, 31–37.
- Jaattela, M., Mouritzen, H., Elling, F., Bastholm, L., 1996. A20 zinc finger protein inhibits TNF and IL-1 signaling. *J. Immunol.* 156, 1166–1173.
- Jibiki, I., Hashimoto, S., Maruoka, S., Gon, Y., Matsuzawa, A., Nishitoh, H., Ichijo, H., Horie, T., 2003. Apoptosis signal-regulating kinase 1-mediated signaling pathway regulates nitric oxide-induced activator protein-1 activation in human bronchial epithelial cells. *Am. J. Respir. Crit. Care Med.* 167, 856–861.
- Julkunen, I., Melen, K., Nyqvist, M., Pirhonen, J., Sareneva, T., Matikainen, S., 2000. Inflammatory responses in influenza A virus infection. *Vaccine* 19 (Suppl. 1), S32–S37.
- Kishimoto, C., Hiraoka, Y., Takada, H., 2004. Effects of immunoglobulin upon murine myocarditis caused by influenza A virus: superiority of intact type to F(ab')<sub>2</sub> type. *J. Cardiovasc. Pharmacol.* 43, 61–67.
- Koura, T., Gon, Y., Hashimoto, S., Azuma, A., Kudoh, S., Fukuda, Y., Sugawara, I., Yodoi, J., Horie, T., 2000. Expression of thioredoxin in granulomas of sarcoidosis: possible role in the development of T lymphocyte activation. *Thorax* 55, 755–761.
- Krikos, A., Laherty, C.D., Dixit, V.M., 1992. Transcriptional activation of the tumor necrosis factor alpha-inducible zinc finger protein, A20, is mediated by kappa B elements. *J. Biol. Chem.* 267, 17971–17976.
- Kujime, K., Hashimoto, S., Gon, Y., Shimizu, K., Horie, T., 2000. p38 mitogen-activated protein kinase and c-jun-NH2-terminal kinase regulate RANTES production by influenza virus-infected human bronchial epithelial cells. *J. Immunol.* 164, 3222–3228.
- Lee, E.G., Boone, D.L., Chai, S., Libby, S.L., Chien, M., Lodolce, J.P., Ma, A., 2000. Failure to regulate TNF-induced NF-kappaB and cell death responses in A20-deficient mice. *Science* 289, 2350–2354.
- Maruoka, S., Hashimoto, S., Gon, Y., Nishitoh, H., Takeshita, I., Asai, Y., Mizumura, K., Shimizu, K., Ichijo, H., Horie, T., 2003. ASK1 regulates influenza virus infection-induced apoptotic cell death. *Biochem. Biophys. Res. Commun.* 307, 870–876.
- Miller, W.E., Mosialos, G., Kieff, E., Raab-Traub, N., 1997. Epstein-Barr virus LMP1 induction of the epidermal growth factor receptor is mediated through a TRAF signaling pathway distinct from NF-kappaB activation. *J. Virol.* 71, 586–594.
- Nimmerjahn, F., Dudziak, D., Dirmeyer, U., Hobom, G., Riedel, A., Schlee, M., Staudt, L.M., Rosenwald, A., Behrends, U., Bornkamm, G.W., Mautner, J., 2004. Active NF-kappaB signalling is a prerequisite for influenza virus infection. *J. Gen. Virol.* 85, 2347–2356.
- Ochiai Ikesue, H.A., Kurokawa, M., Nakajima, K., Nakagawa, H., 1993. Enhanced production of rat interleukin-8 by in vitro and in vivo infections with influenza A NWS virus. *J. Virol.* 67, 6811–6814.
- Opiari, A.W., Boguski Jr, M.S., Dixit, V.M., 1990. The A20 cDNA induced by tumor necrosis factor alpha encodes a novel type of zinc finger protein. *J. Biol. Chem.* 265, 14705–14708.
- Palese, P., 2004. Influenza: old and new threats. *Nat. Med.* 10, S82–S87.
- Peiris, J.S., Yu, W.C., Leung, C.W., Cheung, C.Y., Ng, W.F., Nicholls, J.M., Ng, T.K., Chan, K.H., Lai, S.T., Lim, W.L., Yuen, K.Y., Guan, Y., 2004. Re-emergence of fatal human influenza A subtype H5N1 disease. *Lancet* 363, 617–619.
- Santoro, M.G., Rossi, A., Amici, C., 2003. NF-kappaB and virus infection: who controls whom. *EMBO J.* 22, 2260–2252.
- Seo, S.H., Webster, R.G., 2002. Tumor necrosis factor alpha exerts powerful anti-influenza virus effects in lung epithelial cells. *J. Virol.* 76, 1071–1076.
- Shortridge, K.F., 2003. Severe acute respiratory syndrome and influenza: virus incursions from southern China. *Am. J. Respir. Crit. Care Med.* 168, 1416–1420.
- Song, H.Y., Rothe, M., Goeddel, D.V., 1996. The tumor necrosis factor-inducible zinc finger protein A20 interacts with TRAF1/TRAF2 and inhibits NF-kappaB activation. *Proc. Natl. Acad. Sci. U. S. A.* 93, 6721–6725.
- Tamura, S., Kurata, T., 2004. Defense mechanisms against influenza virus infection in the respiratory tract mucosa. *Jpn. J. Infect. Dis.* 57, 236–247.
- Thompson, W.W., Shay, D.K., Weintraub, E., Brammer, L., Cox, N., Anderson, L.J., Fukuda, K., 2003. Mortality associated with influenza and respiratory syncytial virus in the United States. *JAMA* 289, 179–186.
- Tompkins, S.M., Lo, C.Y., Tumpey, T.M., Epstein, S.L., 2004. Protection against lethal influenza virus challenge by RNA interference in vivo. *Proc. Natl. Acad. Sci. U. S. A.* 101, 8682–8686.
- Traenckner, E.B., Pahl, H.L., Henkel, T., Schmidt, K.N., Wilk, S., Baeuerle, P. A., 1995. Phosphorylation of human I kappa B-alpha on serines 32 and 36 controls I kappa B-alpha proteolysis and NF-kappa B activation in response to diverse stimuli. *EMBO J.* 14, 2876–2883.
- Tran, T.H., Nguyen, T.L., Nguyen, T.D., Luong, T.S., Pham, P.M., Nguyen, V. C., Pham, T.S., Vo, C.D., Le, T.Q., Ngo, T.T., Dao, B.K., Le, P.P., Nguyen, T. T., Hoang, T.L., Cao, V.T., Le, T.G., Nguyen, D.T., Le, H.N., Nguyen, K.T., Le, H.S., Le, V.T., Christiane, D., Tran, T.T., de Menno, J., Schultz, C., Cheng, P., Lim, W., Horby, P., Farrar, J., 2004. Avian influenza A (H5N1) in 10 patients in Vietnam. *N. Engl. J. Med.* 350, 1179–1188.
- Van Reeth, K., 2000. Cytokines in the pathogenesis of influenza. *Vet. Microbiol.* 74, 109–116.
- Webby, R.J., Webster, R.G., 2003. Are we ready for pandemic influenza? *Science* 302, 1519–1522.
- Wurzer, W.J., Ehrhardt, C., Pleschka, S., Berberich-Siebelt, F., Wolff, T., Walczak, H., Planz, O., Ludwig, S., 2004. NF-kappaB-dependent induction of tumor necrosis factor-related apoptosis-inducing ligand (TRAIL) and Fas/FasL is crucial for efficient influenza virus propagation. *J. Biol. Chem.* 279, 30931–30937.
- Yuen, K.Y., Chan, P.K., Peiris, M., Tsang, D.N., Que, T.L., Shortridge, K.F., Cheung, P.T., To, W.K., Ho, E.T., Sung, R., Cheng, A.F., 1998. Clinical features and rapid viral diagnosis of human disease associated with avian influenza A H5N1 virus. *Lancet* 351, 467–471.

Yasuko Shibata · Naomi Ogura · Keisuke Yamashiro  
Shogo Takashiba · Toshiro Kondoh · Keiji Miyazawa  
Masaru Matsui · Yoshimitsu Abiko

## Anti-inflammatory effect of linear polarized infrared irradiation on interleukin-1 $\beta$ -induced chemokine production in MH7A rheumatoid synovial cells

Received: 27 April 2005 / Revised: 10 May 2005 / Accepted: 6 June 2005 / Published online: 27 July 2005  
© Springer-Verlag London Limited 2005

**Abstract** We examined the anti-inflammatory effect of infrared linear polarized light irradiation on the MH7A rheumatoid fibroblast-like synoviocytes (FLS) stimulated with the proinflammatory cytokine interleukin (IL)-1 $\beta$ . Expression of messenger ribonucleic acids (mRNAs) encoding IL-8, RANTES (regulated upon activation, normal T cell expressed and secreted), growth-related gene alpha (GRO $\alpha$ ), and macrophage inflammatory protein-1 $\alpha$  (MIP1 $\alpha$ ) was measured using real-time reverse transcription polymerase chain reaction, and the secreted proteins were measured in the conditioned media using enzyme-linked immunosorbent assays. We found that irradiation with linear polarized infrared light suppressed IL-1 $\beta$ -induced expression of IL-8 mRNA and, correspondingly, the synthesis and release of IL-8 protein in

MH7A cells. This anti-inflammatory effect was equivalent to that obtained with the glucocorticoid dexamethasone. Likewise, irradiation suppressed the IL-1 $\beta$ -induced expression of RANTES and GRO $\alpha$  mRNA. These results suggest that the irradiation of the areas around the articular surfaces of joints affected by rheumatoid arthritis (RA) using linear polarized light may represent a useful new approach to treatment.

**Keywords** Linear polarized light · Super Lizer · Rheumatoid arthritis synoviocytes MH7A · IL-8 · IL-1 $\beta$  · Dexamethasone

Y. Shibata ✉ · Y. Abiko  
Department of Biochemistry and Molecular Biology,  
Nihon University School of Dentistry at Matsudo,  
2-870-1, Sakaecho-Nishi, Matsudo, Chiba 271-8587, Japan  
E-mail: yshibata@mascad.nihon-u.ac.jp  
Tel.: +81-47-3609328  
Fax: +81-47-3609329  
E-mail: yabiko@mascad.nihon-u.ac.jp  
Tel.: +81-47-3609322  
Fax: +81-473-3609329

N. Ogura · T. Kondoh  
Department of Maxillofacial Surgery, Nihon University  
School of Dentistry at Matsudo, 2-870-1, Sakaecho-Nishi,  
Matsudo, Chiba 271-8587, Japan

K. Yamashiro · S. Takashiba  
Department of Pathophysiology, Periodontal Science,  
Okayama University Graduate School  
of Medicine and Dentistry, 2-5-1, Shikata,  
Okayama 700-8525, Japan

K. Miyazawa  
Central Research Laboratories, Kissei Pharmaceutical Co., Ltd,  
4365-1, Hotaka, Minami-azumi, Nagano 399-8304, Japan

M. Matsui  
Tokyo Iken Co., Ltd., 1131-1, Higashi-Naganuma,  
Inagi, Tokyo 206-0802, Japan

### Introduction

Rheumatoid arthritis (RA) is an autoimmune joint disease characterized by the inflammation and destruction of articular surfaces and bone. The pathogenesis of RA involves the proliferation of synovial cells and the invasion of joint cartilage and bone by fibroblast-like synoviocytes (FLS) and other inflammatory cells [1–3]. Indeed, the elastic synovial membrane is an initial target of rheumatic inflammation and, along with chondrocytes, becomes a primary source of inflammatory factors (e.g., cytokines) that are secreted into the synovial fluid [4, 5]. For instance, levels of pro-inflammatory cytokines, such as interleukin (IL)-1 $\beta$ , are known to be elevated in the synovial fluid of RA patients and to play a key role in amplifying and perpetuating inflammation and joint destruction [6, 7].

The MH7A-immortalized rheumatoid FLS line was established by stably transfecting FLS with the SV40 T antigen gene. These cells grow more rapidly than the parental cells and, at this point, have attained over 150 population doublings [8]. The MH7A cells positively stain for IL-1R, intercellular adhesion molecule-1 (ICAM-1), CD16, CD40, CD80, and CD95 [8], and

IL-1 $\beta$  enhances the production of IL-6 and matrix metalloproteinases (MMPs), just as in the parental cells [9, 10]. Thus, MH7A cells appear to be a useful model for investigating the regulation of rheumatoid FLS, the effects of IL-1 $\beta$ , and the potential efficacy of new therapies for treating RA.

Photodynamic laser therapy can be considered as a new way to use arthroscopic techniques to treat inflammation of the synovial membrane in RA [11]. Indeed, following gallium–aluminum–arsenide (Ga–Al–As) laser treatment, histological examination of the irradiated synovial membranes showed a flattening of epithelial cells, decreased villous proliferation, narrower vascular lumens, and lesser infiltration of inflammatory cells than was seen in non-irradiated synovia [7]. An alternative approach makes use of the linear polarized light instrument, which has been used clinically with good effect in several patients with inflammatory disease. It can be applied during physical therapy to relieve pain, and several studies have shown that such irradiation relieves multiple-type alopecia areata [12], improves the structure of stored human erythrocytes [13], improves the flexibility of shoulder and ankle joints [14], and relieves temporomandibular joint pain [15, 16]. The biochemical mechanism of action of linear polarized infrared irradiation is not yet clear, however.

Many cell types are now known to synthesize and release chemokines in response to injury, infection, inflammation, and various other pathological conditions [17–20]. The aim of the present study was to determine whether the proinflammatory cytokine IL-1 $\beta$  would enhance chemokine production in MH7A cells serving as a model of RA synovial cells, and, if so, whether the linear polarized light irradiation would suppress that

effect, thereby, establishing a potential role for linear polarized infrared irradiation in the clinical treatment of inflamed synovial tissue in RA joints.

## Materials and methods

### Human rheumatoid arthritis model

The MH7A cells, which were derived from human FLS isolated from the knee joint of an RA patient and retain the morphologic and functional characteristics of primary synovial cells [8], were obtained from Cell Bank, Riken Bioresource Center (Ibaraki, Japan). The cells were maintained in RPMI-1640 medium (Life Technologies Inc., Grand Island, NY, USA), supplemented with 10% fetal bovine serum and penicillin-streptomycin at 37°C under a 95% air/5% CO<sub>2</sub> atmosphere. For experimentation, MH7A cells were first incubated for 16 h in medium containing 10% fetal calf serum and then in fresh medium containing recombinant human IL-1 $\beta$  (CalBiochem, EMD Bioscience Inc., Darmstadt, Germany).

### Linear polarized infrared irradiation

A Super Lizer (HA2200, Tokyo Iken Co., Ltd., Tokyo, Japan) linear polarized light instrument was used to irradiate cells at wavelengths ranging from 600 nm to 1,600 nm, as shown in Fig. 1a. Dishes containing IL-1 $\beta$ -stimulated MH7A cells were irradiated for 685 s in the CO<sub>2</sub> incubator (Fig. 1b). The depth and intensity of the irradiation were regulated by respectively varying their distance from the laser source and the

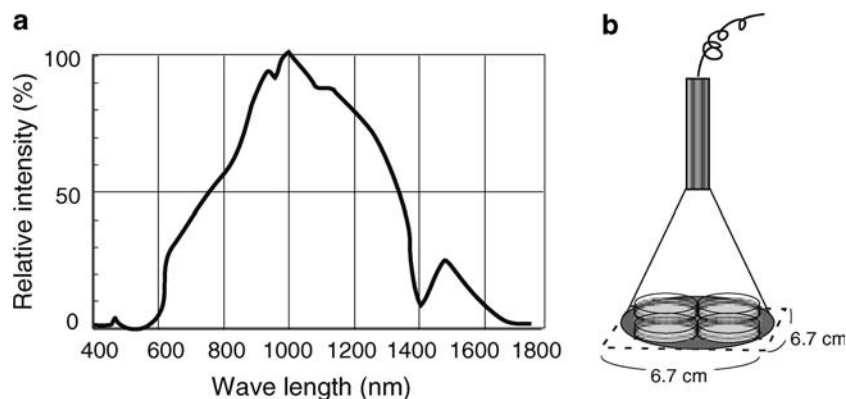


**Fig. 1a, b** An output spectrum from Super Lizer after polarizing plate passage. An output spectrum from Super Lizer (a) was measured by the spectrometer (Yokogawa Electric Co., Tokyo, Japan). The light from a halogen lamp (150 W) is input to a low-pass filter having a film designed to filter out waves of wavelength shorter than 600 nm on a quartz glass. The transmitted light is input to the bundle fiber, then next to square glass pillar, and then a convex lens. Finally, the transmitted light is irradiated to dishes through the polarizing plate in the CO<sub>2</sub> incubator (b). The intensity of the light power was measured using a power meter (thermo-

couple type) (NEOARK Co., Tokyo, Japan). Irradiation occupancy was “0.5,” because the turn on/off of light was every second. The energy density was calculated as follows: (energy density) = (average power of density) × (exposure time). The irradiation area of the laser was 45 cm<sup>2</sup> (6.7 × 6.7 cm). Energy density = 0.0056 W (average power of density) × 685 s (exposure time) = 3.8 J/cm<sup>2</sup> [average power = 0.5 W × 0.5 (occupancy; lamp lighting time/exposure time) = 0.25 W, average power of density = 0.25 W (average power) / 45 cm<sup>2</sup> (irradiation area) = 0.0056 W]

duration of the irradiation. For experimentation, we used pulsed irradiation at a frequency of 1 Hz, which produced an energy density of 3.8 J/cm<sup>2</sup>. The cells were harvested immediately after irradiation, and the ribonucleic acid (RNA) was extracted. In addition, the conditioned media were collected and stored at -20°C for later use.

### Immunoassays

Levels of IL-6, tumor necrosis factor  $\alpha$  (TNF- $\alpha$ ), IL-6, IL-8, and RANTES (regulated upon activation, normal T cell expressed and secreted) protein in media conditioned by MH7A cells grown on 35-mm<sup>2</sup> plates were assayed using commercially available ELISAs (Endogen Inc., Woburn, MA, USA).

### Real-time kinetic RT-PCR

To assess the effects of irradiation on the transcription of genes encoding IL-8, RANTES, growth-related gene alpha (GRO- $\alpha$ ), macrophage inflammatory protein-1 $\alpha$  (MIP1 $\alpha$ ), and the housekeeping enzyme glyceraldehyde-3-phosphate dehydrogenase (GAPDH), MH7A cells grown to 70% confluence on 100-mm<sup>2</sup> plates were irradiated for 2 h using a Super Lizer or left untreated, after which, they were homogenized using TRIzol Reagent (Life Technologies, Gaithersburg, MD, USA), and the total RNA was isolated using a FasRNA kit with a FastPreoFP 120 Instrument (BIO 101 Inc., Vista, CA, USA). The level of expression of specific mRNAs was determined using an ABI Prism 7700 and sequence detection system software (Applied Biosystems, Foster City, CA, USA). The primer sets used for real-time kinetic RT-PCR (polymerase chain reaction) were as follows: for IL-8, 5'-ATC ACT TCC AAG CTG GCC GTG GCT-3' (forward) and 5'-TCT CAG CCC TCT TCA AAA ACT TCT C-3' (reverse) [21]; for RANTES, 5'-TAC ACC AGT GGC AAG TGC TC-3' (forward) and 5'-GAA GCC TCC CAA GCT AGG AC-3' (reverse); for GRO- $\alpha$ , 5'-TGC AGG GAA TTC ACC CCA AG-3' (forward) and 5'-CAG GGC CTC CTT CAG GAA CA-3' (reverse); for MIP1 $\alpha$ , 5'-TTT GGT GTC ATC ACC AGC AT-3' (forward) and 5'-GCC TGA AAC AGC TTC CAC TC-3' (reverse); and for GAPDH, 5'-ATC ACC ATC TTC CAG GAG-3' (forward) and 5'-ATG GAC TGT GGT CAT GAG-3' (reverse).

## Results

### Anti-inflammatory treatment reduces IL-8 production by MH7A cells

The importance of interleukins such as IL-1, IL-6, IL-8, and TNF- $\alpha$  in RA was initially proposed on the basis of analysis of gene regulation at the local site of the disease,

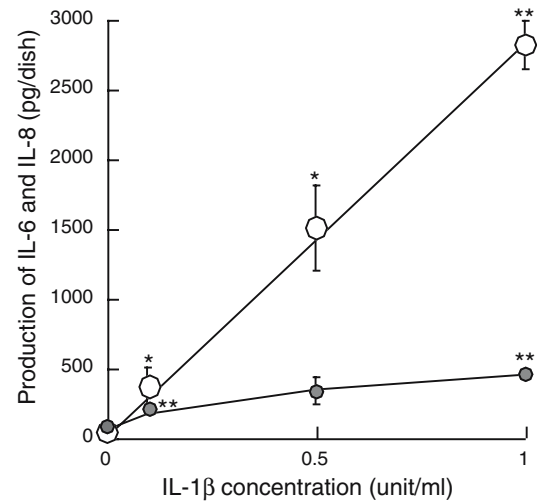


**Fig. 2** Dose-dependent synthesis of IL-8 (open circles) and IL-6 (filled circles) in MH7A cells treated with IL-1 $\beta$ . The cells were incubated with the indicated concentrations of IL-1 $\beta$  for 3 h. The results are expressed as mean  $\pm$  SD ( $n=4$ ); \*  $P < 0.05$ , \*\*  $P < 0.005$  versus control medium without IL-1 $\beta$

the synovium. IL-8 is the prototypical member of a superfamily of small (8–10 kDa), inducible, secreted chemoattractant cytokines (chemokines) that were originally discovered as monocyte-derived factors capable of attracting and activating neutrophils [17–19, 22]. Chemokines, including IL-8, have the function of being key mediators in diverse inflammatory disorders via promoting the recruitment, proliferation, and activation of vascular and immune cells. It has been found

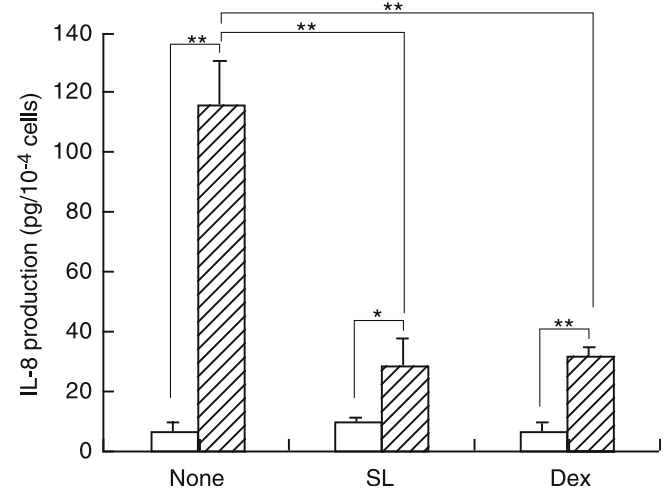


**Fig. 3** Inhibitory effect of linear polarized infrared irradiation using a Super Lizer on the production of IL-8 in MH7A cells. After the addition of a low dose of IL-1 $\beta$  (0.1 units/ml), the cells were irradiated using a Super Lizer (3.8 J/cm<sup>2</sup>) or administered DEX (1  $\mu$ M) and incubated for 3 h in a CO<sub>2</sub> incubator: hatched bars with IL-1 $\beta$ , open bars without IL-1 $\beta$ , None without anti-inflammatory treatment, SL irradiation using a Super Lizer, DEX treatment with 1  $\mu$ M dexamethasone. The results are expressed as mean  $\pm$  SD ( $n=5$ ); \*  $P < 0.05$ , \*\*  $P < 0.005$  versus control medium without IL-1 $\beta$

**Table 1** Chemokine gene expression in MH7A cells stimulated with IL-1 $\beta$ 

	None		SL		DEX	
	None	IL-1 $\beta$	None	IL-1 $\beta$	None	IL-1 $\beta$
IL-8	100	925	91	535	92	109
RANTES	100	173	103	118	122	116
GRO	100	555	60	340	43	179
MIP1 $\alpha$	100	179	68	155	289	287

Effects of irradiation with linear polarized light using a Super Lizer and administration of dexamethasone on the expression of chemokine mRNAs in MH7A cells plated on 100-mm<sup>2</sup> dishes at 1.5 $\times$ 10<sup>5</sup> cells/dish. After incubating for 16 h, fresh medium containing 0.1 U/ml IL-1 $\beta$  was provided, Super Lizer irradiation or DEX was applied, and the incubation was continued for an additional 3 h. The RNA extraction was carried out in a clean box using a FasRNA kit. Five independent extractions were carried out, after which, the extracted RNAs were pooled, measured, and reverse-transcribed. Using real-time kinetic RT-PCR, the expression of several chemokine mRNAs were detected, and their levels were normalized to that of the housekeeping enzyme GAPDH. The data shown are mean percentages normalized to control dishes, which were assigned a value of 100%: *None* no anti-inflammatory therapy, *SL* irradiation with a Super Lizer (3.8 J/cm<sup>2</sup>), *DEX* treatment with dexamethasone (final concentration, 1  $\mu$ M)

that IL-8 is the major chemoattractant in RA synovial tissues [23]. By assaying conditioned media using specific ELISAs, in the present study, we were able to confirm that IL-1 $\beta$  dose-dependently stimulates IL-8 production and release by MH7A cells (Fig. 2). Production of another chemokine, RANTES, and that of cytokines, TNF- $\alpha$ , and IL-6, were also measured in IL-1 $\beta$ -stimulated MH7A cells. A smaller amount of IL-6 than IL-8 was detected from MH7A cells into the medium. The RANTES and TNF- $\alpha$  productions from MH7A cells were not found by the ELISA method (data not shown).

We then evaluated the effect of irradiating the cells with linear polarized infrared light using a Super Lizer on the IL-1 $\beta$ -stimulated production and secretion of IL-8. We found that, after the MH7A cells were stimulated with a low dose (0.1 units/ml) of IL-1 $\beta$ , irradiation reduced the production of IL-8 to 24.4% of that seen in non-irradiated control cells. Notably, this was equivalent to the inhibitory effect obtained with the anti-inflammatory glucocorticoid dexamethasone (DEX) (Fig. 3).

#### Expression of chemokine mRNA in IL-1 $\beta$ -stimulated MH7A cells

Finally, we examined the relative levels of chemokine mRNA expression in MH7A cells using real-time kinetic RT-PCR. We found that IL-1 $\beta$  induced about a nine-fold increase in the expression of IL-8 mRNA, and that infrared Super Lizer irradiation suppressed this effect of IL-1 $\beta$ , though not quite to the degree that DEX did (Table 1). In addition, although we detected no release of RANTES protein from cells by ELISA, the levels of its mRNA were increased 1.7-fold by IL-1 $\beta$  stimulation, and Super Lizer irradiation and DEX suppressed that effect to similar degrees. Expression of GRO $\alpha$ , with and without IL-1 $\beta$  stimulation, was also suppressed by both irradiation and dexamethasone, whereas the expression of MIP1 $\alpha$  mRNA appears to have been suppressed somewhat by Super Lizer irradiation, but not by DEX.

## Discussion

It was recently reported that irradiation with linear polarized light at near-infrared wavelengths using the Super Lizer is an effective short-term treatment in patients with RA-affected temporomandibular pain [15, 16]. However, very little is known about the molecular mechanism by which linear polarized light exerts this effect. In the present study, therefore, we examined the effect of infrared Super Lizer irradiation on IL-1 $\beta$ -induced production of the chemokine IL-8 in the MH7A cultured cell line. The IL-8 levels are known to be elevated in such inflammatory diseases as RA, osteoarthritis, osteomyelitis, and periodontal disease [24]. And although macrophages, neutrophils, and endothelial cells are all considered to be primary sources of IL-8, we found that IL-1 $\beta$  stimulated the immortalized FLS to express IL-8 mRNA and to secrete high levels of IL-8 protein.

Many anti-rheumatic drugs provide relief from RA by acting as immunomodulators [25–30], though some exert an inhibitory effect on various cytokines [27, 28]. In that regard, glucocorticoids (e.g., DEX) reportedly downregulate the expression of several inflammatory genes, including those encoding IL-1, TNF- $\alpha$ , IL-6, and IL-8 [31]. We investigated whether infrared Super Lizer irradiation could influence gene transcription in MH7A cells under basal conditions and following stimulation with IL-1 $\beta$ , and found that the effect of this irradiation on the synthesis and release of IL-8 protein paralleled its effect on the expression of IL-8 mRNA (Table 1). Likewise, the irradiation affected the expression of both RANTES and GRO $\alpha$  mRNA, though the relationship between gene transcription and protein synthesis remains unclear in those cases. It thus appears that Super Lizer irradiation exerts effects on MH7A cells that are similar to those of DEX and are consistent with therapeutic efficacy in RA. Since RA is a chronic inflammatory disease, steroid administration was often in the long-term treatment. Our results demonstrate that the linear polarized infrared irradiation kept the MH7A

cells to their normal state after the stimulation with proinflammatory cytokine, IL-1 $\beta$ , due to the suppressed mRNAs expression of chemokines, as DEX did. Revealing the anti-inflammatory mechanism of the linear polarized infrared irradiation in rheumatoid FLS will contribute to the future treatment of RA patients.

**Acknowledgments** This research was supported in part by a grant from the "Academic Frontier" Project for Private Universities: matching fund subsidy from MEXT (Ministry of Education, Culture, Sports, Science and Technology) 2001–2005 and Grants-in-Aid for Scientific Research (A1; 16209063, A2; 13357017).

## References

- Gay S, Gay RE, Koopman WJ (1993) Molecular and cellular mechanisms of joint destruction in rheumatoid arthritis: two cellular mechanisms explain joint destruction?. *Ann Rheum Dis* 52(Suppl 1):S39–S47
- Firestein GS (1996) Invasive fibroblast-like synoviocytes in rheumatoid arthritis: passive responders or transformed aggressors? *Arthritis Rheum* 39(11):1781–1790
- Pap T, Müller-Ladner U, Gay RE, Gay S (2000) Fibroblast biology. Role of synovial fibroblasts in the pathogenesis of rheumatoid arthritis. *Arthritis Res* 2(5):361–367
- Feldmann M, Brennan FM, Maini RN (1996) Role of cytokines in rheumatoid arthritis. *Annu Rev Immunol* 14:397–440
- Dayer JM (2004) The process of identifying and understanding cytokines: from basic studies to treating rheumatic diseases. *Best Pract Res Clin Rheumatol* 18(1):31–45
- Feldmann M, Maini RN (1999) The role of cytokines in the pathogenesis of rheumatoid arthritis. *Rheumatology* 38(Suppl 2):3–7
- Inoue H, Takamori M, Nagata N, Nishikawa T, Oda H, Yamamoto S, Koshihara Y (2001) An investigation of cell proliferation and soluble mediators induced by interleukin 1 $\beta$  in human synovial fibroblasts: comparative response in osteoarthritis and rheumatoid arthritis. *Inflamm Res* 50(2):65–72
- Miyazawa K, Mori A, Okudaira H (1998) Establishment and characterization of a novel human rheumatoid fibroblast-like synoviocyte line, MH7A, immortalized with SV40T antigen. *J Biochem* 124(2):1153–1162
- Sun H-B, Yokota H (2002) Reduction of cytokine-induced expression and activity of MMP-1, and MMP-13 by mechanical strain in MH7A rheumatoid synovial cells. *Matrix Biol* 21(3):263–270
- Takahashi M, Funato T, Suzuki Y, Fujii H, Kumura-Ishii K, Kaku M, Sasaki T (2002) Chemically modified ribozyme targeting TNF- $\alpha$  mRNA regulates TNF- $\alpha$  and IL-6 synthesis in synovial fibroblasts of patients with rheumatoid arthritis. *J Clin Immunol* 22(4):228–236
- Amano A, Miyagi K, Azuma T, Ishihara Y, Katsube S, Aoyama I, Saito I (1994) Histological studies on the rheumatoid synovial membrane irradiated with a low energy laser. *Laser Surg Med* 15(3):290–294
- Yamazaki M, Miura Y, Tsuboi R, Ogawa H (2003) Linear polarized infrared irradiation using Super Lizer is an effective treatment for multiple-type alopecia areata. *Int J Dermatol* 42(9):738–740
- Yokoyama K, Sugiyama K (2003) Influence of linearly polarized near-infrared irradiation on deformability of human stored erythrocytes. *J Clin Laser Med Surg* 21(1):19–22
- Demura S, Yamaji S, Ikemoto Y (2002) Effect of linear polarized near-infrared light irradiation on flexibility of shoulder and ankle joints. *J Sports Med Phys Fitness* 42(4):438–445
- Yokoyama K, Oku T (1999) Rheumatoid arthritis-affected temporomandibular joint pain analgesia by linear polarized near infrared irradiation. *Can J Anaesth* 46(7):683–687
- Yokoyama K, Sugiyama K (2001) Temporomandibular joint pain analgesia by linearly polarized near-infrared irradiation. *Clin J Pain* 17(1):47–51
- Baggiolini M, Dewald B, Moser B (1994) Interleukin-8 and related chemotactic cytokines—CXC and CC chemokines. *Adv Immunol* 55:97–179
- Ben-Baruch A, Michiel DF, Oppenheim JJ (1995) Signals and receptors involved in recruitment of inflammatory cells. *J Biol Chem* 270(20):11703–11706
- Sozzani S, Locati M, Allavena P, Van Damme J, Mantovani A (1996) Chemokines: a superfamily of chemotactic cytokines. *Int J Clin Lab Res* 26(2):69–82
- Zwahlen R, Walz A, Rot A (1993) In vitro and in vivo activity and pathophysiology of human interleukin-8 and related peptides. *Int Rev Exp Pathol* 34(Pt B):27–42
- Zhong WW, Burke PA, Hand AT, Walsh MJ, Hughes LA, Forse RA (1993) Regulation of cytokine mRNA expression in lipopolysaccharide-stimulated human macrophages. *Arch Surg* 128(2):158–164
- Yoshimura T, Matsushima K, Tanaka S, Robinson EA, Appella E, Oppenheim JJ, Leonard EJ (1987) Purification of a human monocyte-derived neutrophil chemotactic factor that has peptide sequence similarity to other host defense cytokines. *Proc Natl Acad Sci USA* 84(24):9233–9237
- Brennan FM, Zachariae CO, Chantry D, Larsen CG, Turner M, Maini RN, Matsushima K, Feldmann M (1990) Detection of interleukin 8 biological activity in synovial fluids from patients with rheumatoid arthritis and production of interleukin 8 mRNA by isolated synovial cells. *Eur J Immunol* 20(9):2141–2144
- Hebert CA, Baker JB (1993) Interleukin-8: a review. *Cancer Invest* 11(6):743–750
- Hashimoto K, Lipsky PE (1993) Immunosuppression by the disease modifying antirheumatic drug bucillamine: inhibition of human T lymphocyte function by bucillamine and its metabolites. *J Rheumatol* 20(6):953–957
- Brody M, Bohm I, Bauer R (1993) Mechanism of action of methotrexate: experimental evidence that methotrexate blocks the binding of interleukin-1 $\beta$  to the interleukin-1 receptor on target cells. *Eur J Clin Chem Clin Biochem* 31(10):667–674
- Seitz M, Dewald B, Ceska M, Gerber N, Baggiolini M (1992) Interleukin-8 in inflammatory rheumatic diseases: synovial fluid levels, relation to rheumatoid factors, production by mononuclear cells, and effects of gold sodium thiomalate and methotrexate. *Rheumatol Int* 12(4):159–164
- Seitz M, Loetscher P, Dewald B, Towbin H, Rordorf C, Gallati H, Baggiolini M, Gerber NJ (1995) Methotrexate action in rheumatoid arthritis: stimulation of cytokine inhibitor and inhibition of chemokine production by peripheral blood mononuclear cells. *Br J Rheumatol* 34(7):602–609
- Carlin G, Djursater R, Smedegard G (1989) Inhibitory effects of sulfasalazine and related compounds on superoxide production by human polymorphonuclear lymphocytes. *Pharmacol Toxicol* 65:121–127
- Grootveld M, Blake DR, Sahinoglu T, Claxson AW, Mapp P, Stenes C, Allen RE, Furst A (1990) Control of oxidative damage in rheumatoid arthritis by gold(I)-thiolate drugs. *Free Radical Res Commun* 10(4–5):199–220
- Caldenhoven E, Liden J, Wissink S, Van de Stolpe A, Raaijmakers J, Koenderman L, Okret S, Gustafsson JA, Van der Saag PT (1995) Negative cross-talk between RelA and the glucocorticoid receptor: a possible mechanism for the antiinflammatory action of glucocorticoids. *Mol Endocrinol* 9(4):401–412